Universidade Federal do Rio Grande – FURG

Instituto de Oceanografia

Programa de Pós-Graduação em Oceanologia

CARBONO ANTROPOGÊNICO, ACIDIFICAÇÃO OCEÂNICA E OUTRAS MUDANÇAS DO SISTEMA CARBONATO NO OCEANO ATLÂNTICO SUL

ANDRES ELOY PIÑANGO JAUREGUI

Dissertação apresentada ao Programa de Pós-Graduação em Oceanologia, como parte dos requisitos para a obtenção do Título de Mestre.

Orientador: *Prof. Dr.* Rodrigo Kerr Duarte Pereira

Universidade Federal do Rio Grande (FURG), Brasil.

Rio Grande, RS, Brasil

Outubro 2021

CARBONO ANTROPOGÊNICO, ACIDIFICAÇÃO OCEÂNICA E OUTRAS MUDANÇAS DO SISTEMA CARBONATO NO OCEANO ATLÂNTICO SUL

Dissertação apresentada ao Programa de Pós-Graduação em Oceanologia, como parte dos requisitos para a obtenção do Título de Mestre

por

ANDRES ELOY PIÑANGO JAUREGUI

Rio Grande, RS, Brasil

Outubro 2021

PIÑANGO, ANDRES ELOY JAUREGUI

Carbono antropogênico, acidificação oceânica e outras mudanças do sistema carbonato no oceano Atlântico Sul / Andres Eloy Piñango Jauregui – Rio Grande: FURG, 2021.

Número de páginas p. 75

Dissertação (Mestrado) – Universidade Federal do Rio Grande. Mestrado em Oceanologia. Áreas de Concentração: Biogeoquímica, Poluição e Ecossistemas Marinhos; Física dos Oceanos e Clima.

1. Carbono antropogênico. 2. Acidificação dos oceanos.
3. Sistema carbonato marinho. 4. Atlântico Sul.

UNIVERSIDADE FEDERAL DO RIO GRANDE - FURG
IO – INSTITUTO DE OCEANOGRAFIA
PROGRAMA DE PÓS-GRADUAÇÃ0 EM OCEANOLOGIA
E-mail: ccpofqg@furg.br – home-page: www.ppgo.furg.br

ATA ESPECIAL DE DEFESA DE DISSERTAÇÃO DE MESTRADO 05/2021

Às 14h do dia 29 de outubro do ano de dois mil e vinte e um, por Vídeo Conferência, reuniu-se a Comissão Examinadora da Dissertação de **MESTRADO** intitulada: **"Carbono antropogênico, acidificação oceânica e outras mudanças do sistema carbonato no oceano Atlântico Sul",** do **Acad. Andrés Eloy Pinãngo Jáuregui.** A Comissão Examinadora foi composta pelos seguintes membros: Prof. Dr. Rodrigo Kerr Duarte Pereira – (Orientador – IO/FURG), Prof. Dra. Eunice da Costa Machado - (IO-FURG), Profa. Dra. Vanessa Hatje (UFBA) e Profa. Dra. Letícia Cotrim da Cunha (UERJ). Dando início à reunião, o Presidente da sessão, e Coordenador do PPGO, Prof. Dr. Rodrigo Kerr Duarte Pereira, agradeceu a presença de todos, e fez a apresentação da Comissão Examinadora. Logo após, esclareceu que o Candidato teria de 45 a 60 min para explanação do tema, e cada membro da Comissão Examinadora, um tempo máximo de 30 min para perguntas. A seguir, passou à palavra ao Candidato, que apresentou o tema e respondeu às perguntas formuladas. Após ampla explanação, a Comissão Examinadora reuniu-se em reservado para discussão do conceito a ser atribuído ao Candidato. Foi estabelecido que as sugestões de todos os membros da Comissão Examinadora, que seguem em pareceres em anexo, foram aceitas pelo Orientador/Candidato para incorporação na versão final da Dissertação. Finalmente, a Comissão Examinadora considerou o candidato APROVADO por unanimidade. Nada mais havendo a tratar, foi lavrada a presente ATA, que após lida e aprovada, será assinada pela Comissão Examinadora, pelo Candidato e pelo Coordenador o Programa de Pós-Graduação em Oceanologia (PPGO).

Prof. Dr. Rodrigo Kerr Duarte Pereira
Presidente

Profa. Dra. Eunice da Costa Machado

Profa. Dra. Vanessa Hatje

Profa. Dra. Letícia Cotrim da Cunha

Acad. Andrés Eloy Pinãngo Jáuregui

Prof. Dr. Rodrigo Kerr
Coordenador do PPGO

Em memória de Isaura Lobo e Orlando Velásquez

Agradecimentos

Para as coincidências da vida. Muito de quem somos é consequência de coisas fortuitas sobre as quais não temos poder e sinto que é preciso reconhecer isso e agradecer a sorte que me acompanhou até agora. Vou continuar dando o meu melhor, esperando que você não me falhe.

A Marta e Isaac, mis padres, quienes cuidaron de mi tantos años y que siempre han estado ahí brindándome su apoyo, comprensión y cariño. Gracias también a ti Erick, mi vida no sería la misma (ni mejor) de no ser por tu existencia. Sin ustedes este nuevo logro sería imposible, y no hay suficientes palabras en el mundo para expresar cuanto los quiero y cuanto me hacen falta.

A mi segundo hermano Elías, el causante de que hoy este estudiando el océano y quien me brindó un hogar cuando dejé atrás todo lo que conocía. Este trabajo es tanto tuyo como mío.

A mis amigos Luanda, Lineu, Gabriela y Génesis. Aun estando lejos, incluso separados por el Atlántico, han estado presentes dándome aliento. Los llevo siempre conmigo sin importar la distancia.

Ao melhor orientador que já tive na minha vida. Obrigado por todos os ensinamentos Professor Rodrigo. Você não faz ideia de quanta admiração eu tenho por sua ética de trabalho e sua visão do mundo.

A Iole, Thiago e ao Carbon Team em geral. Nossas trocas de conhecimento foram uma influência positiva tanto pessoal quanto profissionalmente.

Agradeço a todas as instituições que permitiram que este projeto fosse possível: ao CAPES, à Universidade Federal de Rio Grande (FURG) e ao Programa de Pós-graduação em Oceanologia.

I would like to thank the supporters, collaborators, and scientists behind the Global Ocean Data Analysis Project (GLODAP) and the Trans-Atlantic II Cruise.

A todos aquellos que de alguna u otra forma colaboraron con esta travesía y no están nombrados aquí.

Índice

Lista de Figuras

CAPÍTULO I

CAPÍTULO IV

Lista de Tabelas

CAPÍTULO II

CAPÍTULO IV

Lista de Acrônimos e Abreviações

A

AABW: *Antarctic Bottom Water*; Água de Fundo Antártica

AAIW: *Antarctic Intermediate Water*; Água Intermediária Antártica

Alk: *Total Alkalinity*; Alcalinidade Total

AOU: *Apparent Oxygen Utilization*; Utilização Aparente de Oxigênio

C

C_{ant}: *Anthropogenic Carbon*; Carbono antropogênico

$CaCO_3$: *Calcium Carbonate*; Carbonato de Calcio

CO_2: *Carbon Dioxide*; Dióxido de Carbono

CO_3^{-2}: *Carbonate Ion*; Íon Carbonato

D

DIC: *Dissolved Inorganic Carbon*; Carbono Inorgânico Dissolvido

E

eMLR: *Extended Multilinear Regression*; Regressão Linear Múltipla Estendida

G

GLODAP: Global Ocean Data Analysis Project

GO-SHIP: Global Ocean Ship-based Hydrographic Investigations Program

Gt: *Gigatonne*; Gigatonelada (10^{15} gramas)

N

NO^{3-}: *Nitrate*; Nitrato

NADW: *North Atlantic Deep Water*; Água Profunda do Atlântico Norte

P

pCO_2: *CO_2 Partial Pressure*; Pressão Parcial de CO_2

Pg: *Petagram*; Petagramas (10^{15} gramas)

ppm: Parts Per Million; Partes Por Milhão

R

RMSE: *Root Mean Square Error*; Erro Quadrático Médio

S

S: *Salinity*; Salinidade

SACW: *South Atlantic Central Water*; Água Central do Atlântico Sul

SAMW: *Subantartic Mode Water*; Água Modal Subantártica

Si: *Silicate*; Silicato

STMW: *Subtropical Mode Water*; Água Modal Subtropical

T

TAII: *Trans-Atlantic II Cruise*; Cruzeiro Trans-Atlantic II

TW: *Tropical Water*; Água Tropical

Grego

γ^n: *Neutral Density*; Densidade Neutra

θ: *Potential Temperature*; Temperatura Potencial

$\Omega_{(Ar/Ca)}$: Aragonite/Calcite Saturation; Saturação de Aragonita ou Calcita

Resumo

As atividades humanas desenvolvidas desde a revolução industrial até hoje originaram o aumento da concentração de dióxido de carbono (CO_2) na atmosfera nos últimos 270 anos em mais de 150 ppm. Os oceanos desempenham um papel importante no equilíbrio do ciclo do carbono, absorvendo ~25% das emissões antropogênicas. No entanto, múltiplas perturbações químicas, entre as quais se destacam a diminuição do pH e da concentração de CO_3^{-2}, surgiram como consequência desta captação anormal de carbono, com o potencial de afetar negativamente ecossistemas inteiros. No oceano Atlântico Sul a camada influenciada pelo vento é ventilada através da formação de massas de água que ocupam as camadas central e intermediária. Por meio dos processos de formação de massa de água, o carbono antropogênico (C_{ant}) é introduzido no interior do oceano, o que, por sua vez, torna a região do Atlântico Sul vulnerável ao processo de acidificação. A concentração de C_{ant} e a acidificação associada já foram estimadas para algumas seções hidrográficas específicas na região desde a década de 1980, sendo ainda necessário uma avaliação abrangente em toda a bacia do oceano Atlântico Sul. Neste estudo, quantificamos as taxas de acumulação de C_{ant} e examinamos as mudanças nas propriedades do sistema carbonato para o Atlântico Sul usando um método modificado de regressão linear múltipla estendida ao longo de seis seções de repetição hidrográfica presentes no banco de dados GLODAPv2.2020. Uma mudança média no inventário de C_{ant} de 0,71 ± 0,35 mol C m^{-2} ano^{-1} foi encontrada de 1989 a 2019. Taxas de acumulação de C_{ant} de 0,89 ± 0,33 µmol kg^{-1} ano^{-1} e 0,30 ± 0,29 µmol kg^{-1} ano^{-1} foram observadas nas águas centrais e intermediárias da área de estudo, acompanhadas por taxas de acidificação de −0,0020 ± 0,0007 unidades de pH ano^{-1} e −0,0009 ± 0,0009 unidades de pH ano^{-1}, respetivamente. Além disso, um aumento da remineralização da matéria orgânica nas águas intermediárias foi observado, amplificando a acidificação dessa massa de água, principalmente na costa africana ao longo de 25°S. Este aumento de carbono inorgânico dissolvido está

provavelmente relacionado ao aumento da atividade biológica, juntamente com mudanças na dinâmica de entrada de águas oriundas do oceano Índico. Assumindo que não haja mudanças nas tendências observadas, as águas intermediárias (água centrais na margem leste) se tornarão insaturadas em aragonita em ~70 anos (~20 anos).

Palavras-Chave: Carbono antropogênico; Acidificação dos oceanos; Sistema carbonato marinho; Atlântico Sul.

Abstract

The wind driven part of the South Atlantic Ocean is primarily ventilated through central and intermediate water formation. Through the water mass formation processes, anthropogenic carbon (C_{ant}) is introduced into the ocean's interior which in turn makes the South Atlantic region vulnerable to ocean acidification. C_{ant} and the accompanying acidification effects have been estimated for individual sections in the region since the 1980s but a comprehensive synthesis for the entire basin is still lacking. Here, we quantified the C_{ant} accumulation rates and examined the changes in the carbonate system properties for the South Atlantic using a modified extended multiple linear regression method applied to six hydrographic sections and data from the GLODAPv2.2020 product. From 1989 to 2019, a mean C_{ant} column inventory change of 0.71 ± 0.35 mol C m^{-2} yr^{-1} was found. C_{ant} accumulation rates of 0.89 ± 0.33 µmol kg^{-1} yr^{-1} and 0.30 ± 0.29 µmol kg^{-1} yr^{-1} were observed in central and intermediate waters, accompanied by acidification rates of −0.0020 ± 0.0007 pH units yr^{-1} and −0.0009 ± 0.0009 pH units yr^{-1}, respectively. Furthermore, increased remineralization was observed in intermediate waters, amplifying the acidification of this water mass, especially at the African coast along 25°S. This increase of dissolved inorganic carbon is likely related to increased biological activity together with changes in the input of Indian Ocean waters. Assuming no changes in the observed trends, intermediate waters (eastern margin central water) will become unsaturated in aragonite in ~70 years (~20 years).

Keywords: Anthropogenic Carbon; Ocean acidification; Carbonate system; South Atlantic Ocean

Capítulo I: Introdução

Múltiplas atividades humanas, tais como a queima de combustíveis fósseis e as mudanças no uso dos solos (e.g., desmatamento), foram responsáveis pela liberação de 700 ± 75 Pg C para a atmosfera desde a Era Industrial (~1750) até o ano 2019 (Friedlingstein et al., 2020). Aproximadamente 41% desse carbono de origem antropogênico (C_{ant}) permanece na atmosfera, aumentando a concentração de dióxido de carbono (CO_2) de 277 partes por milhão (ppm) em 1750 para 409,85 ± 0,10 ppm em 2019 (Dlugokencky & Tans, 2020), i.e. as maiores concentrações registradas nos últimos 800.000 anos (Figura 1). Entretanto, o CO_2 é um gás de efeito estufa e o aumento de sua concentração na atmosfera (junto aos outros gases de efeito estufa, tais como metano ou óxido nitroso) tem causado alterações no balanço radiativo da Terra e, consequentemente, no sistema climático (Cubasch et al., 2013). Estima-se que o restante do C_{ant} liberado (57%) tenha sido capturado pela biosfera terrestre e os oceanos (Friedlingstein et al., 2020), mitigando parte das mudanças no clima da Terra.

No caso dos oceanos, estima-se que eles são responsáveis pela absorção de ~25% das emissões, o que representa um fluxo de 2,5 Gt C por ano (Friedlingstein et al., 2020; Gruber, Clement, et al., 2019). Dois mecanismos

explicam a captação de CO_2 pelos oceanos: a bomba biológica e a bomba física. Na bomba biológica, os organismos vivos transformam o carbono dissolvido nas águas em matéria orgânica durante a fotossíntese, e essa matéria orgânica é transportada para o interior dos oceanos onde é remineralizada, gerando uma variação vertical na concentração de carbono. No caso da bomba física, o CO_2 é dissolvido na interface mar-ar mediante processos físico-químicos (sendo favorecida a solubilidade em águas frias e menos salinas), e essas águas superficiais depois são transportadas para o interior do oceano, armazenando o CO_2 durante décadas ou milênios, dependendo da profundidade (Canadell et al., 2021). Embora ambos processos sejam importantes, a captação de C_{ant} em escala global é controlada primordialmente pela bomba física, visto que a bomba biológica se encontra limitada pela disponibilidade de nutrientes (Broecker, 1991; Sarmiento & Gruber, 2006).

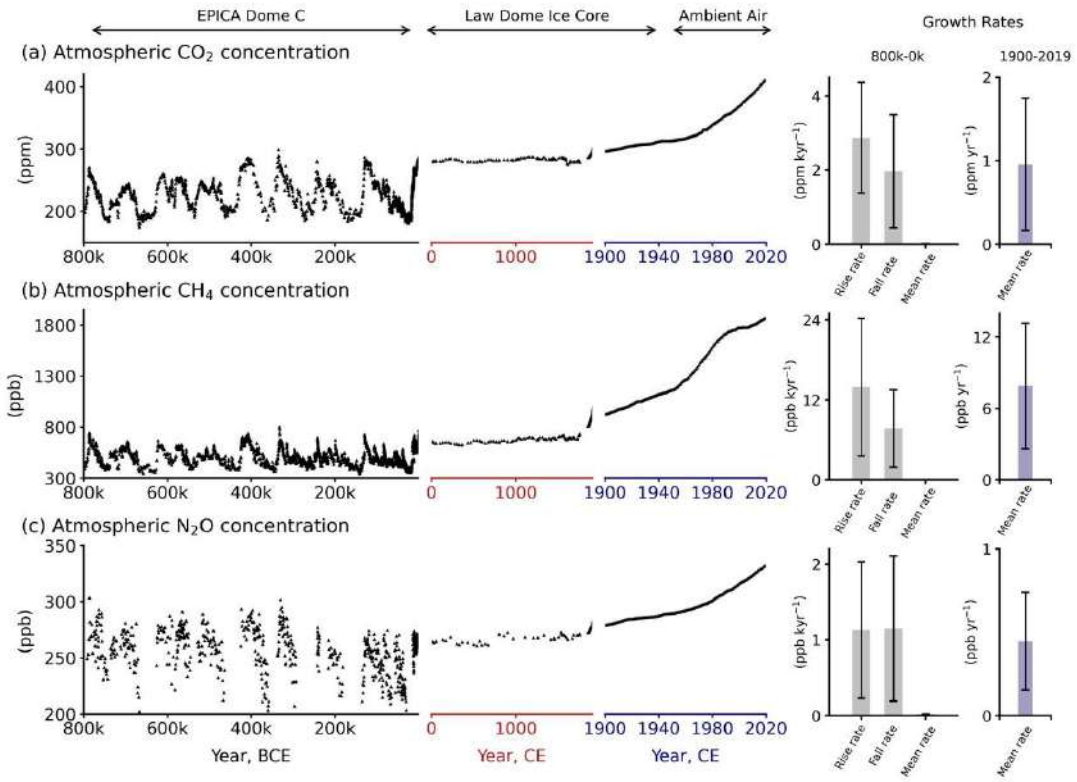

Figura 1. Concentrações dos principais gases de efeito estufa na atmosfera terrestre nos últimos 800.000 anos: (a) dióxido de carbono, (b) metano e (c) oxido nitroso. Os valores anteriores a ~1960 foram obtidos de bolhas de gás aprisionadas em núcleos de gelo e clatratos. Concentrações recentes são medições diretas da atmosfera. Note-se que as taxas de aumento observadas no último século são as maiores de todo o período estudado. Figura extraída de Canadell et al. (2021).

Assim, a absorção, armazenamento e o transporte do C_{ant} nos oceanos estão intimamente relacionados ao processo de formação e circulação das massas de água. Uma relação clara foi identificada entre o transporte e armazenamento de massas de águas centrais, intermediárias e profundas e o conteúdo de C_{ant} no interior do oceano (Gruber, Clement, et al., 2019; Sabine et al., 2004). A captação, exportação e armazenamento de C_{ant} dependem então da ventilação e circulação oceânica, das propriedades das massas de água, das interações oceano-atmosfera, da dinâmica de mesoescala e dos processos biogeoquímicos, resultando em uma distribuição não uniforme ao longo as bacias oceânicas (Gruber, Clement, et al., 2019; Lee et al., 2003; Sabine et al., 2004).

Uma das regiões onde tem sido observada uma acumulação significativa de C_{ant} é o oceano Atlântico Sul (Gruber, Clement, et al., 2019; Sabine et al., 2004; Wanninkhof et al., 2010). Esta região é caracterizada pela presença de um giro subtropical circundado pela Corrente Equatorial Sul, a Corrente do Atlântico Sul, a Corrente de Benguela e a Corrente do Brasil ao norte, sul, leste e oeste, respetivamente (Stramma & England, 1999; Figura 2a). Diversas massas de água compõem a estrutura hidrográfica da região nos primeiros 1500 m: a Água Tropical (AT), variedades de Águas Modais subtropicais (STMW), a Água Central do Atlântico Sul (SACW) e Água Intermediária Antártica (AAIW). Essas massas de água são advectadas para o norte, e representam a conexão principal entre a superfície e o interior do oceano na região subtropical (Azar et al., 2020; de Souza et al., 2018; Stramma & England, 1999; Tanhua et al., 2017; Figura 2b). Abaixo desta profundidade encontra-se a Água Profunda do Atlântico Norte (NADW) fluindo para o sul e, finalmente, a Água de Fundo Antártica (AABW) se movimentando em direção equatorial (Ríos et al., 2015; Stramma & England, 1999). Ao sul do giro subtropical começa o setor Atlântico do oceano Austral, caracterizado pela presença da Corrente Circumpolar Antártica, sendo de especial importância por ser a zona de formação das águas intermediárias encontradas no Atlântico, sujeitas a uma intensa captura de CO_2 (Tanhua et al., 2017; Figura 2b).

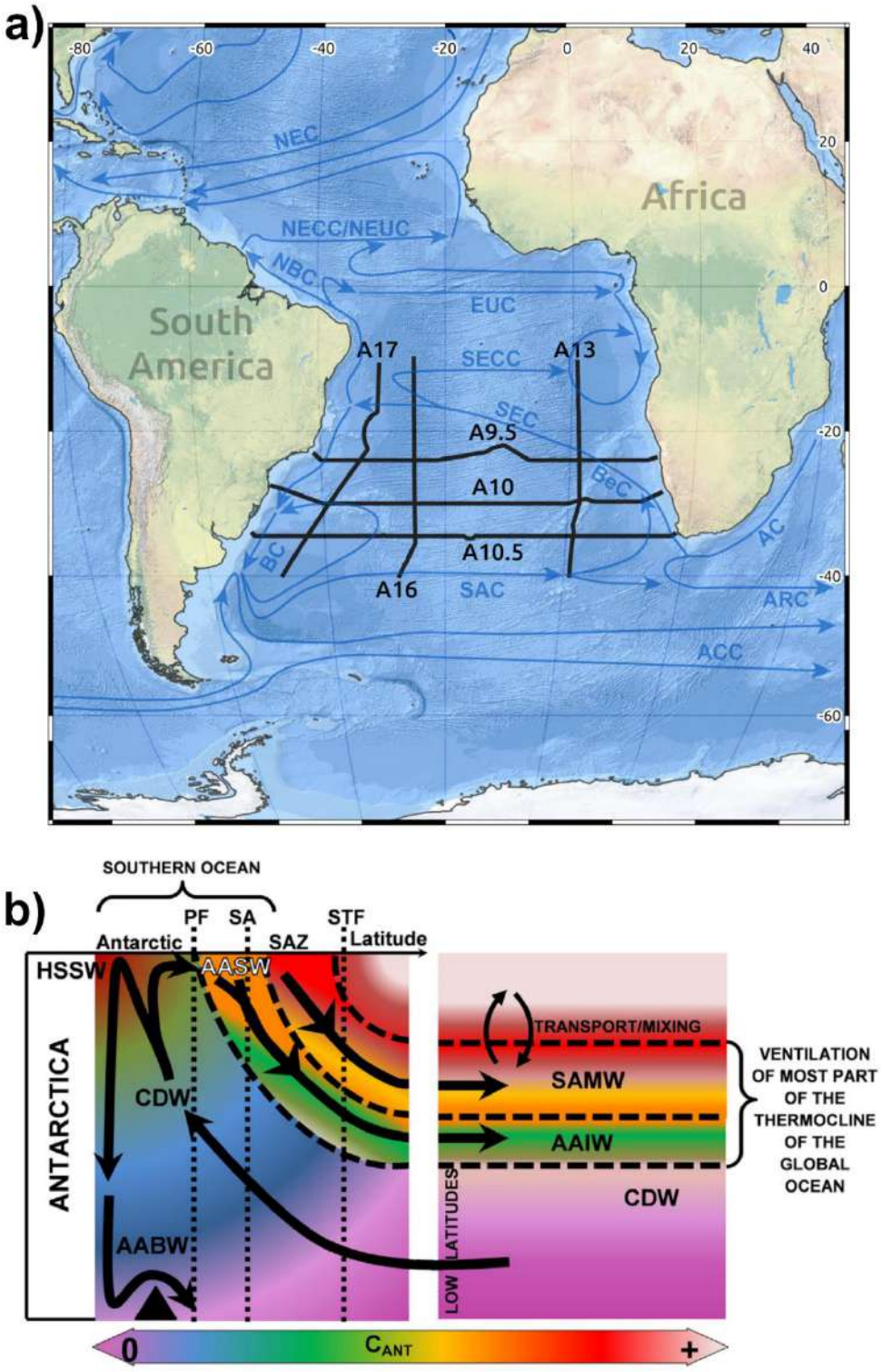

Figura 2. (a) Principais correntes oceânicas superficiais no Atlântico Sul (modificado de Koszalka & Stramma, 2019). As correntes indicadas são: Corrente das Agulhas (AC), Corrente de Retorno das Agulhas (ARC), Corrente Circumpolar Antártica (ACC), Corrente de Benguela (BeC), Corrente do Brasil (BC), Subcorrente Equatorial (EUC), Corrente das Malvinas (MC), Corrente Norte do Brasil (NBC), Corrente Norte Equatorial (NEC), Contracorrente Norte Equatorial (NECC), Subcorrente Norte Equatorial (NEUC), Corrente do Atlântico Sul (SAC), Corrente Sul Equatorial (SEC) e Contracorrente Sul Equatorial (SECC). As líneas pretas indicam a posição das seções hidrográficas utilizadas neste estudo. **(b)** Padrões de circulação e transporte das massas de água em uma seção meridional do oceano Austral (tomado de Pardo et al., 2014). O conteúdo de C_{ant} é indicado pelas cores. A Água Intermediaria Antártica (AAIW) é a Água Modal Subantártica (SAMW) são responsáveis pela ventilação e o transporte de C_{ant} para a termoclina.

A captura do C_{ant} ocasiona a alteração das condições físico-químicas dos oceanos, sendo especialmente afetado o sistema carbonato. Este sistema é responsável pelo controle do pH nos oceanos e por desempenhar um papel importante na concentração de CO_2 na atmosfera em escalas inferiores a 100.000 anos (Ridgwell & Zeebe, 2005). O sistema carbonato consiste num conjunto de reações químicas reversíveis envolvendo: (i) o equilíbrio entre o CO_2 atmosférico e a formação de ácido carbônico, (ii) a dissociação deste ácido em espécies de bicarbonato (HCO_3^-) e carbonato (CO_3^{-2}), com a consequente liberação de íons hidrogênios (H^+), e (iii) a precipitação deste último ânion como carbonato de cálcio ($CaCO_3$) (Millero, 2007). Devido ao aumento da pressão parcial de CO_2 na interface ar-água, o equilíbrio natural é alterado, favorecendo a formação de bicarbonato, com a consequente liberação de prótons e o consumo de carbonato, num fenômeno conhecido como acidificação dos oceanos (Doney, Balch, et al., 2009; Orr et al., 2005).

A acidificação dos oceanos, também conhecido como o “outro” grande problema relacionado às emissões de CO_2 além do aumento da temperatura da superfície terrestre (Doney, Fabry, et al., 2009), é um fenômeno observado em escala global em múltiplas medições (Feely et al., 2009; Lauvset et al., 2020; Orr et al., 2005; Takahashi et al., 2014). Estas alterações químicas da água do mar tem o potencial de afetar negativamente os ecossistemas marinhos, principalmente a os organismos calcificadores, tais como ostracodes, cocolitoforídeos e recifes de coral. Isto ocorre devido à diminuição da saturação de calcita e aragonita (Ω_{Ca} e Ω_{Ar}, respetivamente) na coluna de água (Feely et al., 2009; Hoegh-Guldberg et al., 2007; Millero, 2007). Evidências do registro geológico mostram que múltiplos eventos de acidificação oceânica ocorreram nos últimos 300 milhões de anos e que, na maioria dos casos, estão associados com perdas significativas de biodiversidade e extinções em massa (Honisch et al., 2012).

Embora a captura de C_{ant} e a acidificação dos oceanos sejam fenômenos globais, estes não são espacialmente homogêneos, existindo regiões onde as mudanças são mais acentuadas (Figura 3). Por exemplo, as baixas temperaturas encontradas nas regiões polares originam uma diminuição da pressão parcial de CO_2 nas águas, favorecendo uma maior absorção de C_{ant} em comparação com as regiões tropicais (Figura 3a). Além disso, a temperatura tem um importante

efeito nas propriedades termodinâmicas do sistema carbonato, encontrando-se menores capacidades tampão e maiores mudanças do pH com o descenso da temperatura (Fassbender et al., 2017; Figura 3b). Além da absorção de C_{ant}, outros processos como a remineralização da matéria orgânica e a dissolução de carbonato de cálcio podem alterar a capacidade tampão das águas (Lauvset et al., 2020) e isso tem sido observado, por exemplo, nas águas intermediárias na bacia da Argentina, onde maiores taxas de acidificação foram associadas com uma elevada remineralização de matéria orgânica (Fontela et al., 2021; Ríos et al., 2015).

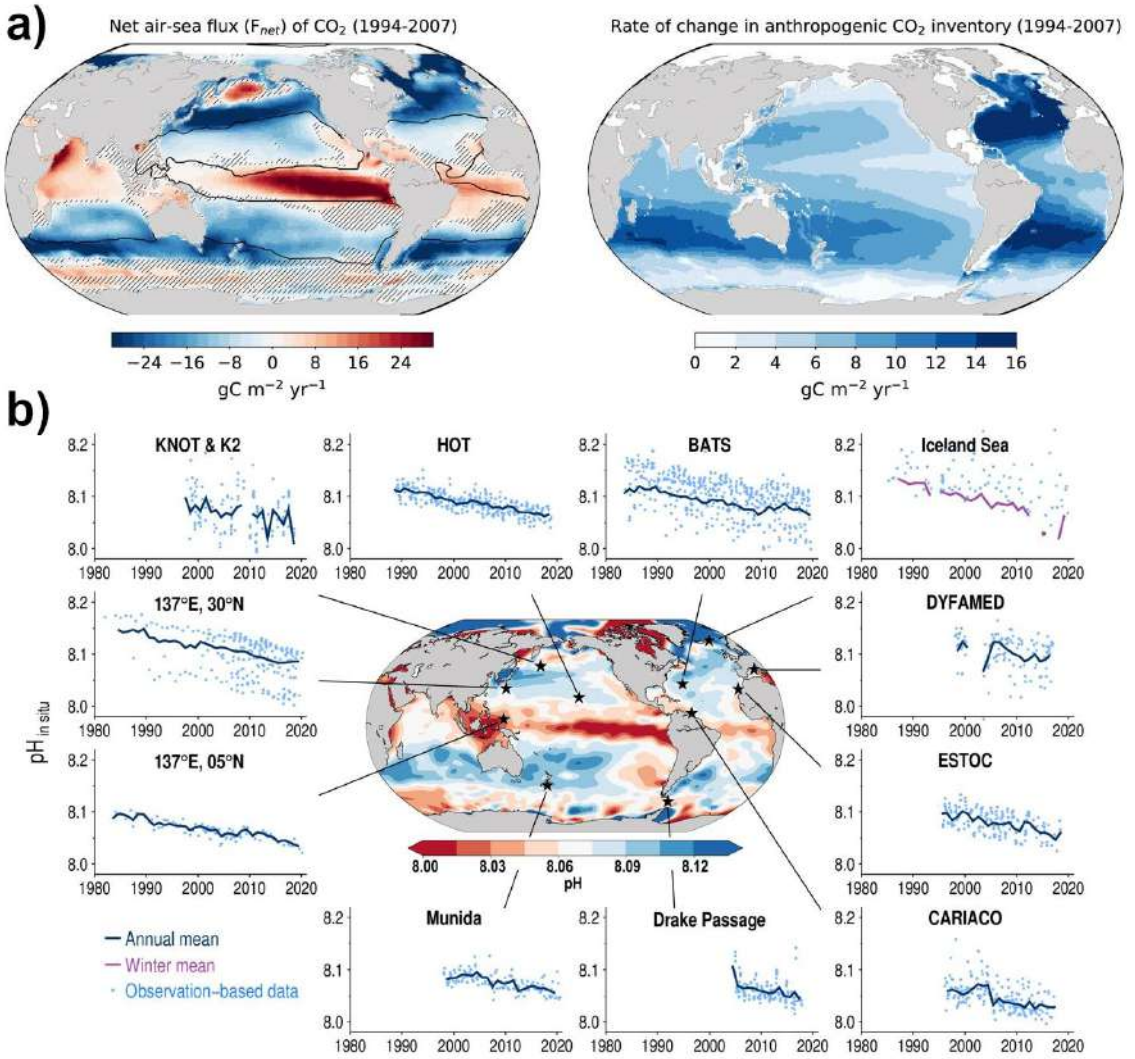

Figura 3. (a) Fluxos de CO_2 na superfície oceânica e mudanças no inventario de C_{ant} no interior do oceano entre 1994 e 2017. Os fluxos de CO_2 são influenciados fortemente pela temperatura, observando-se que a região tropical, mas quente, atua preferencialmente como uma fonte de CO_2 para a atmosfera, enquanto a região subtropical do Atlântico Sul atua como um sumidouro. Os maiores inventários de C_{ant} são encontrados no oceano Atlântico, associados com a formação da Água Profunda do Atlântico Norte (NADW) no Hemisfério Norte e com as águas modais e subtropicais no Hemisfério Sul. **(b)** Mudanças de pH ao longo de distintas regiões oceânicas. Em geral, as mudanças de pH são mais marcadas nas regiões polares, devido a que a capacidade tampão das águas é mais baixa. Figuras extraídas de Canadell et al. (2021).

O C_{ant} não pode ser medido diretamente, tornando a quantificação uma tarefa difícil para comunidade científica que investiga a influência antrópica no ciclo do carbono oceânico desde o fim da década de 1970 (e.g., Brewer, 1978; Chen & Millero, 1979). Uma das abordagens adotadas para superar esse desafio é o estudo das mudanças do carbono inorgânico dissolvido total (DIC) no interior dos oceanos. Variações no DIC por processos naturais estão fortemente associadas às mudanças em outras variáveis biogeoquímicas e físicas, enquanto a absorção do C_{ant} afeta apenas o conteúdo de DIC (Zeebe & Wolf-Gladrow, 2001). Assim, vários métodos que usam esse princípio foram desenvolvidos, como aqueles que dependem de traçadores quase conservativos (e.g., Gruber et al., 1996; Touratier & Goyet, 2004) ou regressões lineares múltiplas (e.g., Friis et al., 2005; Wallace, 1995). O método de regressão linear múltipla estendida (eMLR) desenvolvido por Friis et al. (2005) tornou-se o método mais popular para estimar a captação de C_{ant} a partir de dados de seções hidrográficas repetidas (e.g., Carter et al., 2017; Salt et al., 2015; Tanhua et al., 2017; Wanninkhof et al., 2010; Waters et al., 2011; Woosley et al., 2016).

As primeiras estimativas do conteúdo de C_{ant} no oceano Atlântico Sul datam da década de 1980 (e.g., Chen, 1982). Desde então, o C_{ant} e as taxas de acidificação nas águas centrais (−0,0020 pH ano^{-1}) e intermediárias (−0,0010 pH ano^{-1}) foram estudadas em múltiplas ocasiões (e.g., Carvalho-Borges et al., 2018; Kitidis et al., 2017; Orselli et al., 2018; Ríos et al., 2015; Salt et al., 2015; Woosley et al., 2016). No entanto, a maioria desses estudos tem se concentrado em sub-bacias, pois a distribuição dos dados oceanográficos para toda a região é desigual, principalmente ao longo do tempo. Por exemplo, Fontela et al. (2021) forneceram uma avaliação detalhada da variabilidade do sistema carbonato no oeste do oceano Atlântico Sul nas últimas cinco décadas, encontrando uma concentração decrescente de carbonato como consequência da absorção de C_{ant}, sendo afetada também pela remineralização de matéria orgânica na camada intermediária. No entanto, nenhum estudo existe para a margem oriental do Atlântico Sul. Com a conclusão de novos cruzeiros hidrográficos nos últimos anos (A9.5 24°S, A10.5 34,5°S) no âmbito do *Global Ocean Ship-based Hydrographic Investigations Program* (GO-SHIP), agora é possível avaliar as mudanças nas propriedades do sistema carbonato em toda a bacia.

Nesse contexto, este estudo avaliou a variabilidade espacial do C_{ant} e seu efeito nas taxas de acidificação e outras propriedades do sistema carbonato para o Atlântico Sul nos últimos 30 anos (1989 a 2019). Embora toda a coluna de água abaixo da camada de mistura tenha sido estudada, nosso foco principal foram as camadas de água central e intermediária que ocupam os primeiros 2.000 m da coluna de água. Para isso, uma versão modificada das abordagens mais recentes (Carter et al., 2017, 2019; Gruber, Clement, et al., 2019) desenvolvidas para o cálculo do C_{ant} foi usada.

Capítulo II: Objetivos

A fim de compreender melhor a distribuição do carbono de origem antrópico no oceano Atlântico Sul e sua influência nos parâmetros do sistema carbonato, os seguintes objetivos foram levantados neste estudo.

Objetivo geral

Avaliar a variabilidade espaço-temporal do C_{ant} e os parâmetros do sistema carbonato, assim como sua relação com os processos oceanográficos responsáveis pelas alterações destes no oceano Atlântico Sul.

Objetivos específicos

- Quantificar o C_{ant} nas massas de água do giro subtropical no oceano Atlântico Sul.
- Avaliar o estado de acidificação e as condições do sistema carbonato nas massas de água do Atlântico Sul, a partir de dados novos e pretéritos.
- Identificar os efeitos antropogênicos e naturais nas mudanças do pH e outros parâmetros do sistema carbonato no Atlântico Sul.

Capítulo III: Dados e Métodos

Para atingir os objetivos propostos, uma metodologia composta por três etapas foi utilizada neste estudo. A primeira etapa consistiu na coleta e pré-processamento dos dados oceanográficos disponíveis. Na segunda etapa, o C_{ant} foi quantificado mediante o método de regressões lineares múltiplas estendidas (eMLR). Finalmente, as mudanças de pH e outros parâmetros do sistema carbonato foram estimadas. Uma descrição detalhada de cada etapa pode ser encontrada a seguir.

Seleção é pré-processamento dos dados

Neste estudo, os dados de temperatura, salinidade, oxigênio dissolvido, nutrientes, alcalinidade total e carbono inorgânico dissolvido total de seis seções hidrográficas com duas ou mais ocupações no oceano Atlântico Sul entre 10°S e 40°S (denominadas como A9.5, A10, A10.5 A13, A16 e A17; Figure 1), foram extraídos do *Global Ocean Data Analysis Project versão 2* (GLODAPv2.2020; Olsen et al., 2019, 2020). Além disso, foram usados os dados do cruzeiro *Trans-Atlantic II* (TAII) que ocorreu em 2011 ao longo de 35°S como parte do projeto brasileiro: "*Measurements and modeling of CO2 fluxes in the South Atlantic and Southern Oceans*". No total, dados de 16 cruzeiros, entre 1989 e 2019, foram usados para avaliar as mudanças nas propriedades do sistema carbonato ao

longo do oceano Atlântico Sul. Todos os cruzeiros selecionados seguiram protocolos padrão de amostragem e análise, e uma descrição detalhada pode ser encontrada para cada cruzeiro nos relatórios disponíveis em http://cchdo.ucsd.edu. Informação sobre o cruzeiro TAII pode ser encontrada em Lencina-Avila et al. (2016) e Orselli, Goyet, et al., (2019). Excluindo as seções A13 e A10.5, todas as seções são consistentes espacialmente, com menos de 100 milhas náuticas de distância entre as repetições.

Ao extrair os dados do GLODAPv2.2020, ao invés de usar os dados originais dos cruzeiros, nos beneficiamos do ajuste aplicado nas propriedades que torna todos os dados internamente consistentes (Olsen et al., 2019). Para o cruzeiro TAII que não está no GLODAP, uma análise foi aplicada para avaliar a precisão das medições e avaliar possíveis erros usando a mesma metodologia do GLODAP. Em resumo, uma comparação das propriedades na parte profunda da coluna de água (> 1500 m) entre as estações do cruzeiro TAII e outras estações de cruzeiros na mesma área foi feita mediante o código em MATLAB fornecido por Lauvset e Tanhua (2015) (disponível em https://github.com/sivlauvset/2nd_QC_tool), usando dados do GLODAPv2.2020 como os dados de referência. As medições de salinidade e oxigênio mostraram desvios em comparação com os dados de referência (−0,007 e 0,955, respetivamente) que foram corrigidos seguindo os mesmos princípios usados no conjunto de dados GLODAP (Olsen et al., 2019, 2020).

Como a metodologia utilizada na determinação de C_{ant} e pH depende da existência de dados de alcalinidade total (Alk) e carbono inorgânico dissolvido total (DIC), uma última etapa foi necessária para o cruzeiro TAII, no qual apenas dados de salinidade, temperatura, e oxigênio estavam disponíveis. Então Alk e DIC foram estimados a partir dos parâmetros disponíveis usando o método CANYON-B (Bittig et al., 2018). Outros dados auxiliares como a utilização aparente de oxigênio (AOU), densidade neutra ou temperatura potencial foram calculados mediante o programa Ocean Data View (Schlitzer, R. 2021).

Cálculo do carbono antropogênico

O C_{ant} capturado entre repetições foi estimado para todos os dados abaixo da camada de mistura (para evitar erros associados à atividade biológica e

variabilidade sazonal) usando o método eMLR desenvolvido por Friis et al. (2005), com alguns modificações. O método eMLR clássico faz duas suposições: (1) as regressões lineares múltiplas podem descrever a distribuição natural do DIC, ou seja, as variáveis físicas e biogeoquímicas têm uma relação linear com a variabilidade natural no DIC, e (2) o oceano está em um estado estacionário, o que significa que a correlação entre o DIC e as variáveis independentes não muda com o tempo. Assim, o DIC é ajustado individualmente em ambas ocupações seguindo as Eqs. 1 e 2:

$$DIC_{t1} = a_1 + b_1V1_{t1} + c_1V2_{t1} + \ldots + n_1Vn_{t1} \text{ , (Eq. 1)}$$
$$DIC_{t2} = a_2 + b_2V1_{t2} + c_2V2_{t2} + \ldots + n_2Vn_{t2} \text{ , (Eq. 2)}$$

onde o subscrito t1 e t2 indicam a primeira e a última ocupação, a1 até n1 e a2 até n2 representam os coeficientes da primeira e da segunda regressão respetivamente, e V1 até Vn representam os parâmetros físicos e biogeoquímicos utilizados para descrever a distribuição do DIC. A absorção do C_{ant} entre os dois cruzeiros (ΔC_{ant}) é então calculada subtraindo os coeficientes das Eqs. 1 e 2, e usando os valores dos parâmetros em t2, conforme é mostrado na Eq. 3:

$$\Delta C_{ant} = (a_2 - a_1) + (b_2 - b_1)V1_{t2} + \ldots + (n_2 - n_1)Vn_{t2} \text{ , (Eq. 3)}$$

onde o t1 e os demais termos são equivalentes a descrição das Eqs. 1 e 2.

Embora o método eMLR tenha se mostrado poderoso na identificação de mudanças no conteúdo de C_{ant} em múltiplas pesquisas (e.g., Ríos et al., 2015; Salt et al., 2015; Williams et al., 2015; Woosley et al., 2016), várias modificações foram feitas recentemente, permitindo uma determinação mais precisa do ΔC_{ant} (Carter et al., 2019; Clement & Gruber, 2018). Neste estudo, as seguintes modificações foram utilizadas:

- A coluna de água foi dividida em 13 camadas usando as superfícies isopicnais definidas por Clement e Gruber (2018) para o oceano Atlântico até 28,15 kg m^{-3} (Tabela 1).

Tabela 1. Número de amostras presentes nas 13 camadas isopicnais para cada cruzeiro avaliado neste estudo. As amostras acima de 150 m de profundidade foram excluídas.

Seções	**Camadas isopicnais (kg m^{-3})**												
	< 26.00	**26.00 - 26.50**	**26.50 - 26.75**	**26.75 - 27.00**	**27.00 - 27.25**	**27.25 - 27.50**	**27.50 - 27.75**	**27.75 - 27.85**	**27.85 - 27.95**	**27.95 - 28.05**	**28.05 - 28.10**	**28.10 - 28.15**	**> 28.15**
A9.5-2009	14	31	37	41	52	99	71	20	67	121	114	108	139
A9.5-2018	47	107	78	96	119	182	152	58	133	258	158	151	104
A10-1992	NA	76	65	73	76	96	79	50	76	138	109	60	61
A10-2003	NA	95	89	83	107	147	82	62	79	179	134	74	75
A10-2011	NA	111	121	109	106	145	162	72	107	167	130	59	75
A10.5-2011	NA	32	279	126	142	218	219	75	73	68	NA	NA	NA
A10.5-2017	NA	26	110	99	101	172	136	73	86	134	109	82	159
A17-1994	13	85	70	57	77	146	100	54	97	175	102	81	206
A17-2013	NA	43	50	42	65	75	78	46	70	132	52	28	105
A17-2019	NA	21	23	20	38	53	45	23	33	50	25	16	46
A16-1989	NA	19	30	36	33	64	53	22	27	64	50	27	88
A16-2005	9	63	68	49	49	99	99	33	50	137	75	42	161
A16-2013	12	52	66	69	73	96	116	49	53	114	81	47	171
A13-1995	NA	NA	NA	11	17	23	30	21	37	76	84	104	57
A13-2010	NA	25	48	84	96	112	114	59	86	157	133	202	57

- Conforme sugerido por Clement e Gruber (2018) e Carter et al. (2019), as regressões lineares múltiplas foram ajustadas usando o DIC corrigido pela remineralização da matéria orgânica (DIC_{abio}) ao invés do DIC. O parâmetro DIC_{abio} foi definido conforme mostrado pela Eq. 4:

$$DIC_{abio} = DIC - r_{c:o} \times AOU \text{ , (Eq. 4)}$$

  onde o termo $r_{c:o}$ é a razão de remineralização carbono:oxigênio (117/170) de Anderson e Sarmiento (1994), que explica as mudanças no DIC pela oxidação da matéria orgânica e AOU representa a utilização aparente de oxigênio.

- Temperatura potencial (θ), S, AOU, Alk, Si e NO_3^- foram os parâmetros selecionados para as regressões. θ foi usado ao invés da temperatura para ser consistente com trabalhos anteriores na área (e.g., Salt et al., 2015) e NO_3^- em substituição ao PO_4^{3-} devido a uma maior disponibilidade de dados. Como os dados de nutrientes não estavam disponíveis para a seção A10.5, apenas T, S e AOU foram usados para as regressões lineares múltiplas nesta seção.

- Em vez de uma única regressão linear múltipla, foi feita uma regressão para cada possível combinação dos parâmetros escolhidos, sob a restrição de que pelo menos três variáveis fossem selecionadas, resultando em um total de 42 regressões por camada isopicnal. Isso foi feito para todas as seções, exceto A10.5, onde apenas uma regressão foi utilizada.

- Conforme feito por Carter et al. (2017) foram utilizadas regressões lineares múltiplas robustas, reduzindo a influência de valores anômalos na estimação dos coeficientes.

- Para cada camada isopicnal, foram escolhidas as 10 melhores regressões (aquelas com o menor erro quadrático médio - RMSE total), e o ΔC_{ant} foi

calculado usando a Eq. 3. Finalmente, a média dessas 10 estimativas de ΔC_{ant} foi calculada, sendo esse valor o resultado final utilizado no estudo.

Considerando essas modificações, uma estimativa robusta do C_{ant} no oceano Atlântico Sul foi obtida, com incertezas de ± 3 µmol kg^{-1} (Anexo 1).

Variações naturais do DIC e mudanças do sistema carbonato

As mudanças no pH e outros parâmetros do sistema carbonato devido à remineralização da matéria orgânica e absorção de C_{ant} foram estimadas. A remineralização da matéria orgânica foi o único processo natural levado em consideração por ser o componente natural mais importante que explica os gradientes de pH dentro dos oceanos, e porque a dissolução do carbonato de cálcio só tem influência significativa abaixo das águas intermediárias (Lauvset et al., 2020). A remineralização foi avaliada usando o mesmo princípio do método eMLR, entretanto utilizando-se AOU como o parâmetro dependente nas Eqs. 1 e 2, e com θ e S como variáveis, seguindo as observações de estudos anteriores (e.g., Carter et al., 2017; Sabine et al., 2008). Assim, a mudança na AOU (ΔAOU) entre duas campanhas de amostragem foi calculada aplicando a Eq. 5:

$$\Delta AOU = (a_2 - a_1) + (b_2 - b_1)\theta_{t2} + (c_2 - c_1)S_{t2} \text{ , (Eq. 5)}$$

onde o subscrito t2 indica dados da última ocupação, a1 até c1 e a2 até c2 representam os coeficientes da primeira e da segunda regressão, respetivamente, enquanto θ e S representam a temperatura potencial e a salinidade. O efeito da mudança de AOU no DIC (ΔC_{org}) foi obtido por meio da razão de remineralização ($r_{c:o}$ = 117/170) de Anderson e Sarmiento (1994) seguindo a Eq. 6:

$$\Delta C_{org} = r_{c:o} \times \Delta AOU \text{ , (Eq. 6)}$$

Para cada período analisado, ΔC_{ant} e ΔC_{org} foram subtraídos independentemente dos valores DIC da ocupação mais recente para obter os valores DIC sem a influência desses processos (ou seja, mudança antropogênica: DIC – ΔC_{ant}; mudanças naturais: DIC – ΔC_{org}). Com estes e os valores originais de DIC, o pH

e outros parâmetros do sistema carbonato foram calculados assumindo que a Alk não mudou com o tempo e a diferença entre esses resultados corresponde às mudanças decorrentes de cada processo. Os cálculos do sistema carbonato foram realizados usando a função *carb* do pacote seacarb para R (Gattuso et al., 2020), com as constantes K1 e K2 de Millero et al. (2006), a constante Kf de Perez & Fraga (1987), e as constantes sulfato e borato de Dickson (1990) e Uppström (1974), respetivamente. A constante de Millero et al. (2006) foi usada no lugar da constante de Lueker et al. (2000) para ser consistente com trabalhos anteriores na área (e.g., Carvalho-Borges et al., 2018; Orselli et al., 2018; Woosley et al., 2016). No entanto, não foram encontradas diferenças significativas entre os cálculos feitos com as constantes de Millero et al. (2006) e Lueker et al. (2000).

Capítulo IV: Resultados e Discussão

Para a obtenção do título de Mestre pelo Programa de Pós-Graduação em Oceanologia, é requerido que o discente realize a submissão de pelo menos um artigo científico como primeiro autor em um periódico com corpo indexado. Desse modo, os resultados da pesquisa desenvolvida durante o período de mestrado e a discussão dos resultados serão apresentados em forma de artigo neste capítulo. O manuscrito, de autoria de Andrés Piñango, Rodrigo Kerr, Iole Beatriz Marques Orselli, Andréa da Consolação Oliveira Carvalho, Elias Azar, Johannes Karstensen e Carlos Alberto Eiras Garcia, é intitulado "*Ocean acidification and long-term changes in the carbonate system properties of the South Atlantic Ocean*" e encontra-se em processo de revisão pelos pares para sua posterior publicação no periódico "*Global Biogeochemical Cycles".*

1. Introduction

Multiple human activities, such as the burning of fossil fuels and changes in the use of soils (e.g., deforestation), were responsible for the release of 700 ± 75 Pg C to the atmosphere from the Industrial Era (~1750) until the year 2019 (Friedlingstein et al., 2020). Approximately 41% of this anthropogenic carbon (C_{ant}) has remained in the atmosphere, increasing the concentration of carbon dioxide (CO_2) from 277 parts per million (ppm) in 1750 to 409.85 ± 0.10 ppm in 2019 (Dlugokencky & Tans, 2020). This excess of CO_2 has been causing changes in the radiative balance of the Earth and consequently in the climatic system (Cubasch et al., 2013). The rest of the C_{ant} (57%) has been captured by the terrestrial biosphere and the oceans (Friedlingstein et al., 2020), mitigating part of the changes in the Earth's climate.

In the ocean, the uptake of C_{ant} occurs at the surface by air-sea gas exchange, primarily driven by the solubility pump (Broecker, 1991; Sarmiento & Gruber, 2006). Thus, the C_{ant} uptake and storage are closely related to water mass formation. Indeed a clear linkage has been identified between central, intermediate, and deep water masses transport and storage of C_{ant} in the interior of the ocean (Gruber, Clement, et al., 2019; Sabine et al., 2004). The uptake, export, and storage of C_{ant} depend on ocean ventilation, ocean circulation, water mass properties, ocean-atmosphere interactions, mesoscale dynamics, and biogeochemical processes, resulting in a non-uniform C_{ant} distribution throughout the ocean basins (Gruber, Clement, et al., 2019; Lee et al., 2003; Sabine et al., 2004).

The South Atlantic Ocean is characterized by intense formation of mode and intermediate waters (the former contributing to the central waters). These water masses are advected northward with the wind driven subtropical gyre in what is termed the central and intermediate layers of the South Atlantic Ocean, and they provide the main pathway between the ocean surface and interior (Azar et al., 2020; de Souza et al., 2018; Stramma & England, 1999; Tanhua et al., 2017). In this region, recent estimates have found an increase in the C_{ant} inventory of 5.3 ± 1.2 Pg C up to 3000 m between 1994 and 2007 (Gruber, Clement, et al., 2019)

and a more stable C_{ant} decadal increase has been observed in comparison with the North Atlantic Ocean (Wanninkhof et al., 2010; Woosley et al., 2016).
The uptake of C_{ant} alters the equilibrium of the ocean's carbonate system, reducing the carbonate concentration (and the OH^-) and increasing the concentration of H^+ ions, in a process known as ocean acidification (Doney, Balch, et al., 2009). Ocean acidification, also known as the "other" major problem related to anthropogenic CO_2 emissions (Doney, Fabry, et al., 2009), is a phenomenon observed on a global scale in multiple measurements (e.g., Feely et al., 2009; Lauvset et al., 2020; Orr et al., 2005; Takahashi et al., 2014). The alterations in the marine carbonate chemistry have the potential to disrupt entire ecosystems because calcifying organisms, such as pteropods, coccolithophorids, and coral reefs are especially susceptible to decreased calcite and aragonite saturation states (Ω_{Ca} and Ω_{Ar}, respectively) (Doney et al., 2020; Feely et al., 2009; Millero, 2007; Orr et al., 2005). Evidence from the geological record shows that multiple ocean acidification events have occurred in the past 300 million years, associated with significant losses of biodiversity and mass extinctions (Honisch et al., 2012).

Estimates of the C_{ant} content in the South Atlantic Ocean dates back to the 1980s (e.g., Chen, 1982). Based on repeat section analysis, open ocean acidification rates in central (-0.0020 pH units yr^{-1}) and intermediate (-0.0010 pH units yr^{-1}) water masses have been reported (e.g., Carvalho-Borges et al., 2018; Kitidis et al., 2017; Orselli et al., 2018; Ríos et al., 2015; Salt et al., 2015; Woosley et al., 2016). However, most of these studies have focused on specific sub-basins, as the distribution of oceanographic data for the entire region is uneven, especially over time. For example, Fontela et al. (2021) provided a detailed evaluation of the carbonate system variability in the Argentine Basin (western South Atlantic Ocean) over the last five decades, finding a decreasing carbonate concentration as consequence of C_{ant} uptake enhanced by the remineralization of organic matter in the intermediate layer. However, no such study exists for the eastern South Atlantic margin. With the completion of new hydrographic surveys in recent years (A9.5 24°S, A10.5 34.5°S) and considering also repeat sections in the framework of the Global Ocean Ship-based Hydrographic Investigations Program

(GO-SHIP), it is now possible to assess changes in the carbonate system properties for the entire basin.

Here, we evaluated the spatial variability of the C_{ant} and its effect on the acidification rates and other carbonate system properties for the South Atlantic Ocean over the last 30 years (1989 to 2019). Although the entire water column below the mixed layer was studied, our focus was the central and intermediate water layers that occupy the upper 2000 m and we used a slightly modified version of the latest approaches developed for the calculation of C_{ant} (Carter et al., 2017; Clement & Gruber, 2018).

2. Data and Methods

2.1. Data selection and quality-control processing

The data from six hydrographic repeat sections, with two or more occupations, were extracted from the Global Ocean Data Analysis Project version 2 (GLODAPv2.2020; Olsen et al., 2019, 2020). Additionally, we used the Trans-Atlantic II (TAII) cruise that occurred in 2011 as part of the Brazilian project: "Measurements and modeling of CO_2 fluxes in the South Atlantic and Southern Oceans" (Orselli, Goyet, et al., 2019). In total data from 16 cruises, spanning from 1989 to 2019 were used to evaluate the changes in the carbonate system properties along the South Atlantic Ocean (Figure 1; Table 1). Except for the A13 and A10.5 transects, the sections are spatially consistent, with less than 100 nautical miles of variation between repetitions.

By extracting the data from the GLODAPv2.2020 rather than making use of the original cruise data we benefit from the applied adjustment of the properties that makes all data internally consistent (Olsen et al., 2020). For the TAII cruise (hereafter A10.5-2011) which is not in GLODAP, a crossover analysis was applied to evaluate the accuracy of the measurements and detect possible offsets using the GLODAP methodology (Lauvset & Tanhua, 2015; Olsen et al., 2020). In brief, a comparison of the properties in the deep part of the water column (> 1500 m) between the A10.5-2011 cruise stations and other cruises stations in the same area was done using the MATLAB toolbox provided by Lauvset and Tanhua (2015) (available at https://github.com/sivlauvset/2nd_QC_tool), using data from the GLODAPv2.2020 as the reference data. Salinity and oxygen measurements showed offsets in comparison with the reference data (−0.007

and 0.955 respectively, see Figure S1) which were corrected following the same principles used in the GLODAP dataset (Olsen et al., 2020).

Because the methodology used for the C_{ant} and pH determination depends on the existence of total alkalinity (Alk) and total dissolved inorganic carbon (DIC) data, a last step was necessary for the A10.5-2011 cruise, in which only salinity, temperature, and oxygen data were available. Similar to Orselli, Goyet, et al. (2019), the Alk and DIC were estimated from the available parameters. Here, these estimates were calculated using the LIARv2 (Carter et al., 2018) and the CANYON-B (Bittig et al., 2018) methods. For Alk, better estimates were found using CANYON-B (Figure S2), which were used in the subsequent calculations.

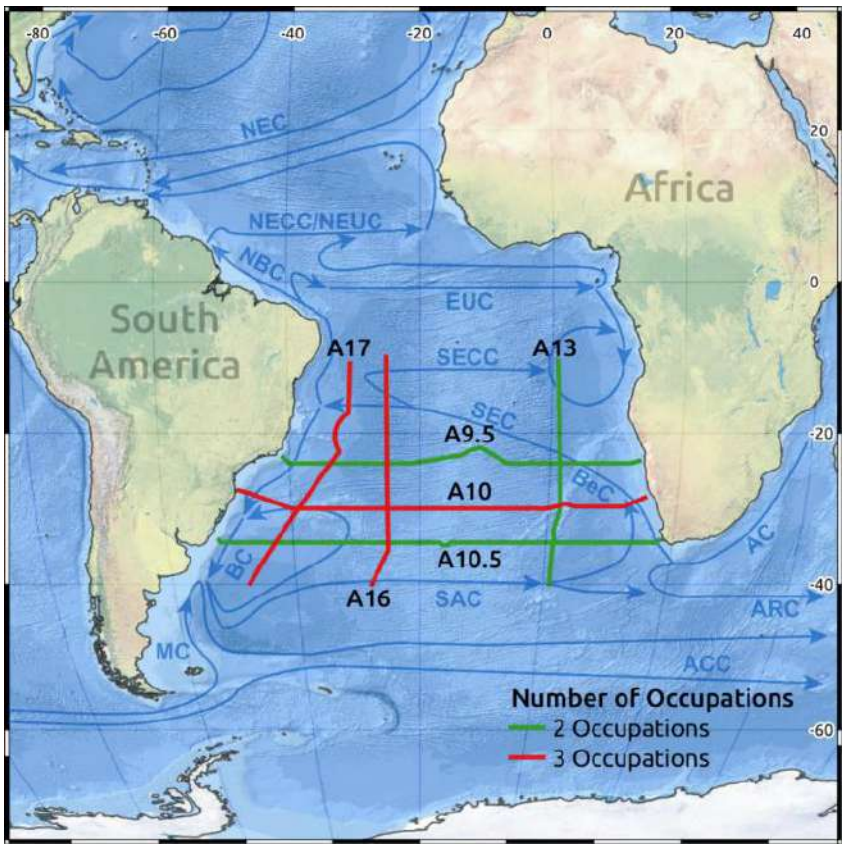

Figure 1. Map of the study region in the South Atlantic Ocean. The colored lines depict the position of the six Global Ocean Ship-based Hydrographic Investigations Program (GO-SHIP) hydrographic sections used in this work, and their color represents the number of occupations: green for two occupations (A9.5, A10.5, and A13 sections) and red for three or more occupations (A10, A16, and A17 sections). Note that the A13 section shows the 33RO20100308 cruise, which corresponds to the GO-SHIP A13.5 section. The blue arrows represent the main upper-ocean currents in the South and Tropical Atlantic (Koszalka & Stramma, 2019). The ocean currents described are: Agulhas Current (AC), Agulhas Return Current (ARC), Antarctic Circumpolar Current (ACC), Benguela Current (BeC), Brazil Current (BC), Equatorial Undercurrent (EUC), Malvinas Current (MC), North Brazil Current (NBC), North Equatorial Current (NEC), North Equatorial Countercurrent (NECC), North Equatorial Undercurrent (NEUC), South Atlantic Current (SAC), South Equatorial Current (SEC) and South Equatorial Countercurrent (SECC).

Table 1. Cruises, nomenclature, and properties used in this work. The acronyms are temperature (T), salinity (S), oxygen (O_2), phosphate (PO_4^{3-}), nitrate (NO_3^-), silicate (Si), total alkalinity (Alk), and total dissolved inorganic carbon (DIC).

Name	Expocode	Date cruise (From/To)	Parameters Available
A9.5 Section – zonal section along 24.5°S			
A9.5-2009	740H20090307	2009-03-07 2009-04-21	T, S, O_2, PO_4^{3-}, NO_3^-, Si, Alk, DIC
A9.5-2018	740H20180228	2018-02-28 2018-04-10	T, S, O2, PO_4^{3-}, NO_3^-, Si, Alk, DIC
A10 Section – zonal section along 30°S			
A10-1992	06MT22_5	1992-12-27 1993-01-31	T, S, O_2, PO_4^{3-}, NO_3^-, Si, Alk, DIC
A10-2003	49NZ20031106	2003-11-06 2003-12-05	T, S, O2, PO_4^{3-}, NO_3^-, Si, Alk, DIC
A10-2011	33RO20110926	2011-09-26 2011-10-31	T, S, O2, PO_4^{3-}, NO_3^-, Si, Alk, DIC
A10.5 Section – zonal section along 34.5°S			
A10.5-2011	TAII Cruise	2011-10-24 2011-11-25	T, S, O_2, Alk[a], DIC[a]
A10.5-2017	06M220170104	2017-01-04 2017-02-01	T, S, O_2, Alk, DIC
A17 Section – longitudinal section along 40°W			
A17-1994	3230CITHER2_1	1994-01-04 1994-03-21	T, S, O_2, PO_4^{3-}, NO_3^-, Si, Alk, DIC
A17-2013	29HE20130320	2013-03-20 2013-05-22	T, S, O_2, PO_4^{3-}, NO_3^-, Si, Alk, pH, DIC
A17-2019	29HE20190406	2019-04-06 2019-05-19	T, S, O2, PO_4^{3-}, NO_3^-, Si, Alk, pH, DIC
A16 Section – longitudinal section along 25°W			
A16-1989	318MSAVE5 318MHYDROS4	1989-01-23 1989-03-08 1989-03-13 1989-04-19	T, S, O_2, PO_4^{3-}, NO_3^-, Si, Alk, DIC
A16-2005	33RO200501	2005-01-11 2005-02-24	T, S, O_2, PO_4^{3-}, NO_3^-, Si, Alk, DIC
A16-2013	33RO20131223	2013-12-23 2014-02-04	T, S, O_2, PO_4^{3-}, NO_3^-, Si, Alk, DIC
A13 Section – longitudinal section along 2°E			
A13-1995	35A3CITHER3_2	1995-02-21 1995-04-02	T, S, O_2, PO_4^{3-}, NO_3^-, Si, Alk, DIC
A13-2010	33RO20100308	2010-03-08 2010-04-18	T, S, O_2, PO_4^{3-}, NO_3^-, Si, Alk, DIC

[a]Estimated from T, S, and O_2 using CANYON-B (Bittig et al., 2018).

2.2. Water masses identification

Our analysis considered the full depth of the water column below the mixed layer. However, we focused on the central and intermediate waters as significant

decadal C_{ant} changes have been observed only in these waters (Wanninkhof et al., 2010; Woosley et al., 2016). Guided by earlier water mass definitions (Hernández-Guerra et al., 2019; Manta et al., 2021; Stramma & England, 1999) we first split the first 1100 m of the water column into two layers (hereafter referred as central and intermediate water layers) and evaluate the changes in the carbonate system properties. The central water layer was defined by neutral density (γ^n) values between 26.2 kg m^{-3} and 27.1 kg m^{-3}, goes from 150 to 750 m and is mainly composed of the South Atlantic Central Water (SACW). The SACW is formed by subduction along the subtropical gyre of the South Atlantic Ocean, north of the subtropical front, being ventilated mainly by three varieties of Subtropical Mode Water (STMW) (Gordon, 1981; Provost et al., 1999; Sato & Polito, 2014). In the western margin, the lower layer of the SACW (γ^n > 27.5 kg m^{-3}) is influenced by the Subantarctic Mode Water (SAMW), formed during the winter by subduction at the north of the Subantarctic Front (Mémery et al., 2000; Tanhua et al., 2017). The intermediate water layer was defined by 27.1 kg m^{-3} < γ^n < 27.65 kg m^{-3}, goes from 750 to 1100 m and is composed of the Antarctic Intermediate Water (AAIW). Both layers are influenced by water masses entering the South Atlantic from the Indian Ocean via the Agulhas Retroflection (Azar et al., 2020; Poole & Tomczak, 1999; de Souza et al., 2018). For a more detailed description of the water masses in the studied region, see Stramma & England (1999) and Hernández-Guerra et al. (2019).

2.3. Anthropogenic carbon calculations

The quantification of the oceanic C_{ant} uptake dates back to the end of the 1970s (e.g., Brewer, 1978; Chen & Millero, 1979; for a historic review see Sabine & Tanhua, 2010). One approach is based on estimating DIC changes comparing repeat hydrographic surveys and decompose these changes into a part that can be associated with natural processes, tightly linked with variations in other biogeochemical and physical variables (Zeebe & Wolf-Gladrow, 2001), and a residue that is interpreted as the C_{ant}. Multiple methods that use this principle have been developed, such as those that depend on quasi-conservative tracers (e.g. Gruber et al., 1996; Touratier & Goyet, 2004) or multiple linear regressions (e.g. Friis et al., 2005; Wallace, 1995). The extended multiple linear regression (eMLR) method developed by Friis et al. (2005) has become one of the most

popular methods to estimate the C_{ant} uptake from repeated hydrographic sections data (e.g., Carter et al., 2017; Salt et al., 2015; Tanhua et al., 2017; Wanninkhof et al., 2010; Waters et al., 2011; Williams et al., 2015; Woosley et al., 2016).

The eMLR method makes two assumptions: (1) the multiple linear regressions can describe the natural distribution of the DIC, i.e., the physical and biogeochemical variables have a linear relationship with the natural variability in DIC, and (2) the ocean is in a steady-state, meaning that the correlation between the DIC and the independent variables do not change with time. Thus, the DIC in both occupations is fitted individually following Eqs. 1 and 2:

$$DIC_{t1} = a_1 + b_1V1_{t1} + c_1V2_{t1} + \ldots + n_1Vn_{t1} \text{ , (Eq. 1)}$$

$$DIC_{t2} = a_2 + b_2V1_{t2} + c_2V2_{t2} + \ldots + n_2Vn_{t2} \text{ , (Eq. 2)}$$

where the subscript *t1* and *t2* indicate the first and the last occupation, a_1 to n_1 and a_2 to n_2 represent the coefficients of the first and the second regression respectively, and *V1* to *Vn* represent the physical and biogeochemical parameters that are used to describe the spatial distribution of the DIC.

The C_{ant} uptake between the two cruises (ΔC_{ant}) is then calculated by subtracting the coefficients from Eq. 1 and Eq. 2 and using the values of the parameters at *t2,* as shown by Eq. 3:

$$\Delta C_{ant} = (a_2 - a_1) + (b_2 - b_1)V1_{t2} + \ldots + (n_2 - n_1)Vn_{t2} \text{ , (Eq. 3)}$$

Although the eMLR method has proven to be powerful identifying the changes in the C_{ant} content in data along repeated surveys (Clement & Gruber, 2018), several considerations have to be taken into account. First, the eMLR assumes that no significant variations in the relationship between the DIC and the independent parameters occur in the time that separates the occupations. Goodkin et al. (2011), based on model data analysis, suggested that under a sampling period of 30 years or more the error in the eMLR method can exceed 20%. Second, the eMLR is very dependent on the parameters chosen for the regression, as shown by Plancherel et al. (2013) and more recently by Woosley et al. (2016), where the utilization of silicate as one of their parameters resulted in a deeper (and not expected) penetration of C_{ant} in the Southern Ocean. Finally,

the eMLR is usually applied along isopycnal surfaces because this is the preferential pathway of water movement and thus penetration of C_{ant} into the ocean (Gruber et al., 1996; Sabine et al., 2004; Wanninkhof et al., 2010) and allowed more robust fits (Clement & Gruber, 2018; Tanhua et al., 2017).

Recently, a few modifications to the eMLR approach have been made, allowing a more precise determination of the ΔC_{ant}. Clement and Gruber (2018) developed a new method capable of estimate the C_{ant} changes for the global ocean through the addition of a probabilistic method for the selection of predictors and the inclusion of C^* (defined as the DIC corrected by the remineralization of organic matter and the calcium carbonate dissolution, see Gruber et al., 1996) rather than DIC in the linear regression. This method was used to quantify the global oceanic sink of C_{ant} over the period from 1994 to 2007. Similarly, modifications proposed by Carter et al. (2017, 2019) allowed further refinement of the C_{ant} accumulation rates in the Pacific Ocean, which showed a lower bias and root mean square error (RMSE) compared to the Friis et al. (2005) method.

Here, we quantified the C_{ant} changes below the surface mixed layer from multiple zonal and meridional hydrographic repeat sections using the eMLR method with some of these modifications, including the utilization of the DIC corrected by the degradation of organic matter (DIC_{abio}) instead of DIC in the multiple linear regressions, and the utilization of the mean C_{ant} value returned by the 10 best regressions (quantified by the lower combined RMSE) as the final estimate (for a full description of the modifications to the approach used here, see Text S1). Considering these modifications, and the fact that the average time between surveys occupations is approximately 10 years, a robust estimation of the C_{ant} in the South Atlantic Ocean was obtained, with uncertainties of ± 3 μmol kg^{-1} (see Text S2 for the uncertainty analysis).

2.4. Changes in the carbonate system properties

Changes in pH and other carbonate system parameters due to organic matter remineralization and C_{ant} uptake were estimated. The organic matter remineralization was the only natural process taken into consideration since it is the most important natural component that explains the gradients of pH inside the oceans, and because the dissolution of calcium carbonate only has a significant influence below the intermediate waters (Lauvset et al., 2020). Remineralization

was evaluated using the same principle of the eMLR method with AOU as the dependent parameter in Eq. 1 and 2 with θ and S as variables, following the observations of previous studies (e.g. Carter et al., 2017; Sabine et al., 2008). Thus, the change in AOU (ΔAOU) between two occupations was calculated by applying Eq. 4:

$$\Delta AOU = (a_2 - a_1) + (b_2 - b_1)\theta_{t2} + (c_2 - c_1)S_{t2} \text{ , (Eq. 4)}$$

where the subscript *t2* indicates data from the last occupation, a_1 to c_1 and a_2 to c_2 represent the coefficients of the first and the second regression respectively, while θ and S represent the potential temperature and salinity. The effect of this AOU change in the DIC (ΔC_{org}) was obtained through the remineralization ratio ($r_{c:o}$ = 117/170) of Anderson and Sarmiento (1994) following Eq. 5:

$$\Delta C_{org} = r_{c:o} \times \Delta AOU \text{ , (Eq. 5)}$$

For each period analyzed, ΔC_{ant} and ΔC_{org} were subtracted independently from the DIC values of the most recent occupation to obtain the DIC values without the influence of these processes (i.e., anthropogenic change: DIC - ΔC_{ant}; natural changes: DIC - ΔC_{org}). With these and the original DIC values, pH and other parameters of the carbonate system were calculated assuming that Alk did not change with time (for an evaluation of the principal changes in the biogeochemical properties see Text S3), and the difference between those results corresponds to changes due to each process. The carbonate system calculations were performed using the *carb* function of the *seacarb* package for R (Gattuso et al., 2020), with the K1 and K2 constant of Millero et al. (2006), the Kf constant of Perez & Fraga (1987), and the sulfate and borate constants of Dickson (1990) and Uppström (1974), respectively. The constant of Millero et al. (2006) was used instead of the constant of Lueker et al. (2000) to be consistent with previous works in the area (e.g., Carvalho-Borges et al., 2018; Orselli et al., 2018; Woosley et al., 2016). However, no significant differences were found between the calculations made using the constants of Millero et al. (2006) and Lueker et al. (2000). All the pH values reported in this work are in the total scale.

3. Results

3.1. Anthropogenic carbon distribution and accumulation rates

A similar vertical distribution of C_{ant} was found in all zonal and meridional sections along the South Atlantic Ocean with more than 6 years between occupations, with statistically significant concentrations of C_{ant} (> 5 µmol kg^{-1} at a confidence of 90%) up to 1000 m, and no significant concentrations in deep and bottom waters (Figure 2, see also Figure S3). In general, higher concentrations of C_{ant} were observed in the sections with the longest time elapsed between occupations (e.g., A17 section from 1994 to 2013), although the accumulation rates showed high spatial variability. The mean C_{ant} accumulation rate was three-fold higher in the central waters than in the intermediate waters, with values of 0.89 ± 0.33 µmol kg^{-1} yr^{-1} and 0.30 ± 0.29 µmol kg^{-1} yr^{-1}, respectively. With exception of the A10.5 section, in which C_{ant} was evenly distributed at a depth of ~1500 m (Figure 2e), all the zonal sections presented a deeper C_{ant} penetration in the western basin than in the eastern basin (Figure 2a-c). Spatial differences were also observed in the meridional sections, with higher C_{ant} concentrations southward. In the A17 section, no C_{ant} was observed below the 27.2 kg m^{-3} isopycnal at the latitude of 12.5°S (Figure 2b), and in the A13 section the depletion of C_{ant} in intermediate waters was located further south, at a latitude of 23°S (Figure 2f).

The C_{ant} spatial variability is more evident in the accumulation rates, especially in central waters, with increasing values southward and westward (Figure 3a-b). The differences in accumulation rates between the south and north (~0.50 µmol kg^{-1} yr^{-1}) were two-fold higher than the east-west differences (~0.25 µmol kg^{-1} yr^{-1}), indicating a higher meridional gradient. In general, for those sections with 3 occupations (A10, A16, and A17), the accumulation rates increased from the 1990s to the 2000s. For example, an increase in the accumulation rates of 0.16 µmol kg^{-1} yr^{-1} was observed between decades in the central waters of the A10 section (Figure 3a), whilst this difference was even higher in the A16 section (Figure 3b), with a value of 0.52 µmol kg^{-1} yr^{-1}. However, this pattern was not present in the intermediate waters of the A10 section, and the central waters of the A17 section, where the accumulation rates of the oldest decade were higher (Figure 3b-c).

In the A10.5 section, the C_{ant} accumulation rates (Figure 3a-c) and column inventories (Figure 3e) showed a different behavior than the rest of the sections and, for this reason, were considered anomalous. The possible origin of this anomaly is discussed in section 4.1. Excluding this section, an average column inventory change of 0.71 ± 0.35 mol C m^{-2} yr^{-1} was found for the South Atlantic Ocean between 1989 and 2019. The column's inventory changes (Figure 3e-f) were consistent with the distribution patterns displayed by the accumulation rates, with higher meridional than zonal variations. The higher accumulation rate observed in the intermediate waters along 30°S (A10 section) between 1992 and 2003 (Figure 3c), particularly at the east of 10°E, was responsible for the higher C_{ant} column inventory obtained in this period, in comparison with the most recent occupation (Figure 3e).

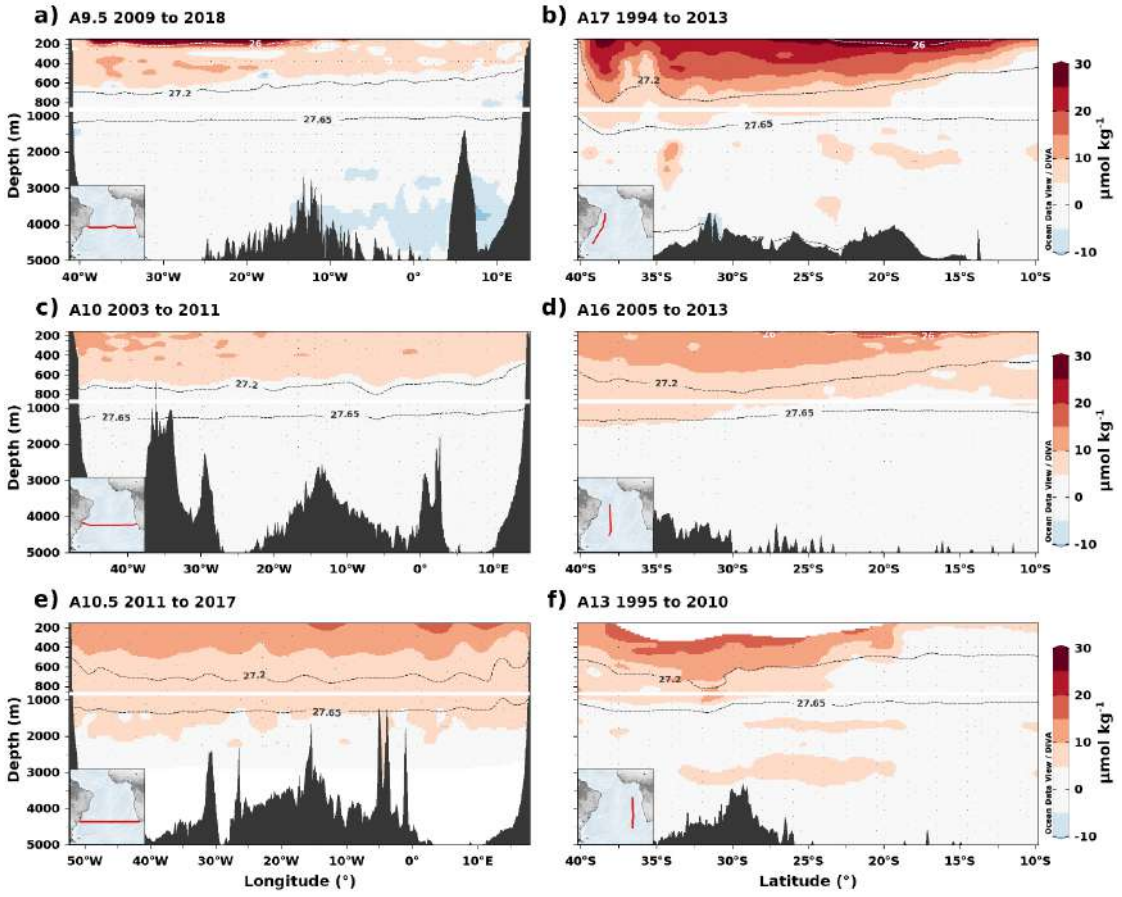

Figure 2. Anthropogenic carbon estimates obtained by the eMLR method in the zonal (left panels) and meridional (right panels) sections evaluated in this study. Colored estimates are statistically distinguishable from 0 with a 90% confidence. The name of the sections and the period of these estimates are shown in the panel titles. The white and black dashed lines depict (from top to bottom) the neutral density of 26 kg m^{-3}, 27.2 kg m^{-3} and 27.65 kg m^{-3}, which correspond to boundaries of the water masses considered (central and intermediate waters). The inset maps indicate the geographic location of the section evaluated.

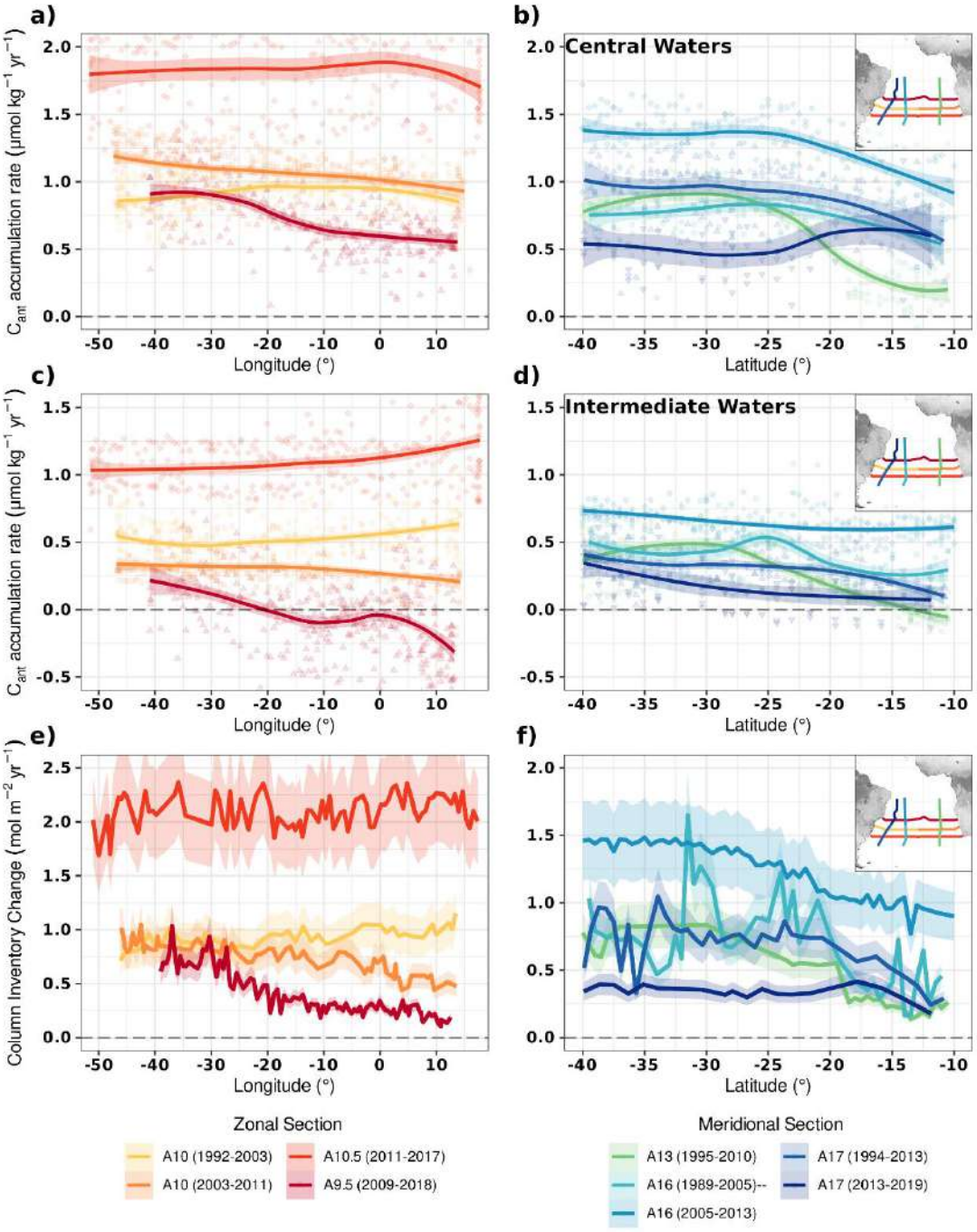

Figure 3. Annual anthropogenic carbon (C_{ant}) accumulation rates (a-d) and column inventory changes (e-f) in the zonal (left panels) and meridional (right panels) sections evaluated in this study. The dots represent the *in-situ* data, while the lines show each section's results, and the colored shadows their uncertainties. Annual C_{ant} accumulation rates were calculated for the central (γ^n < 27.2 kg m^{-3}) and intermediate (27.2 kg m^{-3} < γ^n < 27.65 kg m^{-3}) waters. Column inventory changes were obtained by integration of the C_{ant} concentrations in each station from 150 m to 2000 m and dividing the result by the number of years between each occupation, following the procedure described in Tanhua & Keeling (2012). Section's geographic location is indicated with the same color in the inset maps.

3.2. Influence of natural processes in the DIC distribution

Increased DIC concentrations found in the intermediate waters of the South Atlantic Ocean were associated with positive changes in AOU around the isopycnal of 27.2 kg m^{-3}, particularly between 30°S and 40°S in the meridional sections (Figure 4, see also Figure S4). In those waters, the mean rate of AOU change was 0.31 ± 0.47 µmol kg^{-1} yr^{-1}. Unlike the C_{ant} changes, where the highest concentrations were present in the sections with the longest elapsed time between occupations, the DIC changes associated with the remineralization of organic matter do not show a clear relationship with time. The eastern basin north of 25°S (A9.5 section) was the zone with the most intense organic matter remineralization over the studied region (Figure 4a), with DIC changes above 4.5 µmol kg^{-1} yr^{-1}. However, a similar signal was not seen at 30°S (A10 section) or 35°S (A10.5 section), suggesting that different remineralization dynamics can be found along the African coast. DIC decreases were observed in the central waters in some of the studied sections (e.g., Figure 4d), but in general, those changes were less intense.

3.3. Anthropogenic and natural variations of the carbonate system

The DIC increase induced by both C_{ant} uptake and organic matter remineralization changes have driven the acidification of the South Atlantic Ocean upper waters (Figure 5). The C_{ant} uptake was the main driver controlling the acidification observed in the central waters, while the organic matter remineralization plays a role in the acidification of the intermediate waters below the 27.2 kg m^{-3} isopycnal. The main differences between western and eastern margins (Figure 5a and 5b, respectively) were a slightly higher contribution of remineralization to the pH change in the central and intermediate waters and a lower influence of the C_{ant} in the eastern region. The C_{ant} effect in the pH was not statistically different from zero below the intermediate waters.

The C_{ant} acidification rates observed in the region were −0.0020 ± 0.0007 pH units yr^{-1} and −0.0009 ± 0.0009 pH units yr^{-1} for central and intermediate waters, respectively. Considering only the C_{ant} uptake in the central waters, the pH changes were accompanied by a decrease in calcite and aragonite saturation states, along with an increase in hydrogen ion concentration ($[H^+]$), and in Revelle factor (Figure 6). The anthropogenic changes in the carbonate system properties

showed the same distribution found for the C_{ant} content, with exception of the $[H^+]$, where values higher than expected were observed in the eastern margin of the A9.5a and A10 sections (Figure 6e) and the northern end of the more recent occupation of the A16 section (Figure 6f).

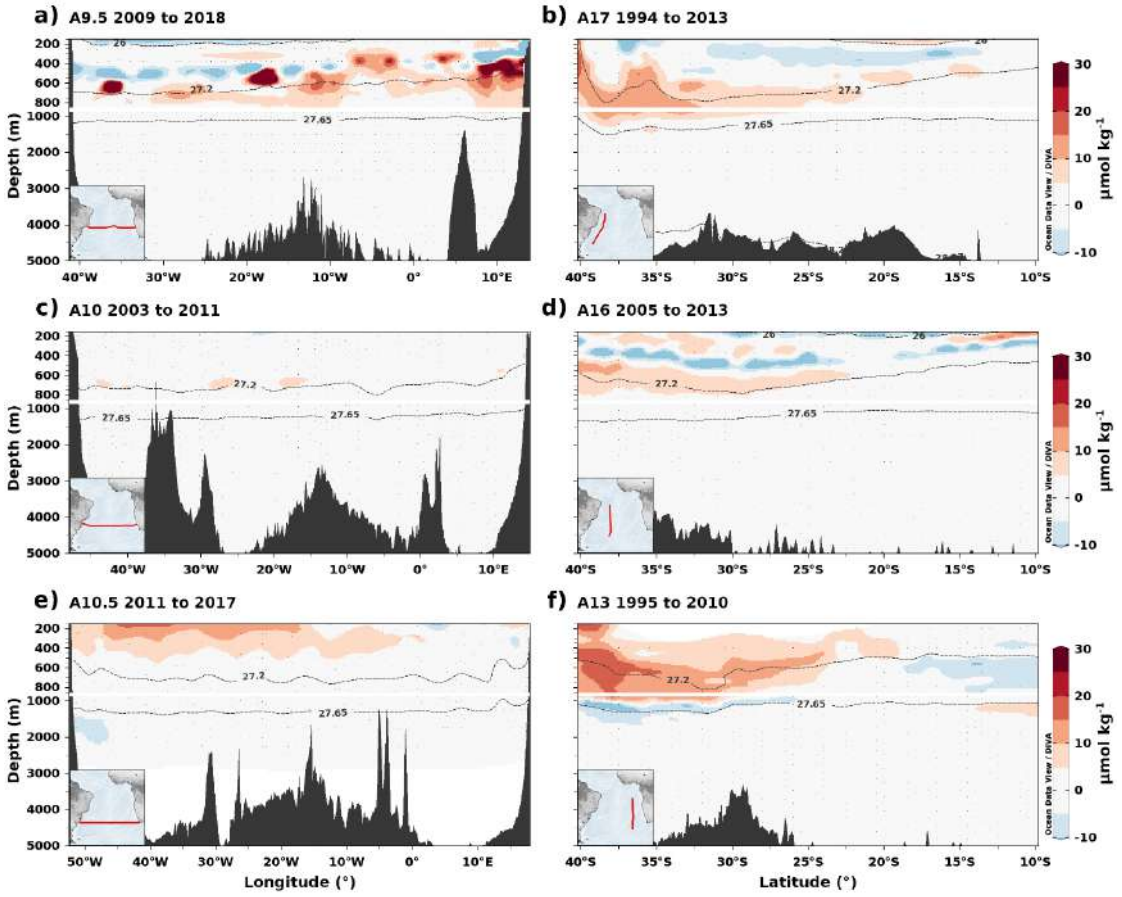

Figure 4. Dissolved inorganic carbon (DIC) changes estimated from the eMLR method applied to apparent oxygen utilization (AOU) data in the zonal (left panels) and meridional (right panels) sections evaluated in this study. Positive (negative) values in red (blue) represent an increase (decrease) since the beginning of the period. The name of the sections and the period of these estimates are shown in the panel titles. The black dashed lines depict (from top to bottom) the neutral density of 26 kg m^{-3}, 27.2 kg m^{-3} and 27.65 kg m^{-3}, which correspond to boundaries of the water masses considered (central and intermediate waters). The inset maps indicate the geographic location of the section evaluated.

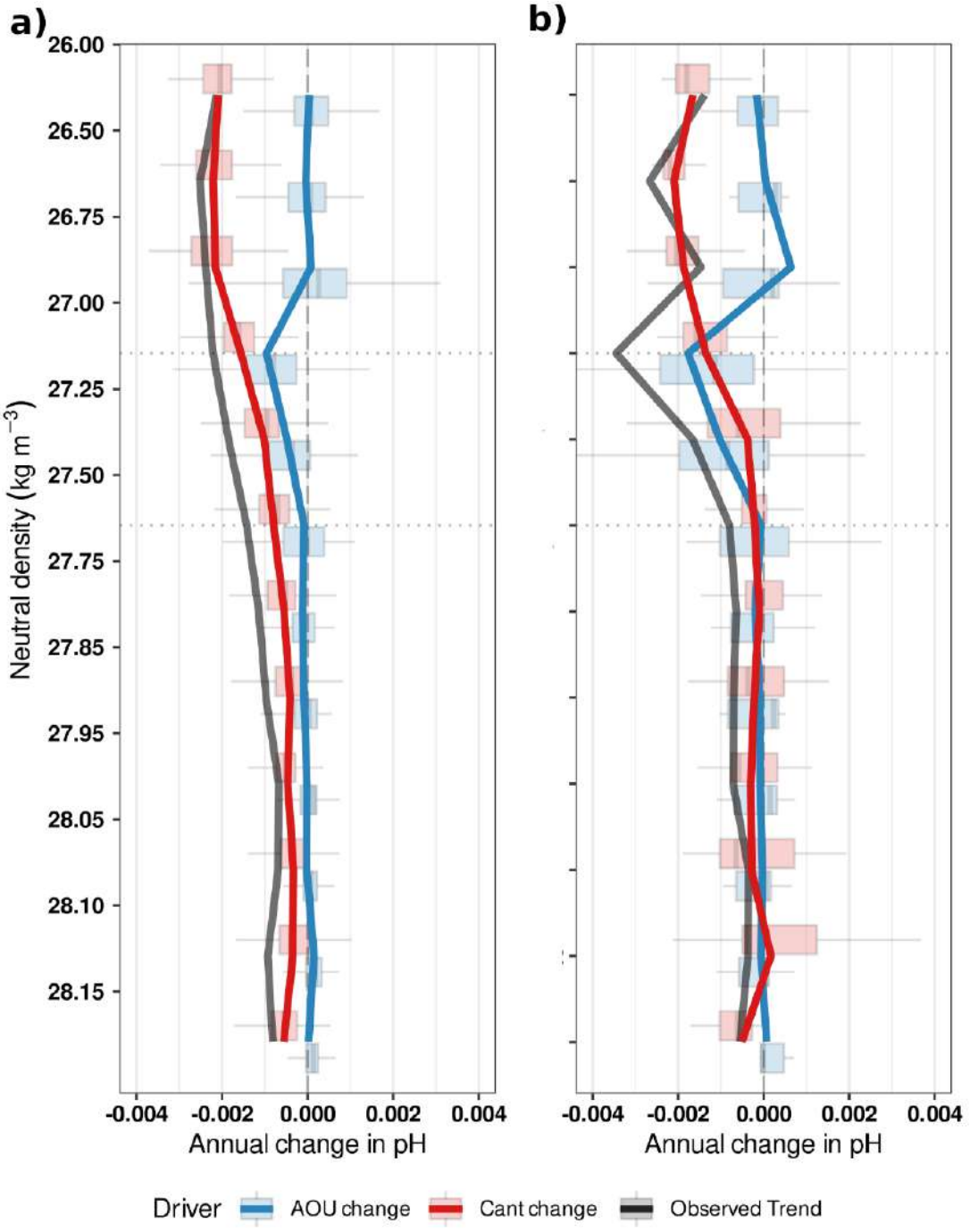

Figure 5. Vertical profile showing the annual acidification rates calculated from the anthropogenic carbon (C_{ant}) changes (in red) and the DIC changes associated with the organic matter remineralization (in blue) over the entire water column at the (a) east and (b) west of 15°W in the South Atlantic Ocean. The acidification rates observed directly between the occupations are indicated by the "observed trend" line in black. Data were binned in 12 intervals of neutral density and the boxplots show a summary of the data distribution. Colored lines represent the median value of each interval of neutral density. The lower limits of the central and intermediate waters are marked by the dotted lines at 27.20 kg m^{-3} and 27.65 kg m^{-3}, respectively.

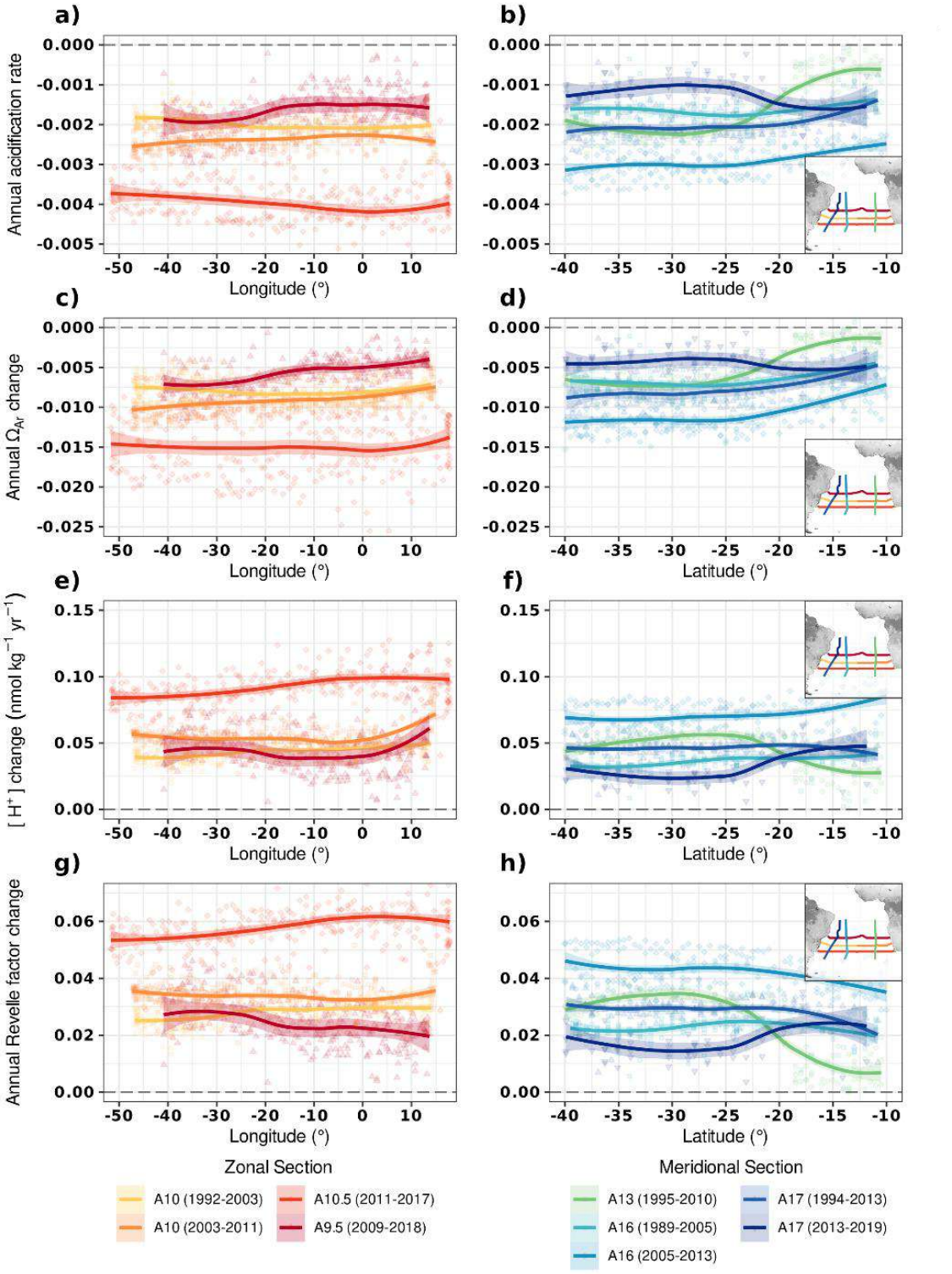

Figure 6. Annual acidification rates (a-b) and annual changes in the calcite saturation state (c-d) the hydrogen ion concentration (e-f) and the Revelle factor (g-h) as result of the absorption of anthropogenic carbon for the central waters of the zonal (left) and meridional (right) sections evaluated in this study. The dots represent the *in-situ* data, while the lines were obtained by local polynomial regression fitting. Uncertainties are shown by the colored shadows. Section's geographic location is indicated with the same color in the inset maps.

4. Discussion

4.1. Anthropogenic changes in the South Atlantic Ocean

The C_{ant} inventory change of 0.71 ± 0.35 mol C m^{-2} yr^{-1} found here for the South Atlantic Ocean between 1989 and 2019 is higher (but within the uncertainty) than the mean global inventory change of 0.65 ± 0.08 mol C m^{-2} yr^{-1} found between 1994 and 2007 (Gruber, Clement, et al., 2019). Higher C_{ant} inventory changes and accumulation rates in this region have been associated with lower Revelle factor values and a high volume of newly formed central and intermediate waters (Sabine et al., 2004). The comparison with recent C_{ant} estimates in the South Pacific Ocean (Carter et al., 2019) shows similar C_{ant} inventory changes along 30°S, an active region of water mass formation in both basins (P06 vs A10; Table 2). However, along meridional transects, inventory changes are higher in the South Atlantic (P16 vs A16; Table 2), likely associated with the differences in ocean circulation and northward water transport between basins (Talley, 2008).

The main pattern found in the spatial distribution of C_{ant} in the South Atlantic Ocean is an increased concentration southward and westward, with a higher variation in the meridional sections in comparison with the zonal sections, except at 25°S (A9.5 section). This pattern can be partially explained by the circulation dynamics in the region and the distance to the water mass formation areas. Wallace (2001) concluded that the southward C_{ant} increase in the AAIW between 10°S and 30°S in the South Atlantic during the 1990s was observed because waters at the south were closest to their formation region. Similarly, Murata et al. (2008) suggested that the formation of STMW in the confluence region between the Brazil and Malvinas Currents contributes to the ventilation of the central waters, resulting in an elevated C_{ant} signal in the western margin. Orselli et al. (2018) also pointed out that the higher C_{ant} in SACW and AAIW samples along the Patagonian shelf-break could be observed because these waters occupy a well-ventilated layer and were sampled geographically close to their formation region. The water age estimates of Fine et al. (2017) at the isopycnal of 26.8 kg m^{-3} validate those observations, and the higher age difference observed longitudinally south of 30°S explains the higher variation in the C_{ant} content in the meridional sections. In latitudes lower than 30°S, older waters are found in the eastern basin as the influence of the eastern boundary shadow zone (Angola

Dome) increases (Karstensen et al., 2008), explaining the results observed at the A9.5 section.

Small differences in the C_{ant} inventory change were observed in sections with more than two occupations (A10, A16, and A17), in line with previous results (Woosley et al., 2016). This suggests that the South Atlantic Ocean shows a lower decadal variability compared to the North Atlantic Ocean, at least in the last 30 years. The higher accumulation rates in most recent decades are coherent with the increased growth rate observed in atmospheric CO_2 (Dlugokencky & Tans, 2020), and a similar pattern has been observed in decadal observations in the Pacific Ocean and on a global scale (Carter et al., 2019; Gruber, Clement, et al., 2019). Although decadal variability is relatively small, and the general trend is an increased C_{ant} concentration over the years, interannual variability can affect the C_{ant} uptake, as observed in the lower accumulation rates in the A17 section between 2013 and 2019. While our temporal resolution does not allow the evaluation of interannual variability, this effect can be seen in the detailed temporal analysis of Fontela et al. (2021), where small variations in the C_{ant} concentrations are observed between years. However, more data are needed to assess whether this interannual variability affects the entire basin or only the western South Atlantic Ocean.

At a regional scale, the accumulation rates and inventories reported here are in good agreement with previous results in the region (Table 2). However, several observations must be made. To exclude the seasonality effect in the upper layer, our inventories account only for data below 200 m. Assuming that the surface waters are in equilibrium with the atmosphere (Sarmiento & Gruber, 2006), the column inventories should be at least 0.18 mol m^{-2} yr^{-1} higher than the reported values (Table 2). Considering this, our C_{ant} values are still within the uncertainty of the previous results. Additionally, oceanic eddies can influence the CO_2 fluxes at the surface, either increasing (Orselli, Kerr, et al., 2019) or decreasing (Pezzi et al., 2021) the oceanic C_{ant} uptake. However, the methodology used here for the C_{ant} calculation does not appear to resolve eddies, as the higher subsurface C_{ant} concentrations in the interior of Agulhas eddies suggested by Woosley et al. (2016) and confirmed by Orselli, Goyet, et al. (2019) in the A10 section are not present in our results. This could be a consequence of the use of an ensemble

step for the C_{ant} calculation, as patterns associated with mesoscale structures are visible in the simpler eMLR method used for the evaluation of natural changes. Finally, the C_{ant} accumulation rates and inventories observed in the A10.5 section are unrealistic, not only because they are higher than the values observed at similar latitudes in the meridional sections, but also because the uptake is higher than that expected when considering the carbonate chemistry (~1.5 µmol kg^{-1} yr^{-1} at the surface, see Text S4). This difference can be likely attributed to the use of reconstructed carbonate system parameters for the earlier occupation and, to a lesser degree, with the parameters used in the regression (temperature, salinity, and oxygen) which are not able to fully describe the variations of DIC. Although reconstructed data has been used successfully in the past for C_{ant} determination since the beginning of the industrial period (Orselli, Goyet, et al., 2019) and even for quasi-decadal (2003-2011) C_{ant} variations (Orselli, Goyet, et al., 2019), our results suggests that this type of data must be carefully evaluated for precise estimation of C_{ant} decadal changes using the eMLR method.

Table 2. Anthropogenic carbon accumulation rates and inventories for the Atlantic Ocean. The acronyms represent the water masses: South Atlantic Central Water (SACW), Antarctic Intermediate Water (AAIW), Subantarctic Modal Water (SAMW), Upper North Atlantic Central Water (uNACW), and South Pacific Central Water (SPCW).

Reference	Section / Position or ocean area	Period	Method	Previous Results		This Study	
				Accumulation Rate μmol kg^{-1} yr^{-1}	Column Inventory mol m^{-2} yr^{-1}	Accumulation Rate μmol kg^{-1} yr^{-1}	Column Inventory mol m^{-2} yr^{-1}
	Atlantic Ocean						
This Study	A13	1995-2010	eMLR			0.59 ± 0.34 (SACW) 0.26 ± 0.25 (AAIW)	0.42 ± 0.22
This Study	A9.5 (24.5°S)	2009-2018	eMLR			0.68 ± 0.38 (SACW) −0.05 ± 0.27 (AAIW)	0.39 ± 0.21
This Study	A10.5 (35°S)	2011-2017	eMLR			1.83 ± 0.37 (SACW) 1.11 ± 0.22 (AAIW)	2.10 ± 0.15
This Study	A17	2013-2019	eMLR			0.53 ± 0.23 (SACW) 0.17 ± 0.19 (AAIW)	0.34 ± 0.05
Murata et al., 2008	A10 (30°S)	1992-2003	ΔnC_T^{CAL}	0.62 ± 0.15 (SAMW)[a] 0.33 ± 0.13 (AAIW)[a]	0.6 ± 0.1	0.91 ± 0.15 (SACW) 0.53 ± 0.15 (AAIW)	0.93 ± 0.09
Woosley et al., 2016	A10 (30°S)	2003-2011	eMLR	0.98 ± 0.17	0.83 ± 0.1	1.08 ± 0.18 (SACW) 0.30 ± 0.15 (AAIW)	0.75 ± 0.13
Wanninkhof et al., 2010	A16 (15°S-60°S)	1989-2005	$eMLR_{dens}$		0.76 ± 0.05	0.75 ± 0.21 (SACW) 0.37 ± 0.22 (SACW)	0.72 ± 0.31
Woosley et al., 2016	A16	2003-2011	eMLR	1.04 ± 0.28		1.28 ± 0.23 (SACW) 0.64 ± 0.09 (AAIW)	1.23 ± 0.21
Ríos et al., 2012	A17 (10°N-55°S)	1972-2003	φC_T^0	0.90 ± 0.04 (SACW) 0.36 ± 0.02 (AAIW)	0.92 ± 0.13		
Ríos et al., 2015	A17 (14°S-50°S)	1994-2013	φC_T^0	1.1 ± 0.1 (SACW)[a] 0.4 ± 0.2 (AAIW)[a]		0.92 ± 0.24 (SACW) 0.31 ± 0.14 (SACW)	0.70 ± 0.19
Salt et al., 2015	A17	1994-2010	eMLR	0.99 ± 0.14 (SACW) 0.36 ± 0.06 (AAIW)			

Wanninkhof et al., 2010	A16 (64°N-60°S)	1989-2003	$eMLR_{dens}$		0.53 ± 0.05
Orselli et al., 2018	Patagonian shelf-break	Preindustrial-2007/2008	TrOCA	0.35 [up to 0.66] (SACW)[b] 0.11 [up to 0.41] (AAIW)[b]	
Carvalho-Borges et al., 2018	South Brazil Bight	Preindustrial-2014	TrOCA	0.32 [up to 0.58] (SACW)[b] 0.14 [up to 0.34] (AAIW)[b]	
Fajar et al., 2015	A7 (7.5°N)	1993-2010	φC_T^0	0.96 ± 0.06 (SACW) 0.33 ± 0.06 (AAIW)	1.07 ± 0.23
Ríos et al., 2015	A17 (18°N-36°N)	1993-2003	φC_T^0	0.8 ± 0.2 (uNACW)[a] 0.2 ± 0.1 (AAIW)[a]	
	Pacific Ocean				
Sabine et al., 2008	P16 (20°S-60°S)	1991-2006	eMLR		0.6 ± 0.1
Carter et al., 2019	P16 (20°S-60°S)	1991-2006	CAREER		0.48 ± 0.13
Waters et al., 2011	P06 (32°S)	1992-2010	eMLR	0.94 ± 0.2 (SPCW) 0.51 ± 0.1 (AAIW)	0.79 ± 0.2
Carter et al., 2019	P06 (32°S)	1992-2017	CAREER		0.74 ± 0.11
	Other Oceans				
Álvarez et al., 2011	I05 (32°S)	1995-2005	eMLR	0.77 ± 0.01 (SAMW)[c]	
Sabine et al., 2008	Global Average	Preindustrial-2005			0.55
Gruber et al., 2019	Global Average	1994-2007	eMLR(C*)		0.65 ± 0.08

[a]Values calculated by dividing the reported average C_{ant} concentrations by the elapsed time between each occupation. [b]Values calculated by dividing the reported average C_{ant} concentrations by the elapsed time since the Industrial Revolution and sampling period (~250 to 260 years). [c]Accumulation rate found in the western Indian Ocean.

4.2. Natural DIC and AOU variations in the South Atlantic Ocean

The eMLR method applied to AOU data has been used in the past to identify DIC changes associated with natural variations, especially in the Pacific Ocean (Carter et al., 2017; Sabine et al., 2008; Williams et al., 2015). Until now, a similar approach had not been utilized in the South Atlantic Ocean. Our results show that the AAIW is becoming less oxygenated, with a mean rate of AOU change of 0.31 ± 0.68 μmol kg^{-1} yr^{-1}. This value is higher than the deoxygenation trend found by Santos et al. (2016) for the AAIW between 1960 and 2015 but agrees well with the observations of Fontela et al. (2021) and Schmidtko et al. (2017) in the Argentine Basin and the South Atlantic Ocean, respectively. Deoxygenation in the upper 1000 m of the ocean has been associated with warming-induced declines in oxygen solubility (Santos et al., 2016; Schmidtko et al., 2017). However, only circulation changes such as the reduced ventilation of the AAIW or an enhanced flux of organic matter can explain the increased remineralization inferred from AOU data. While the identification of the main driver behind those changes is not possible with the available data, we can evaluate if the observed results are consistent with the variations identified in this region.

Decadal ocean circulation changes have been identified previously in the area. Using the distribution of transient tracers and water age models, a decrease in the SAMW age and an increase in the Circumpolar Deep Water (CDW) age was observed along the South Atlantic Ocean (Fine et al., 2017; Tanhua et al., 2017; Waugh et al., 2013). The decrease in SAMW age, evidence of increased ventilation between the 1990s and 2000s, was attributed to the intensification and poleward displacement of westerly winds, which caused an intensification of the northward Ekman transport and increased STMW formation rates over the entire Southern Ocean (Gruber, Landschützer, et al., 2019; Waugh et al., 2013). The decrease of AOU from 1989 to 2013 observed in the central waters along the meridional sections A16 and A17, is coherent with the increased ventilation reported in the SAMW by earlier studies (Fine et al., 2017; Tanhua et al., 2017; Waugh et al., 2013). However, apart from section A17 in 2013-2019, the AOU increase between the isopycnals of 27.2 and 27.65 kg m^{-3} in all meridional sections does not match the transient tracer data, as a conclusive change in the AAIW ventilation has not been previously observed (Tanhua et al., 2017; Waugh

et al., 2013). Moreover, negative C_{ant} anomalies associated with shorter residence times of waters at the surface suggest an enhanced AAIW ventilation in the South Atlantic Ocean between 1994 and 2017 (Gruber, Clement, et al., 2019). These observations show that ventilation changes cannot fully explain the increased remineralization in the AAIW.

Although the consensus is that physical variations are the predominant mechanism of oxygen change in the oceans (Talley et al., 2016; Wanninkhof et al., 2010), and biological productivity is low in the subtropical gyres (Dunne et al., 2007), areas with positive trends in primary productivity have been observed in the last 20 years in South Atlantic gyre (Kulk et al., 2020). Thus, some of the AOU changes in our results can be attributed to increased biological activity, especially in the eastern basin, where the highest phytoplankton biomass concentrations have been found (Carvalho et al., 2021). This is the case of the A9.5 section, where an increase in the AOU is observed east of 10°E around 500 m, in the domain of the Benguela Upwelling System. Primary productivity in the Benguela Upwelling System is controlled by the input of nutrient-rich waters coming from the Angola Gyre (Schmidt & Eggert, 2016). The strength of the upwelling favors a high interannual and decadal variability, associated with shifts in the magnitude and meridional position of the atmospheric South Atlantic Anticyclone (Lamont et al. 2018). Therefore, more intense upwelling and primary productivity in 2018 could explain the increased AOU observed here. The results of Lamont et al. (2018) also show that the upwelling in the Southern Benguela Upwelling System (south of 27°S) is an order of magnitude lower than in the north, which can explain the absence of AOU changes on the east portion of A10 and A10.5 sections.

Another hypothesis is that AOU changes are influenced by the presence of mesoscale structures. Eddies are common in the region, and models have shown that they are capable of transporting oxygen-depleted waters from the African shelf to the open ocean (Schmidt & Eggert, 2016). Similarly, Agulhas eddies carry relatively old waters from the Indian to the Atlantic Ocean. For instance, some of the observed changes in the A9.5 section coincide with the position of eddies. At a larger scale, oxygen gradients (~50 μmol kg^{-1}) have been observed between AAIW formed in the Brazil-Malvinas confluence zone (A-AAIW) and AAIW formed in the Indian Ocean (I-AAIW) that enters the South Atlantic in eddies and

filaments through the Agulhas/Benguela current system (Azar et al., 2020; Gordon et al., 1992; Manta et al., 2021; Rusciano et al., 2012; de Souza et al., 2018). An increased Agulhas leakage could cause a higher input of the I-AAIW variety into the South Atlantic and an increase in the AOU. Previous studies have shown that the intensification and southward displacement of the westerlies observed during the latter decades is responsible for an increased Agulhas leakage (Beal et al., 2011; Biastoch et al., 2009), and the input of waters from the Indian Ocean has a direct effect in the salinity changes observed in the subtropical thermocline (Goes et al., 2014). Therefore, it is reasonable to think that the increased AOU observed in the meridional sections could be, to some degree, the result of changes in the input of I-AAIW caused by the same forcing responsible for the enhanced ventilation of the SAMW.

Finally, it is important to highlight that one potential source of error in our analysis comes from the use of AOU as a proxy of organic matter respiration, as previous works have shown that water masses are not necessarily saturated in oxygen during the subduction (Ito et al., 2004; Russell & Dickson, 2003). However, Carter et al. (2021) showed that the overestimation of organic matter remineralization that comes from the utilization of AOU in the thermocline of the subtropical gyre is small in comparison to the values observed in other regions, such as the Southern Ocean (south of 60°S) and the western North Pacific Ocean. Additionally, the eMLR method would cancel this effect if the oxygen unsaturation has not changed significantly between occupations (Williams et al., 2015).

4.3. Acidification and carbonate changes in the South Atlantic Ocean

The uptake of C_{ant} was the main driver influencing the acidification up to 1100 m along the South Atlantic Ocean, accounting for approximately 90% and 50% of the pH changes observed in central and intermediate waters, respectively. The higher acidification rates associated with this process were found in the central waters, with a mean value of -0.0020 ± 0.0007 yr^{-1} between 1989 and 2018. The central waters in the South Atlantic Ocean are acidifying at a lower rate than their equivalents in the polar regions (Table 3), which is consistent with the decreased buffer capacity observed at higher latitudes (Fassbender et al., 2017; Sabine et al., 2004). At a regional scale, anthropogenic acidification rates in this study agree with previous results. At 30°S (A10 section), our estimates of -0.0020 ± 0.003

yr^{-1} and −0.0024 ± 0.003 yr^{-1} in the central waters between 1993-2003 and 2003-2011 are similar to the values found by Woosley et al. (2016) for the first 250 m during the same periods. For the A16 section, higher estimates were found in comparison with Woosley et al. (2016). This can be partially explained by geographic differences, as their analysis included the North Atlantic Ocean which suffered a lower uptake of C_{ant} during the 1990s (Gruber et al., 2019; Wanninkhof et al., 2010), decreasing their estimate. However, as a higher C_{ant} uptake was observed in the North Atlantic Ocean in the 2000s, the difference between the most recent estimates cannot be attributed to the same effect, suggesting that our estimation of C_{ant} in this section during the 2005-2013 period can be overestimated.

The western basin is the most studied area inside the South Atlantic Ocean, allowing the comparison of anthropogenic acidification rates up to the intermediate waters. Estimates of −0.0020 ± 0.0004 yr^{-1} and −0.0009 ± 0.0004 yr^{-1} in central and intermediate waters found in that region (A17 section) are similar to the previous values reported by Ríos et al. (2015) and Salt et al. (2015) (Table 3). These trends are also in agreement with those reported from the South Brazil Bight (Carvalho-Borges et al., 2018) to the Patagonian shelf-break (Orselli et al., 2018). In the Argentine basin, the acidification values reported by Fontela et al. (2021) are higher in the AAIW, because they represent the total change in pH observed in those waters and not the acidification rate associated only with the C_{ant} increase. However, as 60% of the pH change in the AAIW results from the C_{ant} uptake (Fontela et al., 2021), the approximated acidification rate in those waters of −0.0013 yr^{-1} is in line with our findings. The relatively high acidification found in this region in comparison with the subtropical North Atlantic indicates that the South Atlantic Gyre is acidifying faster than their north counterpart, a phenomenon also observed by Kitidis et al. (2017).

The remineralization of organic matter only has a considerable influence on the pH changes at intermediate waters, but this effect is sufficient to make the total rates of acidification observed in this water mass the highest in the entire water column (Figure 5). This effect is especially noticeable in the eastern basin near the coast of Africa at 25°S, where the highest rates of acidification were found. This pattern of increased acidification in the intermediate waters in comparison

with the upper layer was previously observed by Ríos et al. (2015) and Fontela et al. (2021) along the A17 section, but our results show that a similar feature can also be found along the eastern margin. However, as the available data in this region is scarce, and has a low temporal resolution, new observations are necessary to constraint this effect during the 2010s decade.

Even though the individual impact of each process in the pH changes was evaluated, it is important to highlight that DIC and Alk variations associated with natural processes can alter the buffer capacity, influencing the magnitude of the anthropogenic changes. For instance, the organic matter remineralization increases the DIC and reduces the buffer capacity of the waters, allowing enhanced anthropogenic acidification (Lauvset et al., 2020; Salt et al., 2015). The African coast is the zone most susceptible to this effect in the Subtropical South Atlantic, as we observed high remineralization, a low buffer capacity (represented by higher values in the Revelle factor), and the decoupling between the pH and $[H^+]$ changes (Figure S5). As the C_{ant} concentration is still increasing, the central and intermediate waters in this region are very vulnerable not only to enhanced anthropogenic acidification but also to an aragonite unsaturation in the next 10 to 20 years (Figure S6). A similar combination of physical and biological processes enhancing the changes in the carbonate chemistry have been observed previously in other coastal upwelling systems around the globe (Feely et al., 2018; Lachkar, 2014). For the South Atlantic Ocean, if the anthropogenic changes maintain the present trend, we expect that the AAIW will become unsaturated in aragonite in ~70 years, in line with the predictions of Salt et al. (2015). Regarding the SAMW, aragonite unsaturation is expected in the next century, close to the estimations of Fontela et al. (2021) for the Argentine Basin.

Table 3. Acidification rates and changes in the aragonite saturation (ΔΩAr) in surface/central waters (CW) and intermediate waters (IW) over the Atlantic Ocean and across the world.

Reference	Section / position	Period	Previous results		This study			
			ΔpH (Surface/CW) pH units yr^{-1}	ΔpH (IW) pH units yr^{-1}	ΔpH (CW) pH units yr^{-1}	ΔpH (IW) pH units yr^{-1}	ΔΩAr (CW)	ΔΩAr (IW)
	Atlantic Ocean							
This study	A13 (10°-40°S)	1995-2010			−0.0015 ± 0.0007	−0.0008 ± 0.0007	-0.0047 ± 0.0029	-0.0018 ± 0.0017
This study	A9.5 (24°S)	2009-2018			−0.0016 ± 0.0010	−0.0002 ± 0.0008	-0.0056 ± 0.0031	0.0003 ± 0.0017
This study	A17 (10°-40°S)	2013-2019			−0.0012 ± 0.0005	−0.0005 ± 0.0005	-0.0044 ± 0.0021	-0.0012 ± 0.0014
Woosley et al. (2016)	A10 (30°S)	1992-2003	−0.0020 ± 0.0003		−0.0020 ± 0.0003	−0.0015 ± 0.0004	-0.0079 ± 0.0017	-0.0036 ± 0.0012
Woosley et al. (2016)	A10 (30°S)	2003-2011	−0.0022 ± 0.0004		−0.0024 ± 0.0003	−0.0009 ± 0.0004	-0.0093 ± 0.0020	-0.0021 ± 0.0011
Woosley et al. (2016)	A16 (63°N-30°S)	1989-2005	−0.0011 ± 0.0005		−0.0016 ± 0.0004	−0.0010 ± 0.0006	-0.0065 ± 0.0020	-0.0025 ± 0.0016
Woosley et al. (2016)	A16 (63°N-30°S)	2005-2013	−0.0021 ± 0.0010		−0.0029 ± 0.0004	−0.0019 ± 0.0002	-0.0108 ± 0.0024	-0.0042 ± 0.0008
Ríos et al. (2015)	A17 (14°-50°S)	1994-2013	−0.0020 ± 0.0002[a]	−0.0009 ± 0.0005[a]	−0.0020 ± 0.0004	−0.0009 ± 0.0004	-0.0079 ± 0.0024	-0.0021 ± 0.0010
Ríos et al. (2015)	A17 (18°-36°N)	1993-2003	−0.0015 ± 0.0003[a]	−0.0004 ± 0.0004[a]				
Salt et al. (2015)	A17 (18°-23°S)	1994-2011	−0.0016	−0.0010				
Fontela et al. (2021)	A17 (30°-51°S)	1972-2019	−0.0019 ± 0.0001	−0.0022 ± 0.0002				
Kitidis et al. (2017)	AMT (15°-31°S)	1995-2013	−0.0019					
Kitidis et al. (2017)	AMT (25°-38°S)	1995-2013	−0.0009					
Orselli et al. (2018)	Patagonian shelf-break	Preindustrial-2007/2008	−0.0018	−0.0010				
Carvalho-Borges et al. (2018)	South Brazil Bight	Preindustrial-2014	−0.0017	−0.0010				
Vázquez-Rodríguez et al. (2012)	Ena basin	1981-2008	−0.0009 ± 0.0001	−0.0006 ± 0.0001				
Takahashi et al. (2014)	Drake (SAZ)	2002-2012	−0.0023 ± 0.0007					
	Other Oceans							
Williams et al. (2015)	South Pacific (P16s)	2005-2011	−0.0024 ± 0.0009					
Carter et al. (2017)	Pacific Ocean (60°N-60°S)	1994-2014	−0.0015[a]					
Xue et al. (2014)	Indian Ocean	1962–2012	−0.0016 ± 0.0001					

[a]Values calculated dividing the reported acidification rate by the elapsed time between each occupation.

5. Summary and Conclusions

In this study, we evaluated the C_{ant} distribution, accumulation rates, and its effect on the carbonate system of central and intermediate waters in the South Atlantic Ocean. This was achieved by taking advantage of the availability of new data coming from recent hydrographic surveys of the GO-SHIP program in the region. For this, data from the GLODAPv2.2020 database was analyzed using a modified eMLR approach. The C_{ant} distribution was not spatially uniform, and higher values were observed in the southern and western margin of the subtropical gyre, where the waters are closest to their formation region. From 1989 to 2019, central and intermediate waters accumulated C_{ant} at a rate of 0.89 ± 0.33 μmol kg^{-1} yr^{-1} and 0.30 ± 0.29 μmol kg^{-1} yr^{-1}, respectively. A column inventory change of 0.71 ± 0.35 mol C m^{-2} yr^{-1} was found for the region, which is higher (but within the uncertainty) than the global mean storage rate of 0.65 mol C m^{-2} yr^{-1} reported by Gruber, Clement, et al. (2019). This C_{ant} uptake was the principal process responsible for the acidification of the upper part of the water column, and rates of −0.0020 ± 0.0007 pH units yr^{-1} and −0.0009 ± 0.0009 pH units yr^{-1} were observed in central and intermediate waters, respectively. Under these conditions, it is expected that the AAIW will become unsaturated in aragonite in ~70 years, in line with previous previsions (e.g., Fontela et al., 2021; Salt et al., 2015).

In addition to the C_{ant} estimates, we studied the DIC changes associated with natural processes that have occurred in the South Atlantic Ocean since the 1990s until now. For this, we used the eMLR approach applied to AOU data. The main feature observed was an increased DIC concentration in intermediate waters along the southern limit of the subtropical gyre, and especially at the coast of Africa, north of 25°S. The origin of this signal cannot be totally explained by ventilation changes, and we propose that increased biological activity in union with mesoscale activity and changes in the input of Indian Ocean waters are possible mechanisms behind this increased remineralization. These natural changes coupled with the C_{ant} effect were responsible for the higher acidification of the AAIW, a process previously reported in the western South Atlantic (Fontela et al., 2021; Ríos et al., 2015) but observed here also in the eastern region. Even more, an aragonite unsaturation on central waters along the eastern margin of

the South Atlantic Ocean is expected in the next 10 to 20 years if the anthropogenic changes maintain the present trend. These results highlight the need for more exhaustive monitoring in the eastern margin of the South Atlantic, which will allow us to identify if the interannual variability is similar in both basins, and how much the ecosystems health, marine life, and societies will be affected by these changes.

6. Data Availability Statement

Data from the TAII cruise and the code used for the calculations is available at https://doi.org/10.5281/zenodo.5205939. The GLODAPv2.2020 data was published by Olsen et al. (2020) and can be accessed at the GLODAP website (https://www.glodap.info).

7. Acknowledgments

This study is part of the activities of the Brazilian High Latitude Oceanography Group (GOAL, www.goal.furg.br), the Brazilian Ocean Acidification Network (BrOA, www.broa.furg.br), and the CARBON Team research group (www.carbonteam.furg.br). This study was sponsored by the Brazilian National Council for Scientific and Technological Development (CNPq; grant nos. 443258/2019-8; 442628/2018-8), the Brazilian Improving Coordination of Higher Education Personnel (CAPES, grant no. 23038.001421/2014-30), and supported by the TRIATLAS project, which has received funding from the European Union's Horizon 2020 research and innovation programme under grant agreement no. 817578. The TAII cruise was sponsored by the CNPq grant no. 558267/2009 2, with logistics supported by the Ministry of Science, Technology, Innovation, and Communication (MCTIC), the Brazilian Ministerial Secretary for the Resources of the Sea (SECIRM), and the Brazilian Navy. The authors also acknowledge the support of the Post-Graduate Program in Oceanology from the CAPES Foundation. A. Piñango acknowledges his master's scholarship from CAPES process n°. 88887.374157/2019-00. I. B. M. Orselli acknowledges her CNPq PDJ grant no. 151130/2020-5. R. Kerr and Carlos A. E. Garcia acknowledge their CNPq researcher grants nos. 304937/2018-5 and 309932/2019-0, respectively. We would like to thank the supporters, collaborators, and scientists behind the Global Ocean Data Analysis Project (GLODAP).

8. Supplementary Material

Text S1 describes the principal changes to the extended multiple linear regression (eMLR) method applied in this study. Text S2 contains an analysis of the sources of uncertainty in the estimates of anthropogenic carbon (C_{ant}) and the carbonate system parameters. Text S3 describes the principal changes in oceanographic properties in the studied sections. Text S4 indicates how the expected accumulation rates for the A10.5 section were calculated. The supplementary figures S1 and S2 show information about the data used in the analysis. Figures S3 to S6 display the changes in DIC and pH for the sections not show in the main text. Figures S7 to S10 support Text S3.

Text S1 – Changes to the eMLR method

As indicated in the main text, the C_{ant} changes in the several zonal and meridional hydrographic repeat sections of the South Atlantic Ocean were quantified using the eMLR method with some of the modifications introduced by Clement and Gruber (2018) and by Carter et al. (2017, 2019). The fundamental changes and adjustments in the approach used are the following:

1. The water column was divided into 13 layers using the isopycnal surfaces defined by Clement and Gruber (2018) for the Atlantic Ocean until 28.15 kg m^{-3}. Additionally, we decided to focus on the changes below the surface mixed layer, where the seasonal variability is negligible. Thus, data shallower than 150 m were excluded from the analysis.

2. As suggested by Clement and Gruber (2018) and Carter et al. (2019), MLRs were fit using the DIC corrected by the dissolution of organic matter (DIC_{abio}) instead of the DIC. The DIC_{abio} parameter was defined as shown by Eq. S1:

$$DIC_{abio} = DIC - r_{c:o} \times AOU \text{ , (Eq. S1)}$$

where the $r_{c:o}$ term is the carbon:oxygen remineralization ratio (117/170) of Anderson and Sarmiento (1994), which account for the changes in the DIC by the oxidation of organic matter, and AOU represents the apparent oxygen utilization. DIC_{abio} was used instead of the C* of Clement and

Gruber (2018) because phosphorus data is scarcer in comparison to oxygen data in the study region.

3. Potential temperature (θ), S, AOU, Alk, Si, and NO_3^- were the parameters selected for the eMLRs fits. θ was used instead of temperature to be consistent with previous works in the area (e.g., Salt et al., 2015) and NO_3^- instead of PO_4^{3-} because more data is available. Since nutrients data were not available for the A10.5 section, and because the results showed possible overfitting using Alk, only T, S, and AOU were used for the eMLR fits in this section.

4. As done by Carter et al. (2017) a robust MLR was used, reducing the influence of anomalous values in the estimation of the coefficients. This was done through the RLM function of the MASS package for R (Venables & Ripley, 2002). Like Carter et al. (2017), we used the default values of the Tukey bisquare function, and data with residuals over 4.685 times the standard residuals were given no weight.

5. Instead of a unique MLR, a fit for each possible combination of the chosen parameters was made, under the constraint that at least three variables were selected, resulting in a total of 42 MLR by isopycnal layer. This was done for all sections except the A10.5, where only one MLR was employed.

6. For each isopycnal layer, we selected the best 10 MLR (quantified by the lower combined RMSE), and the ΔC_{ant} was calculated using Eq. 3. Finally, these 10 ΔC_{ant} estimates were averaged and this value was the final result. This approach is the same as the one used by Clement and Gruber (2018) and also is similar to the ensemble method of Carter et al. (2017, 2019).

Text S2 – Determination of uncertainties on calculated parameters

Uncertainties of the C_{ant} estimates obtained by the eMLR method were calculated in two ways: (1) propagating the residuals of the regressions (RMSE) and the

measurements' uncertainties (e.g., Woosley et al. 2016) and (2) applying the method used by Carter et al. (2017), which consisted in the determination and propagation of uncertainties from three different sources (measurement uncertainties, violations of the eMLR assumption that DIC changes from C_{ant} increases are the only nonstationary modes of variability, and the regression constant combinations). In the first approach, the mean RMSE was ± 1.6 µmol kg^{-1}, which combined in quadrature with the measurement uncertainty determined by Friis et al. (2005) of ± 1.0 µmol kg^{-1}, resulted in a total uncertainty of ± 1.9 µmol kg^{-1}. For the second approach, the difference between C_{ant} estimates obtained with and without perturbated data allowed the determination of uncertainties associated with the measured parameters and the violation of the eMLR assumption. The standard deviation of the 10 ΔC_{ant} estimates was used as the uncertainty of the regression constant combinations. The mean uncertainty obtained using this approach for all the cruises was ± 2.7 µmol kg^{-1}. This value was used as the final C_{ant} uncertainty, and similar to Woosley et al. (2016), we round it to ± 3 µmol kg^{-1} to be conservative.

Uncertainties calculation for pH and other carbonate system parameters was performed using the *errors* function of the *seacarb* package, with the constant standard uncertainties described in Orr et al. (2018). The uncertainties used for the input parameters temperature, salinity, phosphate, silicate, Alk and DIC were 0.002 °C, 0.002, 0.01 µmol kg^{-1}, 0.1 µmol kg^{-1}, 2 µmol kg^{-1}, and 2 µmol kg^{-1}, respectively.

Text S3 – Hydrographic and biogeochemical properties changes

For all repeated sections, changes in seawater salinity lower than 1 psu were observed in the upper layer up to 1000 m, with higher variations in the first 600 m, i.e., on both surface and the central waters (Figure S7). Salinity increased mainly along the surface, but with high spatial variability. The intensity of changes in salinity was higher in the western than the eastern basins of the South Atlantic Ocean (see the zonal changes in Figure S7). The presence of mesoscale structures, such as Agulhas eddies, were likely responsible for the salinity changes observed, especially in the zonal sections (Hernández-Guerra et al., 2019; Manta et al., 2021). In contrast, there were little changes in Alk along the

region, with the highest Alk variations (~20 μmol kg^{-1}) closely related to the salinity changes identified in the upper ocean (Figure S8). The lower variability in Alk suggests that the pH errors associated with changes in this parameter should be non-significant in our calculations.

Changes of ~10 – 20 μmol kg^{-1} in AOU were present at all depths (Figure S9) except for the first 150 m, as expected of a surface mixed layer in equilibrium with the atmosphere. AOU variations were higher (> 50 μmol kg^{-1}) near the coast, especially in the eastern margin of the South Atlantic Ocean (Figure S9). For example, a decrease in AOU was observed along the A13 section, at a rate of 2 – 5 μmol kg^{-1} yr^{-1}, and the increases in AOU located in the vicinity of the African coast at the A9.5 section showed a change rate of ~5 μmol kg^{-1} yr^{-1}. A decadal increase in DIC of ~20 μmol kg^{-1} was observed along the region (Figure S10), particularly in the surface and central waters, in agreement with previous studies in the area (Wanninkhof et al., 2010; Woosley et al., 2016). In general, the higher changes in DIC were observed in the sections with elevated elapsed times between occupations, as expected of the C_{ant} uptake. However, below 200 m the highest variations were strongly correlated with AOU changes. This observation indicates that DIC concentrations in the ocean interior were affected not only by an increase in C_{ant} storage but also by natural variability.

Text S4 – Expected Cant accumulation rates in the A10.5 section

As explained by Sarmiento & Gruber (2006), the uptake rate of C_{ant} can be estimated for surface waters knowing their buffer factor and assuming that the inorganic carbon system in the ocean's surface stays in equilibrium with the atmospheric perturbation, following the Eq. S2:

$$\frac{\delta DIC}{\delta t} = \frac{1}{\gamma DIC} \times \frac{DIC}{pCO_2{}^{oc}} \times \frac{\delta pCO_2{}^{atm}}{\delta t}, \text{ (Eq. S2)}$$

where γDIC represents the Revelle factor (buffer factor), DIC and $pCO_2{}^{oc}$ represent the dissolved inorganic carbon and the partial pressure of carbon dioxide in the seawater respectively, while $\delta pCO_2{}^{atm}$ is the change in the partial pressure of carbon dioxide in the atmosphere. Taking into account the average

DIC reconstructed for the first 50 m of the A10.5-2011 cruise (2079 µmol kg^{-1}), the increase rate of CO_2 concentration in the atmosphere between 2011 and 2017 (1.32 µatm yr^{-1}; Dlugokencky & Tans, 2020), the average pCO_2 observed in the surface waters during the A10.5-2011 cruise (335.9 µatm, Lencina-Avila et al., 2016) and a Revelle factor of 10 (Fassbender et al., 2017; Sabine et al., 2004), the expected accumulation rate for the surface waters along 34.5 °S is 1.5 µmol kg^{-1} yr^{-1}, in line with the majority of the results observed in the region.

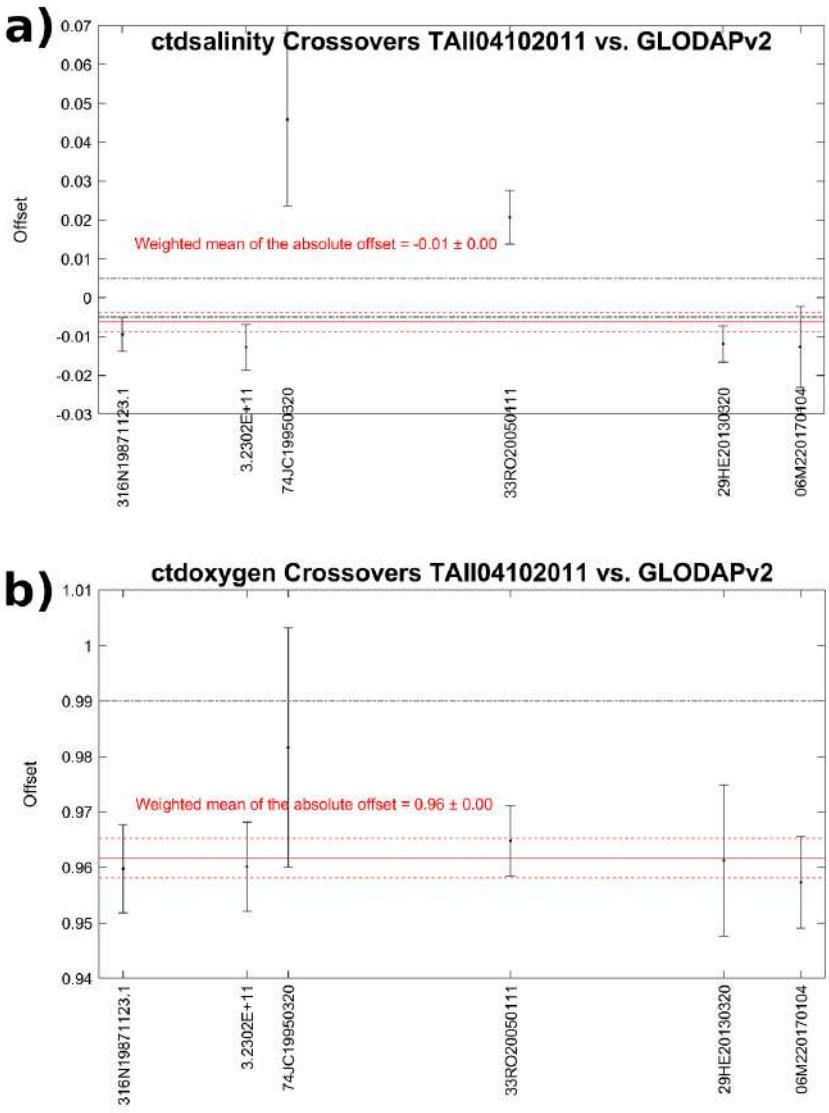

Figure S1. Offsets between the TAII data and the GLODAPV2.2020 database calculated by a crossover analysis using the toolbox for secondary quality control of Lauvset & Tanhua (2015). The expocodes of the cruises matching the stations of the TAII cruise are shown in the horizontal axis. Salinity offsets (a) are additive, and oxygen offsets (b) are multiplicative.

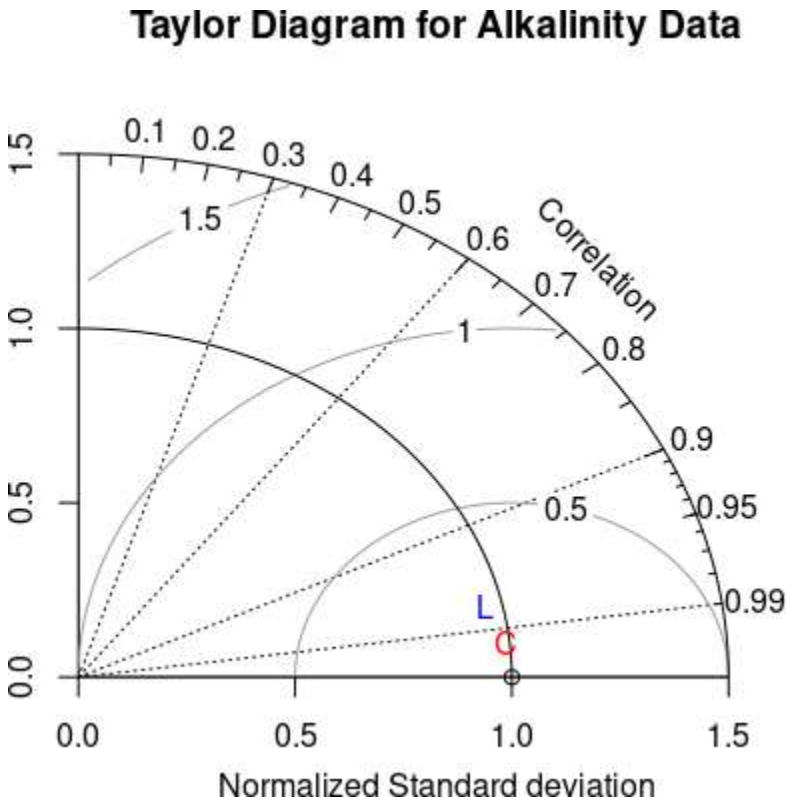

Figure S2. Taylor diagram showing the reconstructed alkalinity data of the A10-2011 section using the LIARv2 method (Carter et al., 2018) (in blue) and the CANYON-B method (Bittig et al., 2018) (in red). A higher correlation and a more similar normalized standard deviation were found between the observed and the predicted values using CANYON-B.

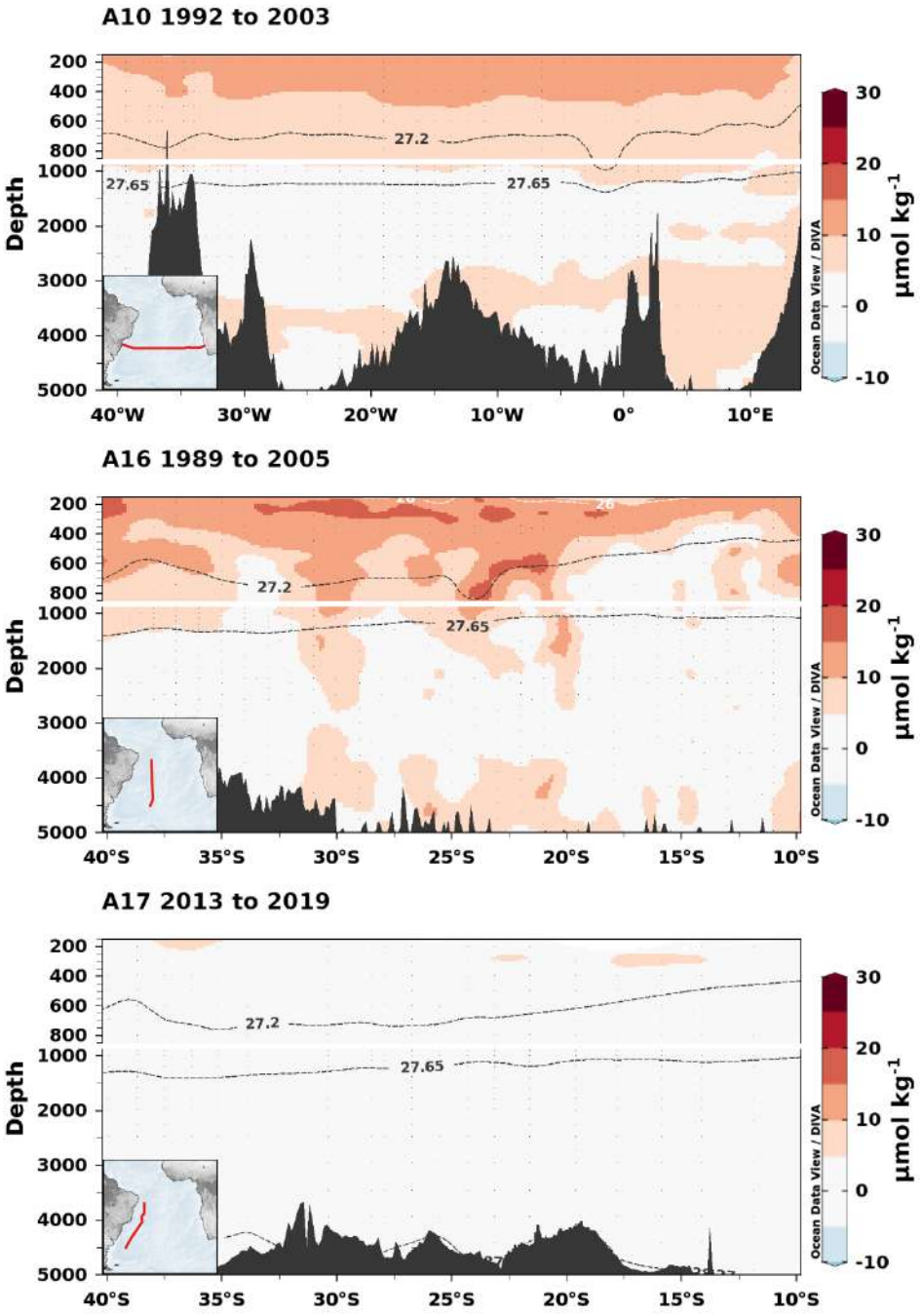

Figure S3. Anthropogenic carbon estimates calculated by the eMLR method for the sections not shown in the main text. Colored estimates are statistically distinguishable from 0 with a 90% confidence. The name of the sections and the period of these estimates are shown in the panel titles. The black dashed lines depict (from top to bottom) the neutral density of 27.2 kg m-3 and 27.65 kg m-3, which correspond to limits between the water masses in the region. Section positions are indicated by the inset maps.

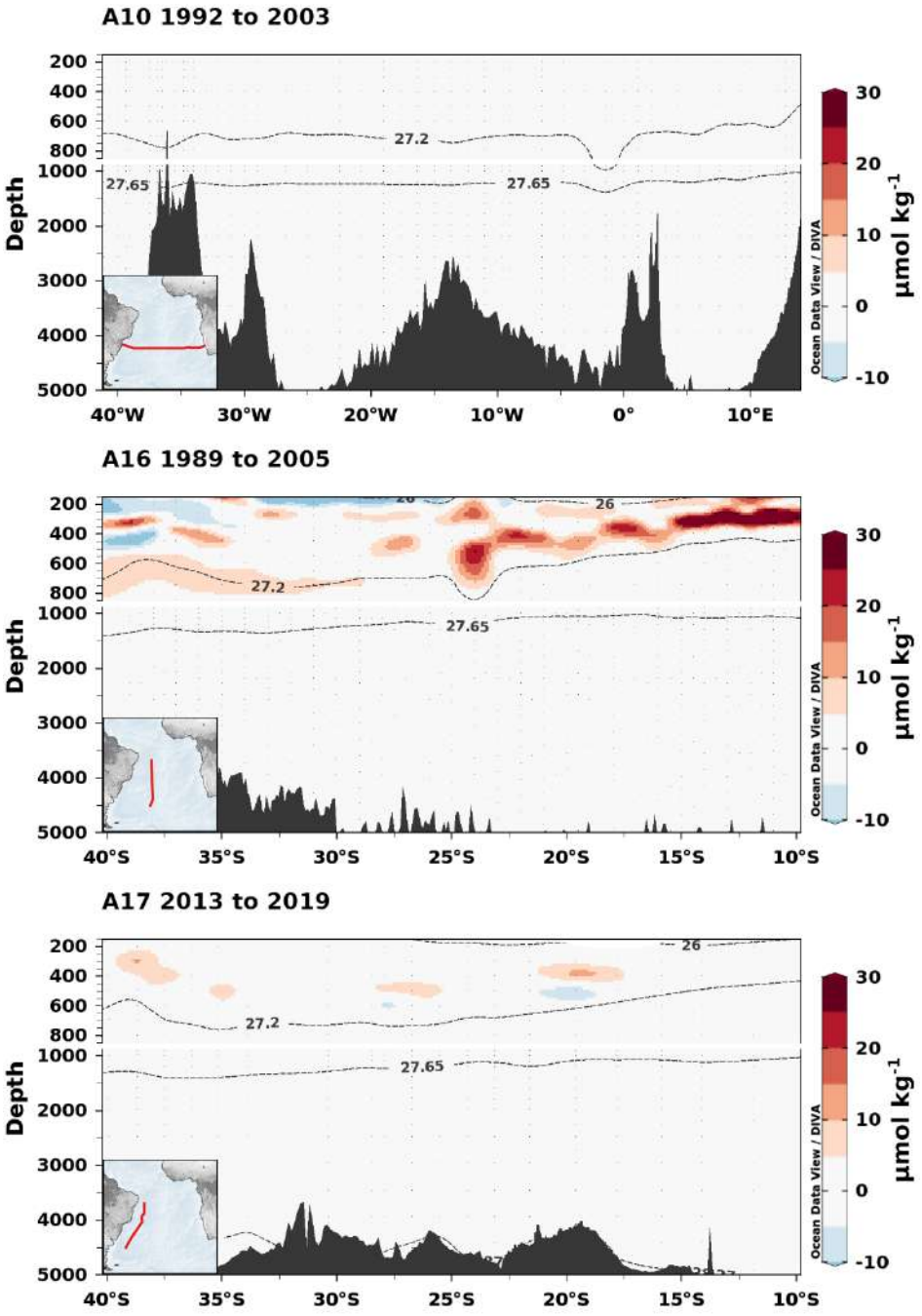

Figure S4. Dissolved inorganic carbon (DIC) changes estimated from the eMLR method applied to apparent oxygen utilization (AOU) data in the sections not shown in the main text. Colored estimates are statistically distinguishable from 0 with a 90% confidence. The name of the sections and the period of these estimates are shown in the panel titles. The black dashed lines depict (from top to bottom) the neutral density of 26 kg m-3, 27.2 kg m-3 and 27.65 kg m-3, which correspond to limits between the water masses in the region. Section positions are indicated by the inset maps.

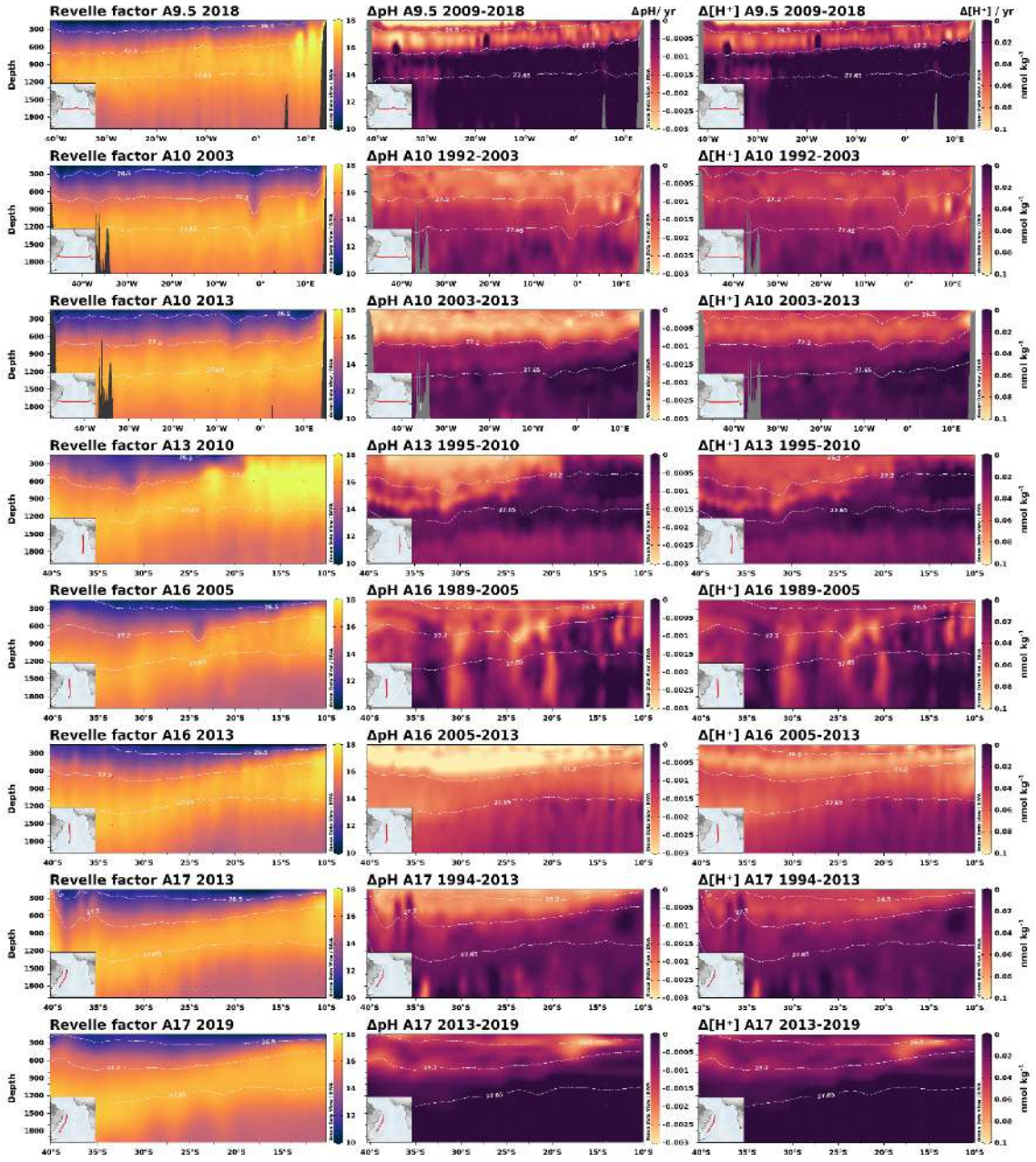

Figure S5. Revelle factor (left panel) and changes in pH and the hydrogen ion concentration (central and right panel) in the first 2000m of the water column for all the studied sections in this work. The name of the sections and the period of these estimates are shown in the panel titles. The white dashed lines depict (from top to bottom) the neutral density of 26 kg m-3, 27.2 kg m-3 and 27.65 kg m-3, which correspond to limits between the water masses in the region. Section positions are indicated by the inset maps.

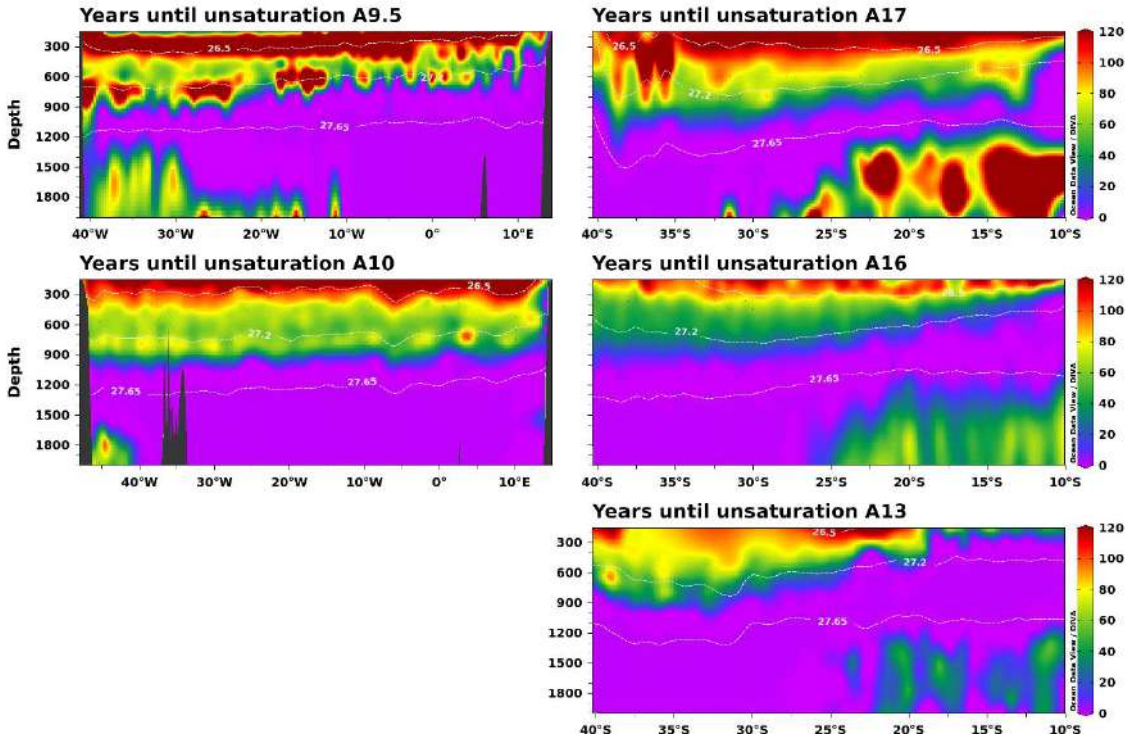

Figure S6. Amount of time (in years) from 2020 until the aragonite saturation reaches a value of 1 in the first 2000 m of the water column in the zonal (left panel) and meridional sections (right panels) evaluated in this study, assuming no change in the observed rates.

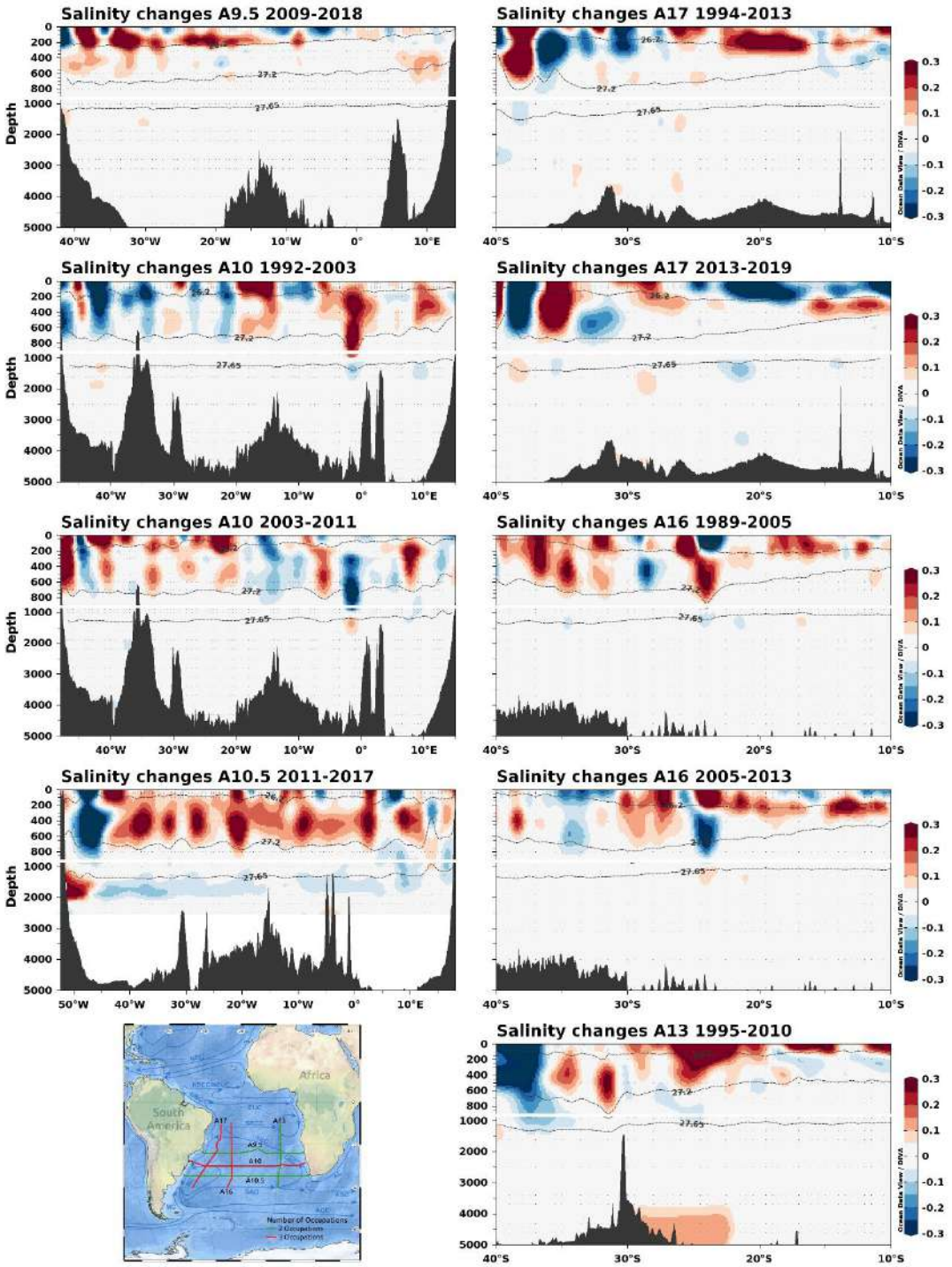

Figure S7. Salinity variations in the zonal (left panels) and meridional section (right panels). Positive (negative) values in red (blue) represent an increase (decrease) since the beginning of the period. The name of the sections and the period of these estimates are shown in the panel titles. The black dashed lines depict (from top to bottom) the neutral density of 26.2 kg m-3, 27.2 kg m-3 and 27.65 kg m-3. The position of the sections is indicated on the map.

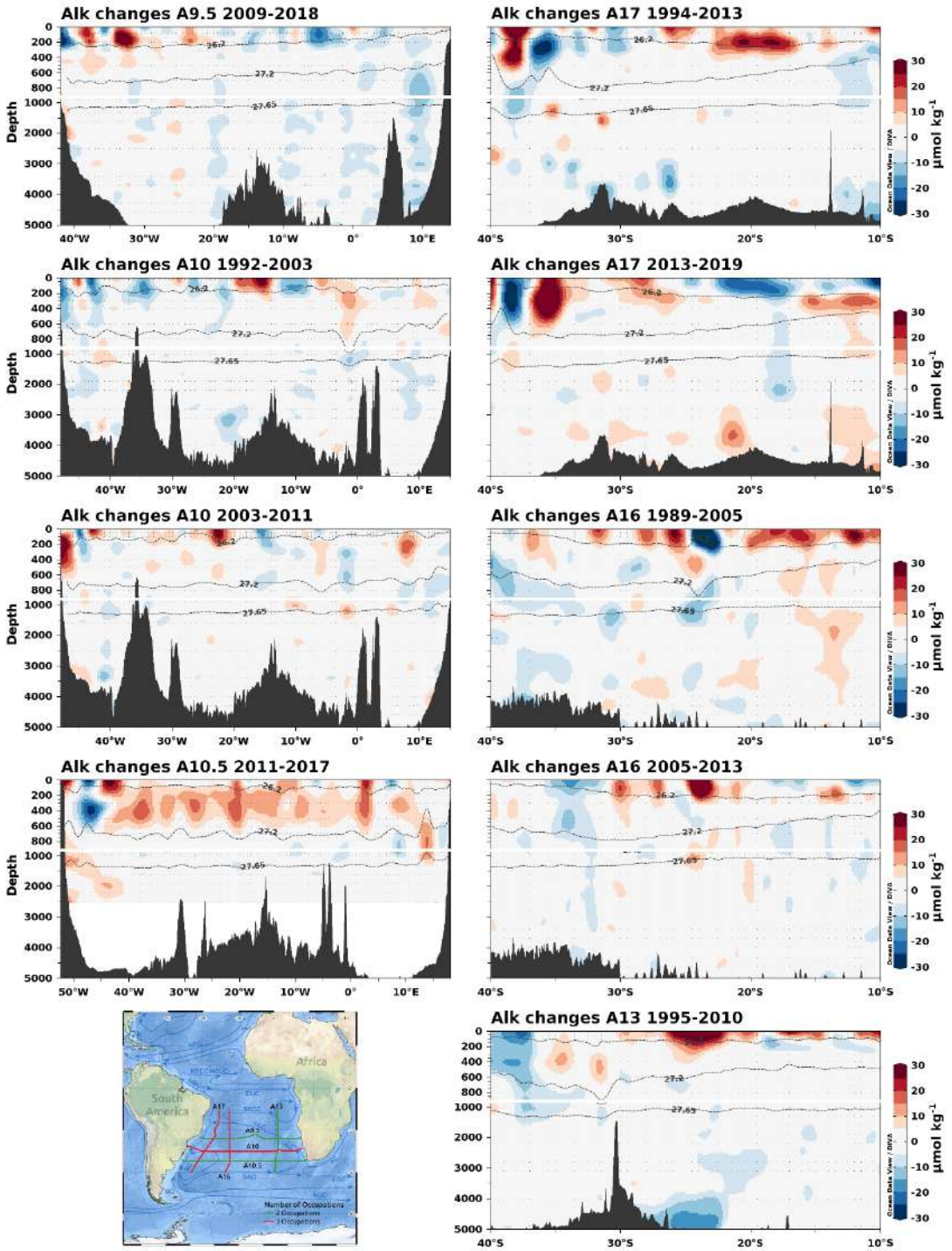

Figure S8. Alkalinity (Alk) variations in the zonal (left panels) and meridional section (right panels). Positive (negative) values in red (blue) represent an increase (decrease) since the beginning of the period. The name of the sections and the period of these estimates are shown in the panel titles. The black dashed lines depict (from top to bottom) the neutral density of 26.2 kg m-3, 27.2 kg m-3 and 27.65 kg m-3. The position of the sections is indicated on the map.

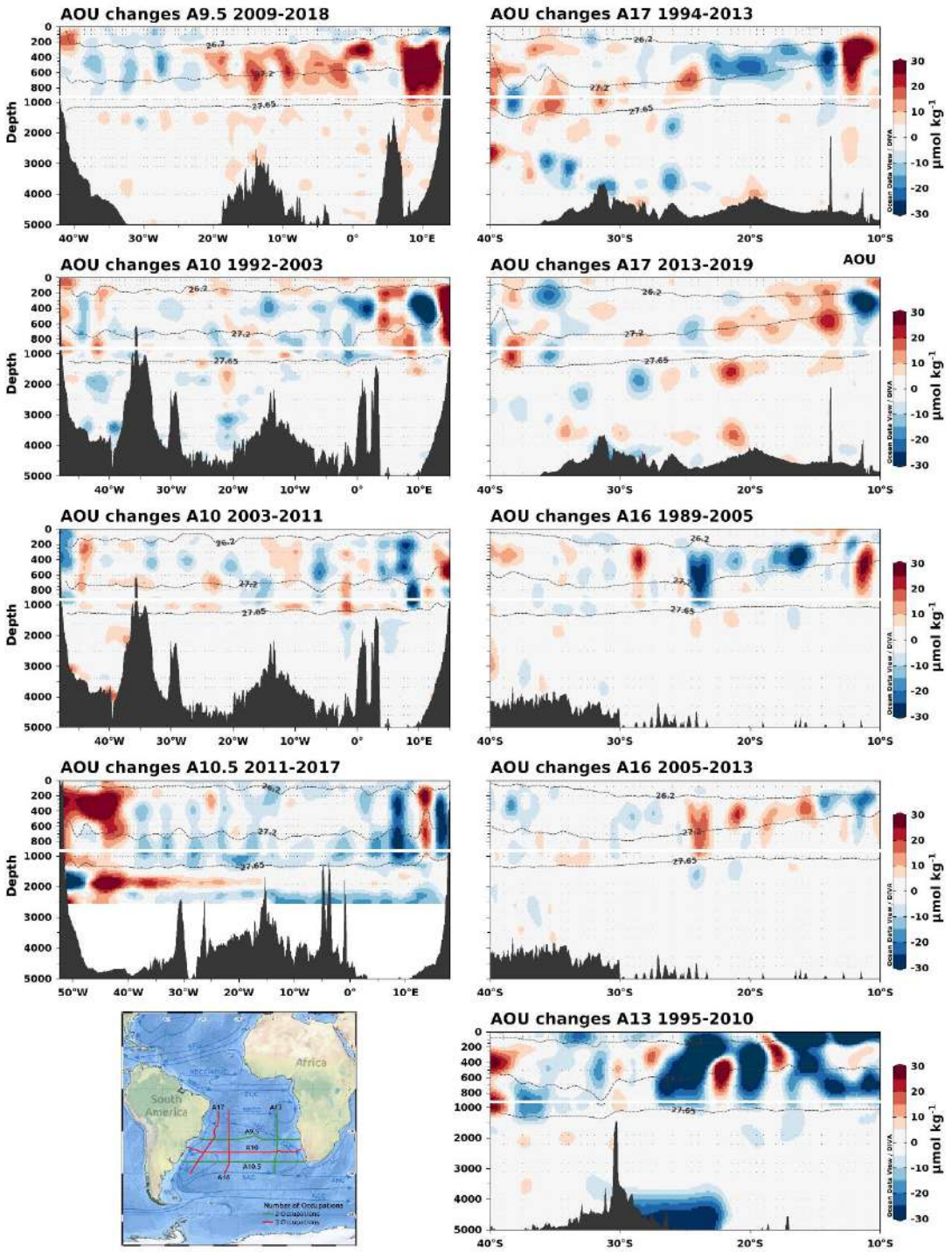

Figure S9. Apparent oxygen utilization (AOU) variations in the zonal (left panels) and meridional section (right panels). Positive (negative) values in red (blue) represent an increase (decrease) since the beginning of the period. The name of the sections and the period of these estimates are shown in the panel titles. The black dashed lines depict (from top to bottom) the neutral density of 26.2 kg m-3, 27.2 kg m-3 and 27.65 kg m-3. The position of the sections is indicated on the map.

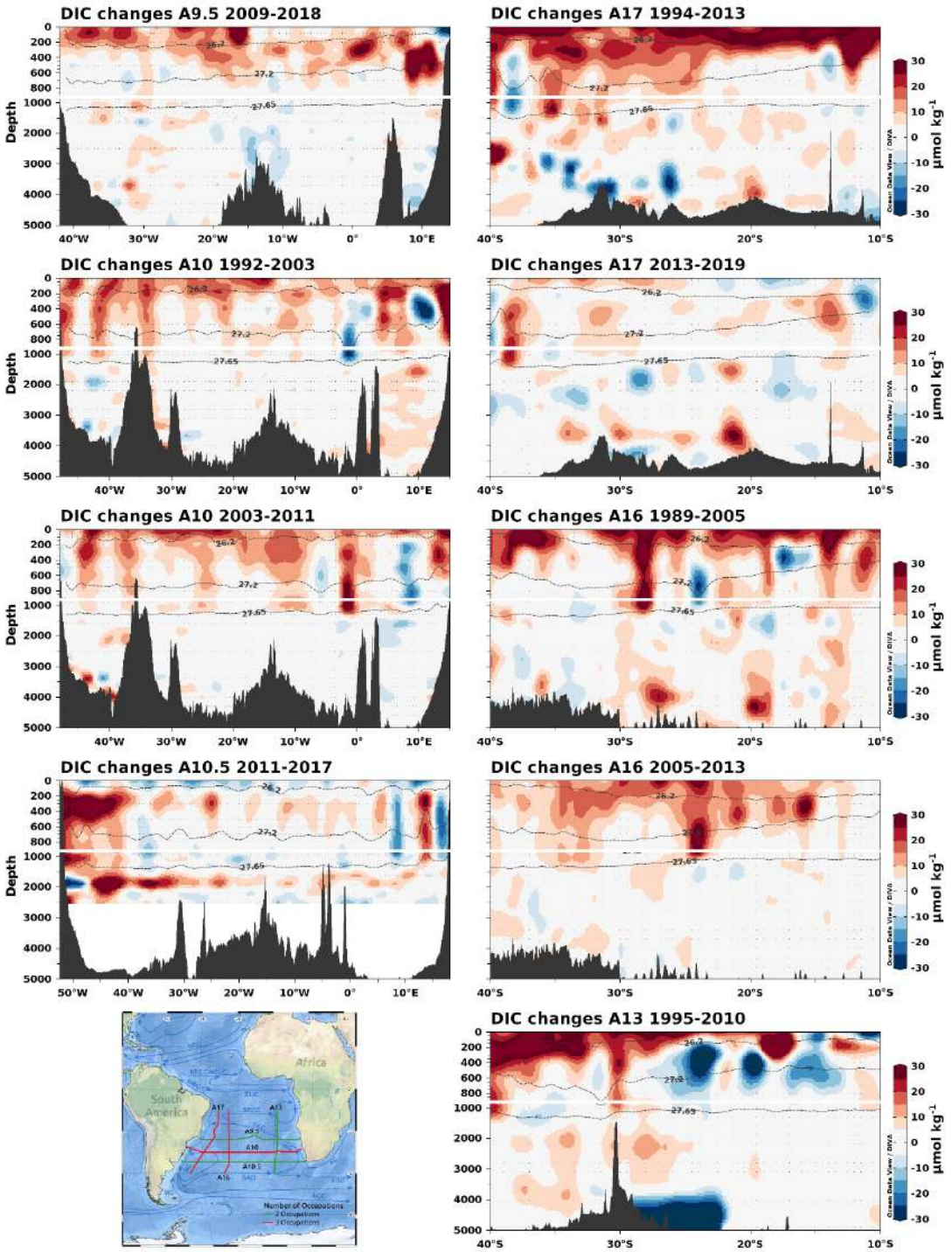

Figure S10. Dissolved inorganic carbon (DIC) variations in the zonal (left panels) and meridional section (right panels). Positive (negative) values in red (blue) represent an increase (decrease) since the beginning of the period. The name of the sections and the period of these estimates are shown in the panel titles. The black dashed lines depict (from top to bottom) the neutral density of 26.2 kg m-3, 27.2 kg m-3 and 27.65 kg m-3. The position of the sections is indicated on the map.

Capítulo V: Síntese da Discussão e Conclusões

Neste estudo, a distribuição espacial e temporal do C_{ant}, suas taxas de acumulação e seu efeito no sistema carbonato foram avaliadas nas águas centrais e intermediárias do oceano Atlântico Sul. Isso foi conseguido aproveitando a disponibilidade de novos dados na região provenientes de cruzeiros hidrográficos pertencentes ao programa GO-SHIP. Para isso, os dados do banco de dados GLODAPv2.2020 foram analisados usando o método eMLR modificado. A distribuição de C_{ant} encontrada não foi espacialmente uniforme, e maiores valores foram observados na margem sul e oeste do giro subtropical, onde as águas estão mais próximas de sua região de formação. De 1989 a 2019, as águas centrais e intermediárias acumularam o C_{ant}, com uma taxa de 0,89 ± 0,33 μmol kg^{-1} ano^{-1} e 0,30 ± 0,29 μmol kg^{-1} ano^{-1}, respetivamente. Uma mudança no inventário da coluna de 0,71 ± 0,35 mol C m^{-2} ano^{-1} foi encontrada para a região, uma taxa que é maior (mas dentro da incerteza) do que a taxa média global de armazenamento de 0,65 mol C m^{-2} ano^{-1} encontrada por Gruber, Clement, et al. (2019). Esta captação de C_{ant} foi o principal processo

responsável pela acidificação da parte superior da coluna de água, e taxas de −0,0020 ± 0,0007 unidades de pH ano^{-1} e −0,0009 ± 0,0009 unidades de pH ano^{-1} foram observadas nas águas centrais e intermediárias, respetivamente. Nessas condições, espera-se que a AAIW se torne insaturada em aragonita em ~70 anos, de acordo as com previsões anteriores (e.g., Fontela et al., 2021; Salt et al., 2015).

Além das estimativas de C_{ant}, as mudanças no DIC associadas às variações na remineralização da matéria orgânica que ocorreram no oceano Atlântico Sul desde a década de 1990 até agora foram estudadas. Para isso, utilizamos a abordagem eMLR aplicada aos dados de AOU. A principal característica observada foi um aumento da concentração de DIC nas águas intermediárias ao longo do limite sul do giro subtropical, e especialmente na costa da África, ao norte de 25°S. A origem deste sinal não pode ser totalmente explicada por mudanças na ventilação. Assim, propomos que o aumento da atividade biológica em união com a atividade de mesoescala e mudanças na entrada de águas do oceano Índico são possíveis mecanismos por trás desse aumento da remineralização. Essas mudanças naturais juntamente com o efeito do C_{ant} foram responsáveis pela maior acidificação da AAIW, um processo previamente relatado no oeste do Atlântico Sul (Fontela et al., 2021; Ríos et al., 2015), e agora também observado na região leste da bacia do Atlântico Sul. Ainda mais, uma insaturação de aragonita em águas centrais ao longo da margem oriental do oceano Atlântico Sul é esperada nos próximos 10 a 20 anos se a absorção de C_{ant} mantem a tendência atual. Esses resultados evidenciam a necessidade de um monitoramento mais exaustivo da margem leste do Atlântico Sul, o que nos permitirá avaliar em que medida a saúde dos ecossistemas, a vida marinha e as sociedades serão afetadas por essas mudanças.

Os resultados apresentados aqui são interessantes porque podem ser usados como valores de referência para o oceano Atlântico Sul, permitindo comparações à medida que mais dados são adquiridos. Novos cruzeiros hidrográficos nas seções menos estudadas (A10.5 e A13) estão sendo planejados para os próximos anos (https://www.go-ship.org/CruisePlans.html), sendo encorajada a determinação do C_{ant} nestas seções para uma melhor compreensão das mudanças no ciclo do carbono oceânico durante a última década. Uma das

principais limitações deste trabalho é que não foi possível observar o efeito dos vórtices de mesoescala, possivelmente em decorrência da metodologia utilizada. Embora o papel dos vórtices das Agulhas nos fluxos de carbono, a atividade biológica e o armazenamento de C_{ant} já foi avaliado recentemente (e.g., Carvalho et al., 2021; Orselli, Goyet, et al., 2019; Orselli, Kerr, et al., 2019), o uso de dados provenientes de boias biogeoquímicas ARGO pode complementar esses estudos, ampliando a resolução espacial e temporal. Da mesma forma, o uso de boias biogeoquímicas pode ajudar a entender se as variações interanuais no C_{ant} observadas em estudos anteriores (Fontela et al., 2021) se estendem por toda a bacia ou se são de natureza local. Por fim, recomenda-se o estudo de outros processos que podem estar influenciando localmente o conteúdo de C_{ant} nas massas de água superficiais do oceano Atlântico Sul, como a presença de efeitos topográficos nas ilhas e montes submarinos da região.

ANEXO I

Este anexo contém uma descrição do método utilizado para o cálculo das incertezas associadas à determinação do C_{ant} mediante o método eMLR, assim como uma descrição do cálculo da taxa de acumulação de C_{ant} esperada na seção A10.5 a partir dos dados hidrográficos disponíveis.

Determinação das incertezas nos parâmetros calculados

As incertezas do C_{ant} estimado pelo método eMLR foram calculadas mediante dois métodos: **(1)** propagando o erro quadrático médio (RMSE) das regressões e as incertezas associadas às medições das variáveis utilizadas nas regressões seguindo as observações de Woosley et al. (2016) e **(2)** aplicando o método de Carter et al. (2017), que consistiu na determinação e propagação das incertezas de três fontes diferentes:

1. Incertezas de medição das variáveis utilizadas nas regressões.
2. Violações da suposição de que as mudanças do DIC pela absorção do C_{ant} é a única fonte de variabilidade identificada pelo método.
3. Incertezas associadas com as distintas combinações de variáveis utilizadas nas regressões.

Para a primeira abordagem, o RMSE médio foi de ± 1,6 μmol kg^{-1}, e a soma em quadratura com a incerteza de medição determinada por Friis et al. (2005) de ± 1,0 μmol kg^{-1} resultou em uma incerteza total de ± 1,9 μmol kg^{-1}. Para a segunda abordagem, a diferença entre as estimativas de C_{ant} obtidas com e sem dados perturbados permitiu a determinação das incertezas associadas com os parâmetros medidos e a violação da suposição do método. Os dados perturbados foram gerados subtraendo a incerteza de cada variável dos dados (e.g. subtraendo 0,002 dos dados de temperatura e salinidade). O desvio padrão das 10 estimativas de ΔC_{ant} foi usado como a incerteza das combinações das variáveis utilizadas nas regressões. A incerteza média obtida usando esta abordagem para todos os cruzeiros foi de ± 2,7 μmol kg^{-1}. Este valor foi usado como a incerteza final do C_{ant} e semelhante a Woosley et al. (2016), nós o aproximamos a ± 3 μmol kg^{-1} para ser conservadores.

O cálculo das incertezas para o pH e outros parâmetros do sistema de carbonato foi realizado usando a função ***errors*** do pacote ***seacarb***, usando as incertezas das constantes do sistema carbonato descritas em Orr et al. (2018). As incertezas usadas para os parâmetros de entrada: temperatura, salinidade, fosfato, silicato, Alk e DIC foram 0,002 °C, 0,002, 0,01 μmol kg^{-1}, 0,1 μmol kg^{-1}, 2 μmol kg^{-1} e 2 μmol kg^{-1}, respetivamente.

Taxas esperadas de acumulação de C_{ant} na seção A10.5

Conforme explicado por Sarmiento & Gruber (2006), a taxa de absorção de C_{ant} pode ser estimada para as águas superficiais conhecendo seu fator tampão e assumindo que o sistema de carbono inorgânico na superfície do oceano permanece em equilíbrio com a perturbação atmosférica, seguindo a Eq. S2:

$$\frac{\delta DIC}{\delta t} = \frac{1}{\gamma DIC} \times \frac{DIC}{pCO_2{}^{oc}} \times \frac{\delta pCO_2{}^{atm}}{\delta t}, \text{ (Eq. S2)}$$

onde γDIC representa o fator de Revelle (capacidade tampão), DIC e $pCO_2{}^{oc}$ representam o carbono inorgânico dissolvido e a pressão parcial de dióxido de carbono na água do mar respetivamente, enquanto $\delta pCO_2{}^{atm}$ é a mudança na pressão parcial de dióxido de carbono na atmosfera. Levando em consideração o DIC médio reconstruído para os primeiros 50 m do cruzeiro A10.5-2011 (2079 μmol kg^{-1}), a taxa de aumento da concentração de CO_2 na atmosfera entre 2011 e 2017 (1,32 μatm ano^{-1}; Dlugokencky & Tans, 2020), o pCO_2 médio observado nas águas superficiais durante o cruzeiro A10.5-2011 (335,9 μatm, Lencina-Avila et al., 2016) e um fator de Revelle de 10 (Fassbender et al., 2017; Sabine et al., 2004), a taxa de acumulação esperada para as águas superficiais ao longo de 34,5°S é de 1,5 μmol kg^{-1} ano^{-1}, semelhante à maioria dos resultados observados na região.

Referências bibliográficas

Álvarez, M., Tanhua, T., Brix, H., Monaco, C. L., Metzl, N., McDonagh, E. L., & Bryden, H. L. (2011). Decadal biogeochemical changes in the subtropical Indian Ocean associated with Subantarctic Mode Water. *Journal of Geophysical Research: Oceans*, *116*(C9). https://doi.org/10.1029/2010JC006475

Anderson, L. A., & Sarmiento, J. L. (1994). Redfield ratios of remineralization determined by nutrient data analysis. *Global Biogeochemical Cycles*, *8*(1), 65–80. https://doi.org/10.1029/93GB03318

Azar, E., Piñango, A., Wallner-Kersanach, M., & Kerr, R. (2020). Source waters contribution to the tropical Atlantic central layer: New insights on the Indo-Atlantic exchanges. *Deep Sea Research Part I: Oceanographic Research Papers*, 103450. https://doi.org/10.1016/j.dsr.2020.103450

Beal, L. M., De Ruijter, W. P. M., Biastoch, A., & Zahn, R. (2011). On the role of the Agulhas system in ocean circulation and climate. *Nature*, *472*(7344), 429–436. https://doi.org/10.1038/nature09983

Biastoch, A., Böning, C. W., Schwarzkopf, F. U., & Lutjeharms, J. R. E. (2009). Increase in Agulhas leakage due to poleward shift of Southern Hemisphere westerlies. *Nature*, *462*(7272), 495–498. https://doi.org/10.1038/nature08519

Bittig, H. C., Steinhoff, T., Claustre, H., Fiedler, B., Williams, N. L., Sauzède, R., et al. (2018). An Alternative to Static Climatologies: Robust Estimation of Open Ocean CO2 Variables and Nutrient Concentrations From T, S, and O2 Data Using Bayesian Neural Networks. *Frontiers in Marine Science*, *5*, 328. https://doi.org/10.3389/fmars.2018.00328

Brewer, P. G. (1978). Direct observation of the oceanic CO2 increase. *Geophysical Research Letters*, *5*(12), 997–1000. https://doi.org/10.1029/GL005i012p00997

Broecker, W. S. (1991). Keeping global change honest. *Global Biogeochemical Cycles*, *5*(3), 191–192. https://doi.org/10.1029/91GB01421

Canadell, J. G., Monteiro, P. M. S., Costa, M. H., Cotrim da Cunha, L., Cox, P. M., Eliseev, A. V., et al. (2021). Global Carbon and other Biogeochemical Cycles and Feedbacks. In V. Masson-Delmotte, P. Zhai, A. Pirani, S. L. Connors, C. Péan, S. Berger, et al. (Eds.), *Climate Change 2021: The Physical Science Basis. Contribution of Working Group I to the Sixth Assessment Report of the Intergovernmental Panel on Climate Change*. Cambridge: Cambridge University Press.

Carter, B. R., Feely, R. A., Mecking, S., Cross, J. N., Macdonald, A. M., Siedlecki, S. A., et al. (2017). Two decades of Pacific anthropogenic carbon storage and ocean acidification along Global Ocean Ship-based Hydrographic Investigations Program sections P16 and P02. *Global Biogeochemical Cycles*, *31*(2), 306–327. https://doi.org/10.1002/2016GB005485

Carter, B. R., Feely, R. A., Williams, N. L., Dickson, A. G., Fong, M. B., & Takeshita, Y. (2018). Updated methods for global locally interpolated estimation of alkalinity, pH, and nitrate. *Limnology and Oceanography: Methods*, *16*(2), 119–131. https://doi.org/10.1002/lom3.10232

Carter, B. R., Feely, R. A., Wanninkhof, R., Kouketsu, S., Sonnerup, R. E., Pardo, P. C., et al. (2019). Pacific Anthropogenic Carbon Between 1991 and 2017. *Global Biogeochemical Cycles*, 2018GB006154. https://doi.org/10.1029/2018GB006154

Carter, B. R., Feely, R. A., Lauvset, S. K., Olsen, A., DeVries, T., & Sonnerup, R. (2021). Preformed Properties for Marine Organic Matter and Carbonate Mineral Cycling Quantification. *Global Biogeochemical Cycles*, *35*(1), e2020GB006623. https://doi.org/10.1029/2020GB006623

Carvalho, A. C. O., Kerr, R., Mendes, C. R. B., Azevedo, J. L. L., & Tavano, V. M. (2021). Phytoplankton strengthen CO2 uptake in the South Atlantic Ocean. *Progress in Oceanography*, *190*, 102476. https://doi.org/10.1016/j.pocean.2020.102476

Carvalho-Borges, M. de, Orselli, I. B. M., Ferreira, M. L. de C., & Kerr, R. (2018). Seawater acidification and anthropogenic carbon distribution on the continental shelf and slope of the western South Atlantic Ocean. *Journal of Marine Systems*, *187*, 62–81. https://doi.org/10.1016/j.jmarsys.2018.06.008

Chen, C.-T. A. (1982). On the distribution of anthropogenic CO2 in the Atlantic and Southern oceans. *Deep Sea Research Part A. Oceanographic Research Papers*, *29*(5), 563–580. https://doi.org/10.1016/0198-0149(82)90076-0

Chen, C.-T. A., & Millero, F. J. (1979). Gradual increase of oceanic CO 2. *Nature*, *277*(5693), 205–206. https://doi.org/10.1038/277205a0

Clement, D., & Gruber, N. (2018). The eMLR(C*) Method to Determine Decadal Changes in the Global Ocean Storage of Anthropogenic CO2. *Global Biogeochemical Cycles*, *32*(4), 654–679. https://doi.org/10.1002/2017GB005819

Cubasch, U., Wuebbles, D., Chen, D., Facchini, M. C., Frame, D., Mahowald, N., & Winther, J.-G. (2013). Introduction. In D. F. Stocker, D. Qin, G.-K. Plattner, M. Tignor, S. K. Allen, J. Boschung, et al. (Eds.), *Climate Change 2013: The Physical Science Basis. Contribution of Working Group I to the Fifth Assessment Report of the Intergovernmental Panel on Climate Change* (pp. 119–158). Cambridge: Cambridge University Press.

Dickson, A. G. (1990). Standard potential of the reaction: AgCl(s) + 1/2H 2 (g) = Ag(s) + HCl(aq), and the standard acidity constant of the ion HSO4- in synthetic sea water from 273.15 to 318.15 K. *The Journal of Chemical Thermodynamics*, *22*(2), 113–127. https://doi.org/10.1016/0021-9614(90)90074-z

Dlugokencky, E., & Tans, P. (2020). Trends in atmospheric carbon dioxide, National Oceanic and Atmospheric Administration, Earth System

Research Laboratory (NOAA/ESRL). Retrieved December 15, 2020, from http://www.esrl.noaa.gov/gmd/ccgg/trends/global.html

Doney, S. C., Balch, W., Fabry, V., & Feely, R. A. (2009). Ocean Acidification: A Critical Emerging Problem for the Ocean Sciences. *Oceanography*, *22*(4), 16–25. https://doi.org/10.5670/oceanog.2009.93

Doney, S. C., Fabry, V. J., Feely, R. A., & Kleypas, J. A. (2009). Ocean Acidification: The Other CO2 Problem. *Annual Review of Marine Science*, *1*(1), 169–192. https://doi.org/10.1146/annurev.marine.010908.163834

Doney, S. C., Busch, D. S., Cooley, S. R., & Kroeker, K. J. (2020). The Impacts of Ocean Acidification on Marine Ecosystems and Reliant Human Communities. *Annual Review of Environment and Resources*, *45*(1), 83–112. https://doi.org/10.1146/annurev-environ-012320-083019

Dunne, J. P., Sarmiento, J. L., & Gnanadesikan, A. (2007). A synthesis of global particle export from the surface ocean and cycling through the ocean interior and on the seafloor. *Global Biogeochemical Cycles*, *21*(4). https://doi.org/10.1029/2006GB002907

Fajar, N. M., Guallart, E. F., Steinfeldt, R., Ríos, A. F., Pelegrí, J. L., Pelejero, C., et al. (2015). Anthropogenic CO2 changes in the Equatorial Atlantic Ocean. *Progress in Oceanography*, *134*, 256–270. https://doi.org/10.1016/j.pocean.2015.02.004

Fassbender, A. J., Sabine, C. L., & Palevsky, H. I. (2017). Nonuniform ocean acidification and attenuation of the ocean carbon sink. *Geophysical Research Letters*, *44*(16), 8404–8413. https://doi.org/10.1002/2017GL074389

Feely, R. A., Doney, S. C., & Cooley, S. (2009). Ocean Acidification: Present Conditions and Future Changes in a High-CO2 World. *Oceanography*, *22*(4), 36–47. https://doi.org/10.5670/oceanog.2009.95

Feely, R. A., Okazaki, R. R., Cai, W.-J., Bednaršek, N., Alin, S. R., Byrne, R. H., & Fassbender, A. (2018). The combined effects of acidification and hypoxia on pH and aragonite saturation in the coastal waters of the California current ecosystem and the northern Gulf of Mexico. *Continental Shelf Research*, *152*, 50–60. https://doi.org/10.1016/j.csr.2017.11.002

Fine, R. A., Peacock, S., Maltrud, M. E., & Bryan, F. O. (2017). A new look at ocean ventilation time scales and their uncertainties. *Journal of Geophysical Research: Oceans*, *122*(5), 3771–3798. https://doi.org/10.1002/2016JC012529

Fontela, M., Velo, A., Gilcoto, M., & Pérez, F. F. (2021). Anthropogenic CO2 and ocean acidification in Argentine Basin Water Masses over almost five decades of observations. *Science of The Total Environment*, *779*, 146570. https://doi.org/10.1016/j.scitotenv.2021.146570

Friedlingstein, P., O'Sullivan, M., Jones, M. W., Andrew, R. M., Hauck, J., Olsen, A., et al. (2020). Global Carbon Budget 2020. *Earth System Science Data*, *12*(4), 3269–3340. https://doi.org/10.5194/essd-12-3269-2020

Friis, K., Körtzinger, A., Pätsch, J., & Wallace, D. W. R. (2005). On the temporal increase of anthropogenic CO2 in the subpolar North Atlantic. *Deep Sea Research Part I: Oceanographic Research Papers*, *52*(5), 681–698. https://doi.org/10.1016/j.dsr.2004.11.017

Gattuso, J.-P., Epitalon, J.-M., Lavinge, H., & Orr, J. C. (2020). seacarb: seawater carbonate chemistry. (Version R package version 3.2.13.). Retrieved from http://CRAN.R-project.org/package=seacarb

Goes, M., Wainer, I., & Signorelli, N. (2014). Investigation of the causes of historical changes in the subsurface salinity minimum of the South Atlantic. *Journal of Geophysical Research: Oceans*, *119*(9), 5654–5675. https://doi.org/10.1002/2014JC009812

Goodkin, N. F., Levine, N. M., Doney, S. C., & Wanninkhof, R. (2011). Impacts of temporal CO2 and climate trends on the detection of ocean anthropogenic CO2 accumulation. *Global Biogeochemical Cycles*, *25*(3). https://doi.org/10.1029/2010GB004009

Gordon, A. L. (1981). South Atlantic thermocline ventilation. *Deep Sea Research Part A. Oceanographic Research Papers*, *28*(11), 1239–1264. https://doi.org/10.1016/0198-0149(81)90033-9

Gordon, A. L., Weiss, R. F., Smethie, W. M., & Warner, M. J. (1992). Thermocline and intermediate water communication between the south Atlantic and Indian oceans. *Journal of Geophysical Research: Oceans*, *97*(C5), 7223–7240. https://doi.org/10.1029/92JC00485

Gruber, N., Sarmiento, J. L., & Stocker, T. F. (1996). An improved method for detecting anthropogenic CO2 in the oceans. *Global Biogeochemical Cycles*, *10*(4), 809–837. https://doi.org/10.1029/96GB01608

Gruber, N., Clement, D., Carter, B. R., Feely, R. A., van Heuven, S., Hoppema, M., et al. (2019). The oceanic sink for anthropogenic CO2 from 1994 to 2007. *Science*, *363*(6432), 1193–1199. https://doi.org/10.1126/science.aau5153

Gruber, N., Landschützer, P., & Lovenduski, N. S. (2019). The Variable Southern Ocean Carbon Sink. *Annual Review of Marine Science*, *11*(1), 159–186. https://doi.org/10.1146/annurev-marine-121916-063407

Hernández-Guerra, A., Talley, L. D., Pelegrí, J. L., Vélez-Belchí, P., Baringer, M. O., Macdonald, A. M., & McDonagh, E. L. (2019). The upper, deep, abyssal and overturning circulation in the Atlantic Ocean at 30°S in 2003 and 2011. *Progress in Oceanography*, *176*, 102136. https://doi.org/10.1016/j.pocean.2019.102136

Hoegh-Guldberg, O., Mumby, P. J., Hooten, A. J., Steneck, R. S., Greenfield, P., Gomez, E., et al. (2007). Coral Reefs Under Rapid Climate Change and Ocean Acidification. *Science*, *318*(5857), 1737–1742. https://doi.org/10.1126/science.1152509

Honisch, B., Ridgwell, A., Schmidt, D. N., Thomas, E., Gibbs, S. J., Sluijs, A., et al. (2012). The Geological Record of Ocean Acidification. *Science*, *335*(6072), 1058–1063. https://doi.org/10.1126/science.1208277

Ito, T., Follows, M. J., & Boyle, E. A. (2004). Is AOU a good measure of respiration in the oceans? *Geophysical Research Letters*, *31*(17). https://doi.org/10.1029/2004GL020900

Karstensen, J., Stramma, L., & Visbeck, M. (2008). Oxygen minimum zones in the eastern tropical Atlantic and Pacific oceans. *Progress in Oceanography*, *77*(4), 331–350. https://doi.org/10.1016/j.pocean.2007.05.009

Kitidis, V., Brown, I., Hardman-Mountford, N., & Lefèvre, N. (2017). Surface ocean carbon dioxide during the Atlantic Meridional Transect (1995–2013); evidence of ocean acidification. *Progress in Oceanography*, *158*, 65–75. https://doi.org/10.1016/j.pocean.2016.08.005

Koszalka, I. M., & Stramma, L. (2019). Current Systems in the Atlantic Ocean. In J. K. Cochran, H. J. Bokuniewicz, & P. L. Yager (Eds.), *Encyclopedia of Ocean Sciences (Third Edition)* (pp. 204–211). Oxford: Academic Press. https://doi.org/10.1016/B978-0-12-409548-9.11291-6

Kulk, G., Platt, T., Dingle, J., Jackson, T., Jönsson, B. F., Bouman, H. A., et al. (2020). Primary Production, an Index of Climate Change in the Ocean: Satellite-Based Estimates over Two Decades. *Remote Sensing*, *12*(5), 826. https://doi.org/10.3390/rs12050826

Lachkar, Z. (2014). Effects of upwelling increase on ocean acidification in the California and Canary Current systems. *Geophysical Research Letters*, *41*(1), 90–95. https://doi.org/10.1002/2013GL058726

Lamont, T., García-Reyes, M., Bograd, S. J., van der Lingen, C. D., & Sydeman, W. J. (2018). Upwelling indices for comparative ecosystem studies: Variability in the Benguela Upwelling System. *Journal of Marine Systems*, *188*, 3–16. https://doi.org/10.1016/j.jmarsys.2017.05.007

Lauvset, S. K., & Tanhua, T. (2015). A toolbox for secondary quality control on ocean chemistry and hydrographic data. *Limnology and Oceanography: Methods*, *13*(11), 601–608. https://doi.org/10.1002/lom3.10050

Lauvset, S. K., Carter, B. R., Perez, F. F., Jiang, L. -Q., Feely, R. A., Velo, A., & Olsen, A. (2020). Processes Driving Global Interior Ocean pH Distribution. *Global Biogeochemical Cycles*, *34*(1). https://doi.org/10.1029/2019GB006229

Lee, K., Choi, S.-D., Park, G.-H., Wanninkhof, R., Peng, T.-H., Key, R. M., et al. (2003). An updated anthropogenic CO2 inventory in the Atlantic Ocean. *Global Biogeochemical Cycles*, *17*(4), n/a-n/a. https://doi.org/10.1029/2003GB002067

Lencina-Avila, J. M., Ito, R. G., Garcia, C. A. E., & Tavano, V. M. (2016). Sea-air carbon dioxide fluxes along 35°S in the South Atlantic Ocean. *Deep Sea Research Part I: Oceanographic Research Papers*, *115*, 175–187. https://doi.org/10.1016/j.dsr.2016.06.004

Lueker, T. J., Dickson, A. G., & Keeling, C. D. (2000). Ocean pCO2 calculated from dissolved inorganic carbon, alkalinity, and equations for K1 and K2: validation based on laboratory measurements of CO2 in gas and seawater

at equilibrium. *Marine Chemistry*, *70*(1), 105–119. https://doi.org/10.1016/S0304-4203(00)00022-0

Manta, G., Speich, S., Karstensen, J., Hummels, R., Kersalé, M., Laxenaire, R., et al. (2021). The South Atlantic Meridional Overturning Circulation and Mesoscale Eddies in the First GO-SHIP Section at 34.5°S. *Journal of Geophysical Research: Oceans*, *126*(2). https://doi.org/10.1029/2020JC016962

Mémery, L., Arhan, M., Alvarez-Salgado, X. A., Messias, M.-J., Mercier, H., Castro, C. G., & Rios, A. F. (2000). The water masses along the western boundary of the south and equatorial Atlantic. *Progress in Oceanography*, *47*(1), 69–98. https://doi.org/10.1016/S0079-6611(00)00032-X

Millero, F. J. (2007). The Marine Inorganic Carbon Cycle. *Chemical Reviews*, *107*(2), 308–341. https://doi.org/10.1021/cr0503557

Millero, F. J., Graham, T. B., Huang, F., Bustos-Serrano, H., & Pierrot, D. (2006). Dissociation constants of carbonic acid in seawater as a function of salinity and temperature. *Marine Chemistry*, *100*(1), 80–94. https://doi.org/10.1016/j.marchem.2005.12.001

Murata, A., Kumamoto, Y., Sasaki, K., Watanabe, S., & Fukasawa, M. (2008). Decadal increases of anthropogenic CO2 in the subtropical South Atlantic Ocean along 30°S. *Journal of Geophysical Research*, *113*(C6), C06007. https://doi.org/10.1029/2007JC004424

Olsen, A., Lange, N., Key, R. M., Tanhua, T., Álvarez, M., Becker, S., et al. (2019). GLODAPv2.2019 – an update of GLODAPv2. *Earth System Science Data*, *11*(3), 1437–1461. https://doi.org/10.5194/essd-11-1437-2019

Olsen, A., Lange, N., Key, R. M., Tanhua, T., Bittig, H. C., Kozyr, A., et al. (2020). GLODAPv2.2020 - the second update of GLODAPv2. *Earth System Science Data Discussions*, 1–41. https://doi.org/10.5194/essd-2020-165

Orr, J. C., Fabry, V. J., Aumont, O., Bopp, L., Doney, S. C., Feely, R. A., et al. (2005). Anthropogenic ocean acidification over the twenty-first century and its impact on calcifying organisms. *Nature*, *437*(7059), 681–686. https://doi.org/10.1038/nature04095

Orr, J. C., Epitalon, J.-M., Dickson, A. G., & Gattuso, J.-P. (2018). Routine uncertainty propagation for the marine carbon dioxide system. *Marine Chemistry*, *207*, 84–107. https://doi.org/10.1016/j.marchem.2018.10.006

Orselli, I. B. M., Kerr, R., Ito, R. G., Tavano, V. M., Mendes, C. R. B., & Garcia, C. A. E. (2018). How fast is the Patagonian shelf-break acidifying? *Journal of Marine Systems*, *178*, 1–14. https://doi.org/10.1016/j.jmarsys.2017.10.007

Orselli, I. B. M., Goyet, C., Kerr, R., Azevedo, J. L. L. de, Araujo, M., Galdino, F., et al. (2019). The Effect of Agulhas Eddies on Absorption and Transport of Anthropogenic Carbon in the South Atlantic Ocean. *Climate*, *7*(6), 84. https://doi.org/10.3390/cli7060084

Orselli, I. B. M., Kerr, R., Azevedo, J. L. L. de, Galdino, F., Araujo, M., & Garcia, C. A. E. (2019). The sea-air CO2 net fluxes in the South Atlantic Ocean and the role played by Agulhas eddies. *Progress in Oceanography*, *170*, 40–52. https://doi.org/10.1016/j.pocean.2018.10.006

Pardo, P. C., Pérez, F. F., Khatiwala, S., & Ríos, A. F. (2014). Anthropogenic CO2 estimates in the Southern Ocean: Storage partitioning in the different water masses. *Progress in Oceanography*, *120*, 230–242. https://doi.org/10.1016/j.pocean.2013.09.005

Perez, F. F., & Fraga, F. (1987). Association constant of fluoride and hydrogen ions in seawater. *Marine Chemistry*, *21*(2), 161–168. https://doi.org/10.1016/0304-4203(87)90036-3

Pezzi, L. P., de Souza, R. B., Santini, M. F., Miller, A. J., Carvalho, J. T., Parise, C. K., et al. (2021). Oceanic eddy-induced modifications to air–sea heat and CO2 fluxes in the Brazil-Malvinas Confluence. *Scientific Reports*, *11*(1), 10648. https://doi.org/10.1038/s41598-021-89985-9

Plancherel, Y., Rodgers, K. B., Key, R. M., Jacobson, A. R., & Sarmiento, J. L. (2013). Role of regression model selection and station distribution on the estimation of oceanic anthropogenic carbon change by eMLR. *Biogeosciences*, *10*(7), 4801–4831. https://doi.org/10.5194/bg-10-4801-2013

Poole, R., & Tomczak, M. (1999). Optimum multiparameter analysis of the water mass structure in the Atlantic Ocean thermocline. *Deep Sea Research Part I: Oceanographic Research Papers*, *46*(11), 1895–1921. https://doi.org/10.1016/S0967-0637(99)00025-4

Provost, C., Escoffier, C., Maamaatuaiahutapu, K., Kartavtseff, A., & Garçon, V. (1999). Subtropical mode waters in the South Atlantic Ocean. *Journal of Geophysical Research: Oceans*, *104*(C9), 21033–21049. https://doi.org/10.1029/1999JC900049

Ridgwell, A., & Zeebe, R. (2005). The role of the global carbonate cycle in the regulation and evolution of the Earth system. *Earth and Planetary Science Letters*, *234*(3–4), 299–315. https://doi.org/10.1016/j.epsl.2005.03.006

Ríos, A. F., Velo, A., Pardo, P. C., Hoppema, M., & Pérez, F. F. (2012). An update of anthropogenic CO2 storage rates in the western South Atlantic basin and the role of Antarctic Bottom Water. *Journal of Marine Systems*, *94*, 197–203. https://doi.org/10.1016/j.jmarsys.2011.11.023

Ríos, A. F., Resplandy, L., García-Ibáñez, M. I., Fajar, N. M., Velo, A., Padin, X. A., et al. (2015). Decadal acidification in the water masses of the Atlantic Ocean. *Proceedings of the National Academy of Sciences*, *112*(32), 9950–9955. https://doi.org/10.1073/pnas.1504613112

Rusciano, E., Speich, S., & Ollitrault, M. (2012). Interocean exchanges and the spreading of Antarctic Intermediate Water south of Africa. *Journal of Geophysical Research: Oceans*, *117*(C10). https://doi.org/10.1029/2012JC008266

Russell, J. L., & Dickson, A. G. (2003). Variability in oxygen and nutrients in South Pacific Antarctic Intermediate Water. *Global Biogeochemical Cycles*, *17*(2). https://doi.org/10.1029/2000GB001317

Sabine, C. L., & Tanhua, T. (2010). Estimation of Anthropogenic CO2 Inventories in the Ocean. *Annual Review of Marine Science*, *2*(1), 175–198. https://doi.org/10.1146/annurev-marine-120308-080947

Sabine, C. L., Feely, R. A., Gruber, N., Key, R. M., Lee, K., Bullister, J. L., et al. (2004). The Oceanic Sink for Anthropogenic CO2. *Science*, *305*(5682), 367–371. https://doi.org/10.1126/science.1097403

Sabine, C. L., Feely, R. A., Millero, F. J., Dickson, A. G., Langdon, C., Mecking, S., & Greeley, D. (2008). Decadal changes in Pacific carbon. *Journal of Geophysical Research: Oceans*, *113*(C7). https://doi.org/10.1029/2007JC004577

Salt, L. A., van Heuven, S. M. A. C., Claus, M. E., Jones, E. M., & de Baar, H. J. W. (2015). Rapid acidification of mode and intermediate waters in the southwestern Atlantic Ocean. *Biogeosciences*, *12*(5), 1387–1401. https://doi.org/10.5194/bg-12-1387-2015

Santos, G. C., Kerr, R., Azevedo, J. L. L., Mendes, C. R. B., & da Cunha, L. C. (2016). Influence of Antarctic Intermediate Water on the deoxygenation of the Atlantic Ocean. *Dynamics of Atmospheres and Oceans*, *76*, 72–82. https://doi.org/10.1016/j.dynatmoce.2016.09.002

Sarmiento, J. L., & Gruber, N. (2006). *Ocean biogeochemical dynamics*. Princeton: Princeton University Press.

Sato, O. T., & Polito, P. S. (2014). Observation of South Atlantic subtropical mode waters with Argo profiling float data. *Journal of Geophysical Research: Oceans*, *119*(5), 2860–2881. https://doi.org/10.1002/2013JC009438

Schmidt, M., & Eggert, A. (2016). Oxygen cycling in the northern Benguela Upwelling System: Modelling oxygen sources and sinks. *Progress in Oceanography*, *149*, 145–173. https://doi.org/10.1016/j.pocean.2016.09.004

Schmidtko, S., Stramma, L., & Visbeck, M. (2017). Decline in global oceanic oxygen content during the past five decades. *Nature*, *542*(7641), 335–339. https://doi.org/10.1038/nature21399

de Souza, A. G. Q. de, Kerr, R., & Azevedo, J. L. L. de. (2018). On the influence of Subtropical Mode Water on the South Atlantic Ocean. *Journal of Marine Systems*, *185*, 13–24. https://doi.org/10.1016/j.jmarsys.2018.04.006

Stramma, L., & England, M. (1999). On the water masses and mean circulation of the South Atlantic Ocean. *Journal of Geophysical Research: Oceans*, *104*(C9), 20863–20883. https://doi.org/10.1029/1999JC900139

Takahashi, T., Sutherland, S. C., Chipman, D. W., Goddard, J. G., Ho, C., Newberger, T., et al. (2014). Climatological distributions of pH, pCO2, total CO2, alkalinity, and CaCO3 saturation in the global surface ocean, and temporal changes at selected locations. *Marine Chemistry*, *164*, 95–125. https://doi.org/10.1016/j.marchem.2014.06.004

Talley, L. D. (2008). Freshwater transport estimates and the global overturning circulation: Shallow, deep and throughflow components. *Progress in Oceanography*, *78*(4), 257–303. https://doi.org/10.1016/j.pocean.2008.05.001

Talley, L. D., Feely, R. A., Sloyan, B. m., Wanninkhof, R., Baringer, M. o., Bullister, J. l., et al. (2016). Changes in Ocean Heat, Carbon Content, and Ventilation: A Review of the First Decade of GO-SHIP Global Repeat Hydrography. *Annual Review of Marine Science*, *8*(1), 185–215. https://doi.org/10.1146/annurev-marine-052915-100829

Tanhua, T., & Keeling, R. F. (2012). Changes in column inventories of carbon and oxygen in the Atlantic Ocean. *Biogeosciences*, *9*(11), 4819–4833. https://doi.org/10.5194/bg-9-4819-2012

Tanhua, T., Hoppema, M., Jones, E. M., Stöven, T., Hauck, J., Dávila, M. G., et al. (2017). Temporal changes in ventilation and the carbonate system in the Atlantic sector of the Southern Ocean. *Deep Sea Research Part II: Topical Studies in Oceanography*, *138*, 26–38. https://doi.org/10.1016/j.dsr2.2016.10.004

Touratier, F., & Goyet, C. (2004). Applying the new TrOCA approach to assess the distribution of anthropogenic CO2 in the Atlantic Ocean. *Journal of Marine Systems*, *46*(1–4), 181–197. https://doi.org/10.1016/j.jmarsys.2003.11.020

Uppström, L. R. (1974). The boron/chlorinity ratio of deep-sea water from the Pacific Ocean. *Deep Sea Research and Oceanographic Abstracts*, *21*(2), 161–162. https://doi.org/10.1016/0011-7471(74)90074-6

Venables, W. N., & Ripley, B. D. (2002). *Modern Applied Statistics with S* (Fourth). New York: Springer. Retrieved from http://www.stats.ox.ac.uk/pub/MASS4/

Wallace, D. W. R. (1995). *Monitoring global ocean carbon inventories*. College Station, Tex.: Ocean Observing System Development Panel.

Wallace, D. W. R. (2001). Chapter 6.3 Storage and transport of excess CO2 in the oceans:The JGOFS/WOCE global CO2 survey. In G. Siedler, J. Church, & J. Gould (Eds.), *International Geophysics* (Vol. 77, pp. 489–L). Academic Press. https://doi.org/10.1016/S0074-6142(01)80136-4

Wanninkhof, R., Doney, S. C., Bullister, J. L., Levine, N. M., Warner, M., & Gruber, N. (2010). Detecting anthropogenic CO2 changes in the interior Atlantic Ocean between 1989 and 2005. *Journal of Geophysical Research*, *115*(C11), C11028. https://doi.org/10.1029/2010JC006251

Waters, J. F., Millero, F. J., & Sabine, C. L. (2011). Changes in South Pacific anthropogenic carbon. *Global Biogeochemical Cycles*, *25*(4), n/a-n/a. https://doi.org/10.1029/2010GB003988

Waugh, D. W., Primeau, F., DeVries, T., & Holzer, M. (2013). Recent Changes in the Ventilation of the Southern Oceans. *Science*, *339*(6119), 568–570. https://doi.org/10.1126/science.1225411

Williams, N. L., Feely, R. A., Sabine, C. L., Dickson, A. G., Swift, J. H., Talley, L. D., & Russell, J. L. (2015). Quantifying anthropogenic carbon inventory changes in the Pacific sector of the Southern Ocean. *Marine Chemistry*, *174*, 147–160. https://doi.org/10.1016/j.marchem.2015.06.015

Woosley, R. J., Millero, F. J., & Wanninkhof, R. (2016). Rapid anthropogenic changes in CO2 and pH in the Atlantic Ocean: 2003–2014. *Global Biogeochemical Cycles*, 21.

Zeebe, R. E., & Wolf-Gladrow, D. (Eds.). (2001). Chapter 1 Equilibrium. In *Elsevier Oceanography Series* (Vol. 65, pp. 1–84). Elsevier. https://doi.org/10.1016/S0422-9894(01)80002-7